HELICAL MODE INSTABILITY IN A HIGHLY IONIZED PLASMA

by

CHIA-HWA TAO

A dissertation submitted to the Graduate Faculty in Engineering in partial fulfillment of the requirements for the degree of Doctor of Philosophy, The City University of New York.

1971

This manuscript has been read and accepted for the Graduate Faculty in Engineering in satisfaction of the dissertation requirement for the degree of Doctor of Philosophy.

1/13/1971
date

Chairman of Examining Committee

13 Jan 1971
date

Executive Officer

Professor R. F. Dressler

Professor L. A. Ferrari

Professor C. M. Tchen

Professor N. C. Jen, Chairman
Supervisory Committee

The City University of New York

ABSTRACT

The helical instability in a weakly ionized plasma, known as Kadomtsev instability, has been extensively investigated in recent years. In this study, a series of experimental results of such instability for highly ionized plasma is presented. The experiments were conducted in a single-ended quiescent plasma machine at the Magnetohydrodynamics Laboratory of the City University of New York with a degree of ionization over 90%. In addition to the Langmuir probe measurement, the helical mode and its time evolution and the instantaneous density distribution across the column have been successfully recorded by the newly developed high speed photographic technique which is known as the plasma camera.

The experimental results are summarized as follows:

(1) The helical instability occurs when the longitudinal current presents and the magnetic field exceeds the critical magnetic field of 700 gauss.

(2) The helix rotates in the direction of the electron diamagnetic drift. The pitch of the helix, as recorded by the plasma camera, varies with the magnetic field and has a dimension comparable to or less than the length of the plasma column.

(3) The instability criterion is not sensitive to the background pressure of the system. The longitudinal current is essential for the helical instability to occur, but its magnitude does not have significant effect on the amplitude of the instability.

(4) The direct measurements of plasma diffusion across the magnetic field indicates that the diffusion follows the classical theory up to the critical magnetic field. Enhanced diffusion occurs immediately above the critical magnetic field and then is followed by Bohm diffusion before the plasma becomes fully turbulent. Under the turbulent state, the diffusion coefficient is inversely proportional to the square of the magnetic field, similar to the classical case. The experimental results have shown that Bohm diffusion corresponds closely to large amplitude oscillations and turbulent diffusion associates with break down of the coherent waves.

The above results are significantly different from the case of weakly ionized plasma; they present a physical model of the helical instability of a highly ionized plasma column and offer a base for theoretical investigations.

ACKNOWLEDGEMENTS

I am deeply indebted to my mentor, Professor Norman C. Jen who suggested the topic of research and directed it from its inception. His expert guidance, unfailing effort and inspiration throughout the research and writing of the thesis are gratefully appreciated.

For their interest and guidance I would like to thank the members of my Doctoral Committee: Professors L. Diesendruck, R.F. Dressler, M. Ettenberg, L.A. Ferrari, H. Lashinsky and C.M. Tchen.

Thanks are due to Professors Joseph C. Cataldo and K.L. Li for useful discussions. The assistance of Mr. Ira Mansfield in performing the experiment is much appreciated.

I would like to thank both the City University of New York and the United States Air Force Office of Scientific Research for the financial support given to me personally and to the Magnetohydrodynamic Laboratory, without which this work would not have been possible. I would like to thank the United States Naval Ordnance Laboratory for the use of the Dynafax high speed camera. The financial aid and services provided by The City College and the Department of Civil Engineering are gratefully acknowledged.

TABLE OF CONTENTS

LIST OF ILLUSTRATIONS

LIST OF TABLES

CHAPTER 1

INTRODUCTION

Due to the direct association of the diffusion of charged particles across a magnetic field and the instability of the confined plasma column, the understanding of instability becomes primary importance in the field of plasma physics and controlled thermonuclear fusion research. Instabilities of various types have been observed and investigated, and almost all of them lead to enhanced diffusion in the direction transverse to the confining magnetic field[1-6]. According to the mode of instabilities, they are classified as drift instability[7-9], flute instability[10] and helical instability[11-15]. Considerable effort, both theoretical and experimental, has been made in the study of these instabilities except the helical instability for a highly ionized plasma case. For weakly ionized plasma, Lehnert and Hoh established the physical model through their gas discharge experiment and then Kadomtsev and Nedospasov derived the theory. Up to this date, the understanding of the helical instability in a highly ionized plasma is lacking, yet it is rather important.

Physically the instabilities between the weakly ionized and the highly ionized cases are very different. For the weakly ionized case, the collisions among electrons and neutrals provide luminous pictures of the helical motion which can be observed easily. For highly ionized plasma, the collisional phenomenon is completely different and the physical picture of the helical motion becomes impossible to be observed by ordinary means.

Because of the lack of actual physical picture of the helical instability for highly ionized plasma, theoretical analysis and better understanding of the instability becomes almost impossible.

The purpose of this thesis is to identify the existence of such instability in a highly ionized plasma column and to study its properties, driving mechanism, parametric effects on the transverse diffusion and visualization by means of conducting a set of experiments. It is hoped that theseexperimental results and the actual picture of the dynamic of helical instability present a physical model for theoretical investigation in the future.

1.1 Review of Work on Helical Instability

The helical instability of a weakly ionized gas discharge was first observed by Lehnert and Hoh in the study of the diffusion process of the gas discharge in a magnetic field. The rate of diffusion agreed with the classical theory of ambipolar diffusion in a range of magnetic field up to a critical value. Above this value an instability set in, and the diffusion increased with magnetic field, resulting in a diffusion rate much higher than that by the classical collision theory. The mechanism of the helical instability was not determined in their experiment. Hoh[16] later gave a theoretical explanation showing that the condition for maintaining a stable wall sheath of the gas discharge could not be satisfied when the magnetic field was above the critical value.

Kadomtsev and Nedospasov in their theoretical analysis of the anomalous diffusion of the positive column identified the instability as diffusive and called it the current-convective instability. They indicated that the longitudinal electric current and its interaction with the magnetic field ($\underline{j} \times \underline{B}$ force) were the cause of the helical instability. A dispersion relation and the frequency of oscillations were obtained by a linear analysis. Comparison between the theoretical values of the critical magnetic field and experimental data were given. The plasma was predicted to become turbulent at strong magnetic field as a result of this instability.

The properties and the growth of the helical instability were further investigated experimentally by Paulikas and Pyle. Quantitative comparisons between their experiment and the theory of Hoh and the theory of Kadomtsev and Nedospasov showed good agreement with the latter theory. They also studied the properties of waves and found that the density oscillation is of the form of a rotating helix with a pitch (or the longitudinal wave length) shorter than the length of the column.

Guest and Simon[17] in a stability analysis similar to that of Kadomtsev and Nedospasov indicated that the driving mechanism of the helical instability was due to the force from charge separation produced by the difference in a streaming velocity of the electrons and ions to the end walls. Hence a longitudinal electric current is necessary for the helical instability to occur. Woods[18] further showed theoretically that the helical mode instability is due to the coupling between a steady

electric current along the magnetic field lines and a transverse variation in resistivity of the plasma.

The significance of the effect of the longitudinal electric current on the helical instability was demonstrated by Akhmedov and Zaitsev[19] in their experiment on He and Ne gas discharges. It was found that the increase of the longitudinal current lowered the critical magnetic field at which the onset of the instability occurred.

In addition, much work has been carried out in recent years on the helical instability in weakly ionized plasmas, for example, theoretically on the improvement of Kadomtsev type analyses[20-22], and experimentally on the studies of effects of various parameters on the instability[23-26]. The above results are in sharp contrast to the case of highly ionized plasmas, particularly for the plasma produced in a Q-machine, with which the helical instability has yet to be investigated.

1.2 Investigation of the Helical Instability in a Highly Ionized Plasma - Some Salient Features

Investigation of the helical instability in a highly ionized potassium plasma may differ from its counterpart in a weakly ionized positive column due to their differences in the constituents and the way the plasma is

created. In the weakly ionized plasma the collision between ions and neutrals is dominant. The ion-neutral collision frequency is much greater than the ion cyclotron frequency and the frequency of the observed oscillations, and the effect of the magnetic field on the ions as well as the inertia and diffusion of ions are negligible. In the highly or fully ionized plasma the transverse motion of the ions is governed by the magnetic field, and the electron-ion collision is important[27]. With the presence of the radial density gradient the plasma is subject to an azimuthal drift similar to that of the "Universal" instability[28].

The positive column is created by accelerating electrons from the cathode to the anode, and the electrons encounter the gas neutrals resulting in ionization. An electric current flow, of the order of 1 amp., is kept by the longitudinal electric field. On the other hand, the potassium plasma is generated by surface ionization at the hot ionizer, and no ionization is taking place in the body of the quasi-neutral plasma. Because of current collection, recombination losses, and thermal motion, the plasma streams to the cold plate. The losses of electrons and ions may differ due to the biased end conditions. The overall balanace of electron and ion densities relies on the readjustment at the sheath of the hot ionizer. Therefore, the longitudinal electric flow, which affects the stability of the column, is limited by the ability of readjustment of the ionizer sheath conditions. Under the experimental conditions where the permissible electric current is relatively small (of the order of 10^{-2} amp.), the electric current effect

on the helical instability is not as pronounced. The helical instability may, therefore, not always arise.

The difficulties in the experimental investigation of the helical instability in a highly ionized plasma lie in the direct measurement of the transverse diffusion, the positive identification of the helical mode oscillation and the observation of its time volution. In the case of the weakly ionized gas discharge, the diffusion of particles across the magnetic field was measured indirectly by the change of the axial field required to maintain the discharge column. The sudden change in the effective diffusion corresponds to the onset of the helical instability at the critical magnetic field. The critical magnetic field can also be determined by observing the change in intensity of the glow of the discharge[29]. Since the gas discharge is self-luminous, the helical density oscillation can be identified by observing its helicity with a streak camera and photomultipliers as well as by measuring the mode number (m = 1) of the azimuthal propagation and the longitudinal wave length of the oscillations. This conventional photographic technique, however, cannot be adapted to the highly ionized potassium plasma as it is not self-luminus.

To overcome the above-mentioned difficulties, a specially developed photographic technique using the high speed plasma camera[30,31] and a diffusion flux collector are used in conjunction with the Langmuir probes in the experiment. The high speed plasma camera is able to record the instantaneous density distribution of the plasma over a time scale. This

furnishes the time evolution of the helical instability. It can also provide visualization of the turbulent density distribution of the column under strong magnetic fields. The diffusion collector measures the transverse plasma flux, hence it gives the rate of diffusion of plasma across the magnetic field in the presence of the helical instability. The properties of the instability and various components of the waves are studied by using the Langmuir probe technique.

1.3 Summary

In this chapter a review of earlier work on the helical instability and the importance of the present investigation have been given. Factors essential to the study of the helical instability in a highly ionized plasma have been discussed. The incorporation of the high speed photography using the high speed plasma camera and the method for direct measurement of diffusion by the diffusion collector with the Langmuir probes have been described.

Chapter 2 gives a description of the apparatus used in the experiment. Chapter 3 presents the theory and principle of the major diagnostic techniques. Calibration of equipment and preparatory experiment are given in Chapter 4, and results of the experiment are presented in Chapter 5. The analysis and discussion of the experimental findings and a conclusion are given in Chapter 6.

CHAPTER 2

EXPERIMENT APPARATUS

The experiment has been conducted on the Q-machine at The City College Magnetohydrodynamic Laboratory of the City University of New York. The Q-machine, high speed plasma camera, Langmuir probe and the auxiliary equipment are shown in Fig. 2.1.

2.1 The Q-machine

The Q-machine is a quiescent, thermally ionized alkali metal plasma generator which is noted for producing a steady, quiescent and highly ionized plasma suitable for investigations of plasma instabilities, magnetic field confinement, diffusion and turbulence.

2.1.1 The Theory of Q-machine

The generation of plasma is attained by contact ionization of the neutral potassium vapor from an atomic beam oven sprayed onto a hot tungsten plate in an evacuated chamber. A high degree of ionization is achieved by keeping the chamber walls at a low temperature so that neutrals condense on them and are quickly pumped out of the system. The operation may be single-ended having the hot tungsten plate and the atomic beam oven at one end of the chamber and a cold collector plate at the other end, or double-ended with one hot plate located at each end of the chamber, each provided with an oven.

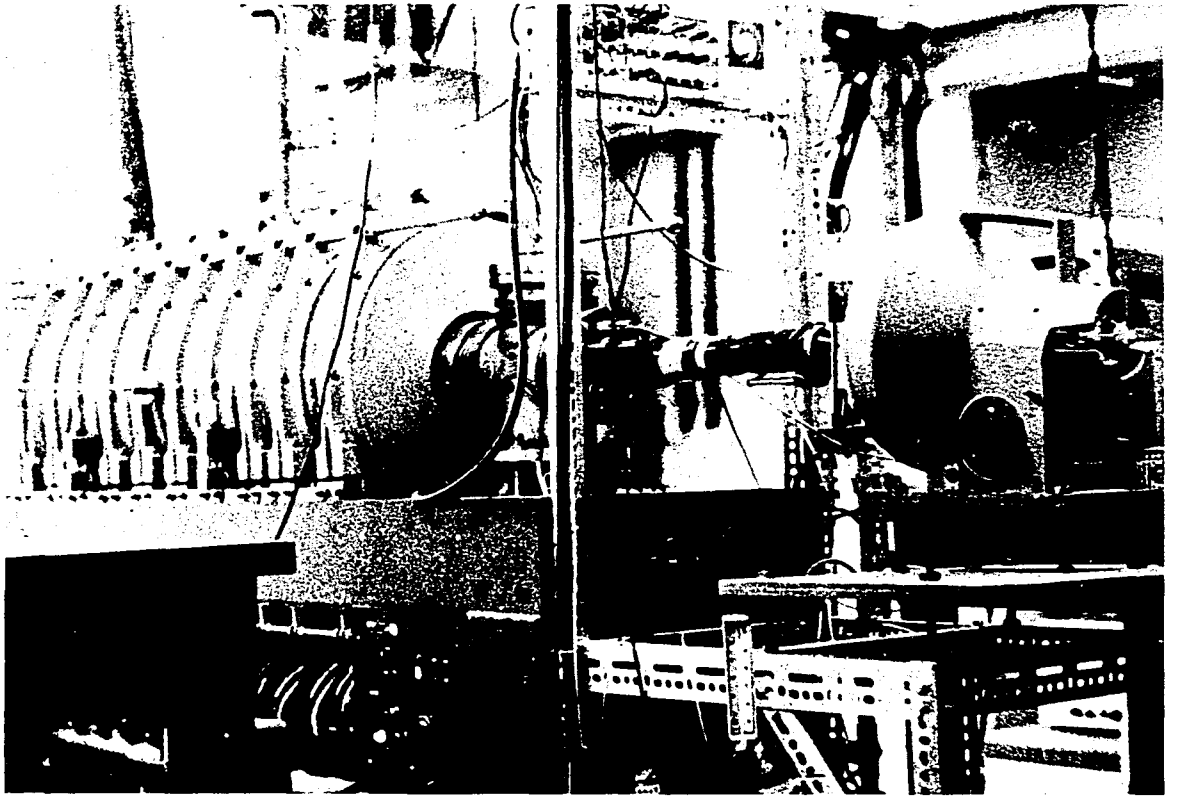

Figure 2.1 General View of the Q-machine

The theory and operation of the quiescent plasma generating device, as shown below, was first presented by Rynn and D'Angelo[32]. Due to the configuration of the plasma column and the way it is produced the radial density distribution has strong dependency on the confining magnetic field and the azimuthal drifts always exist.

In the present study the Q-machine is operated single-ended. Figure 2.2 is a schematic diagram of the Q-machine. The dependence of the radial density distribution on the magnetic field and the rotational drift velocities are derived. As the plasma is highly ionized and steady, time-independent hydromagnetic equations of the two-fluid model are employed. Using cylindrical coordinates and the origin at the hot ionizer surface and the z-axis coinciding with the axis of the plasma column, the equations of continuity are

$$\nabla \cdot (n \underline{v}_i) + \alpha n^2 = 0 \qquad (2.1a)$$

$$\nabla \cdot (n \underline{v}_e) + \alpha n^2 = 0 \qquad (2.1b)$$

where n is the density, $\underline{v}$ is the velocity , α is the recombination coefficient, and the subscripts i and e refer to ions and electrons respectively. The equations of motion are

$$n m_i \underline{v}_i \cdot \nabla \underline{v}_i + k T \nabla n - n e(\underline{E} + \underline{v}_i \times \underline{B}) = - \eta e^2 n^2 (\underline{v}_i - \underline{v}_e) \qquad (2.2a)$$

$$n m_e \underline{v}_e \cdot \nabla \underline{v}_e + k T \nabla n + n e(\underline{E} + \underline{v}_e \times \underline{B}) = \eta e^2 n^2 (\underline{v}_i - \underline{v}_e) \qquad (2.2b)$$

where m_i and m_e are the ion mass and the electron mass respectively, $\underline{E}$ is the electric field, $\underline{B}$ is the magnetic field, η is the electric resistivity,

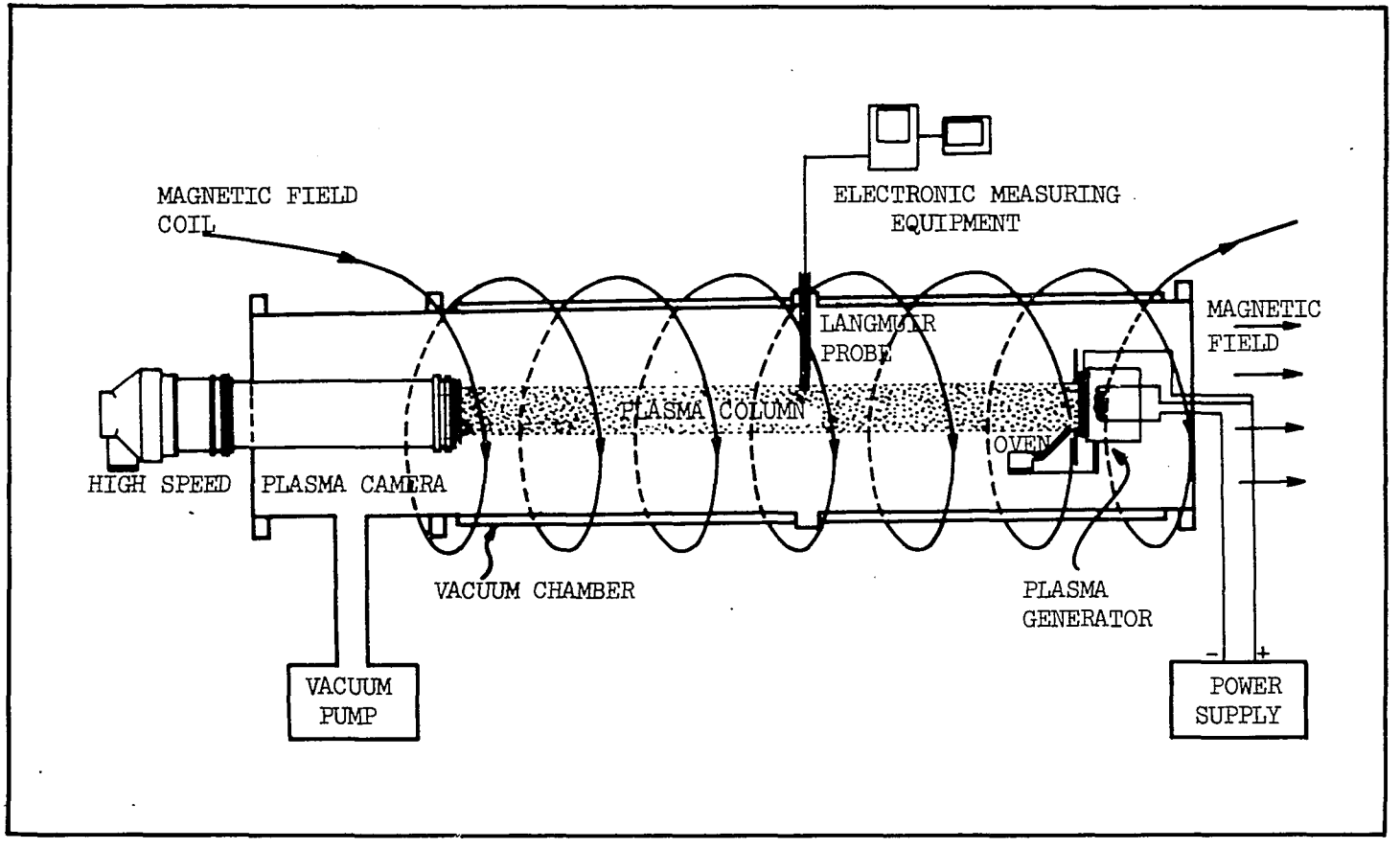

Figure 2.2 Schematic Diagram of the Q-machine

and e is the electron charge.

In the above equations it has been assumed that

$$n_i = n_e = n$$

and

$$T_i = T_e = T$$

It is further assumed that $\underline{v} \cdot \nabla \underline{v}$ is negligible and all quantities have no θ-dependence.

The equations of continuity become

$$\frac{1}{r}\frac{\partial}{\partial r}(r n v_{ir}) + \frac{\partial}{\partial z}(n v_{iz}) = -\alpha n^2 \tag{2.3a}$$

$$\frac{1}{r}\frac{\partial}{\partial r}(r n v_{er}) + \frac{\partial}{\partial z}(n v_{ez}) = -\alpha n^2 \tag{2.3b}$$

With $\underline{B} = (0,0,B)$ and $\underline{E} = (E_r, 0, 0)$ (The radial electric field is due to the potential gradient near the edge of the column.), the equations of motion are, from Eqs. (2.2a) and (2.2b)

$$\left[kT\frac{\partial n}{\partial r} - n e v_{i\theta} B - n e E_r + \eta e^2 n^2 (v_{ir} - v_{er})\right]\hat{r}$$

$$+ \left[n e v_{ir} B + \eta e^2 n^2 (v_{i\theta} - v_{e\theta})\right]\hat{\theta}$$

$$+ \left[\frac{\partial n}{\partial z} + \eta e^2 n^2 (v_{iz} - v_{ez})\right]\hat{z} = 0 \tag{2.4a}$$

$$\left[kT\frac{\partial n}{\partial r} + n e v_{e\theta} B + n e E_r - \eta e^2 n^2 (v_{ir} - v_{er})\right]\hat{r}$$

$$+ \left[-n e v_{er} B - \eta e^2 n^2 (v_{i\theta} - v_{e\theta})\right]\hat{\theta}$$

$$+ \left[\frac{\partial n}{\partial z} - \eta e^2 n^2 (v_{iz} - v_{ez})\right]\hat{z} = 0 \tag{2.4b}$$

Add Eq. (2.4a) to Eq. (2.4b), we have

$$\text{r-component:}\quad 2\,kT\frac{\partial n}{\partial r} - ne(v_{i\theta} - v_{e\theta})B = 0 \tag{2.5}$$

$$\theta\text{-component:}\qquad v_{ir} = v_{er} = v_r \tag{2.6}$$

$$\text{z-component:}\qquad \frac{\partial n}{\partial z} = 0 \tag{2.7}$$

Equation (2.6) indicates that ions and electrons have the same radial drift velocity. This is true for a highly ionized plasma in which the diffusion is ambipolar. Equation (2.7) shows that there is no density gradient along the column.

Subtracting Eq. (2.4b) from Eq.(2.4a) and with the aid of Eq. (2.6) we have

$$\text{r-component:}\quad E_r = -\frac{(v_{i\theta} + v_{e\theta})B}{2} \tag{2.8}$$

$$\theta\text{-component:}\quad v_r = -\frac{1}{B}\eta en\,(v_{i\theta} - v_{e\theta}) \tag{2.9}$$

$$\text{z-component:}\qquad v_{iz} = v_{ez} \tag{2.10}$$

With the aid of Maxwell's equations

$$\nabla \times \underline{B} = 4\pi \underline{j}$$

$$\frac{1}{r}\frac{\partial B}{\partial \theta}\hat{r} - \frac{\partial B}{\partial r}\hat{\theta} = 4\pi en\,(v_{i\theta} - v_{e\theta})\,\hat{\theta} \tag{2.11}$$

It gives that

$$\frac{\partial B}{\partial \theta} = 0 \tag{2.12}$$

i.e. the magnetic field is independent of θ, and

$$\frac{\partial B}{\partial r} = -4\pi e n (v_{i\theta} - v_{e\theta}) \tag{2.13}$$

From Eq. (2.5) and Eq. (2.13)

$$\frac{dB}{dr} = \frac{8\pi k T}{B} \frac{dn}{dr}$$

Integrate to get

$$\frac{B^2}{16\pi} + kTn = \frac{B_o^2}{16\pi} \tag{2.14}$$

It renders that $B \cong B_o$, where B_o is the external confining magnetic field. It is evident that B, n, v_r, v_θ, and $\frac{\partial v_z}{\partial z}$ depend on r. It is reasonable to assume the dependence of v_z on r and z as

$$v_z = f(r)\, z \tag{2.15}$$

where f(r) is a function related to the distribution of the potassium onto the hot ionizer.

From Eqs. (2.5) and (2.9) one obtains

$$v_r = -\frac{2\eta k T}{B_o^2} \frac{\partial n}{\partial r} \tag{2.16}$$

Substituting v_r and v_z of Eqs. (2.15) and (2.16) into Eq. (2.3) we get, after rearrangement

$$\frac{d^2(n^2)}{dr^2} + \frac{1}{r}\frac{d(n^2)}{dr} - \frac{2\alpha}{A} n^2 = -\frac{2\mu}{A}$$

where $A \equiv \frac{2\eta k T}{B_o^2}$ and $\mu = -n f(r)$. μ depends on the distribution of the

potassium neutral flux at the hot ionizer plate. For the atomic beam mode of operation uniform distribution of neutrals on the hot plate can be attained. Hence μ is considered constant in the region $0 \leq r \leq R$, while $\mu = 0$ in the region $r \geq R$, where R is the radius of the plasma column dictated by the opening of the aperture limiter. (Fig. 2.2) Therefore we have

$$\frac{d^2(n^2)}{dr^2} + \frac{1}{r}\frac{d(n^2)}{dr} - \frac{2\alpha}{A}n^2 = -\frac{2\mu}{A} \qquad (2.17)$$

(region $0 \leq r \leq R$)

$$\frac{d^2(n^2)}{dr^2} + \frac{1}{r}\frac{d(n^2)}{dr} - \frac{2\alpha}{A}n^2 = 0 \qquad (2.18)$$

(region $r \geq R$)

For $0 \leq r \leq R$, solutions are Bessel functions of the first kind, and for $r \geq R$, solutions are Bessel functions of the second kind, with the boundary conditions that $n = n_o$ at $r = 0$, $n = 0$ at $r = \infty$, and the densities and their derivatives of the two regions match at $r = R$.

Figure 2.3 shows the calculated radial density profiles for the case where $T = 2,000\,^{o}K$, $\eta = 4.4 \times 10^{8}$ emu and $\alpha = 3 \times 10^{-10}$ cm^3/sec. The plasma column is less spread and it has a sharper boundary at its edge for high magnetic field, showing the effect of confinement.

Figure 2.4 gives a plot of the angular velocity, Ω of the plasma at a magnetic field of 2000 gauss. It is shown that the plasma has azimuthal drifts and the maximum azimuthal drift velocity of about one-tenth of the

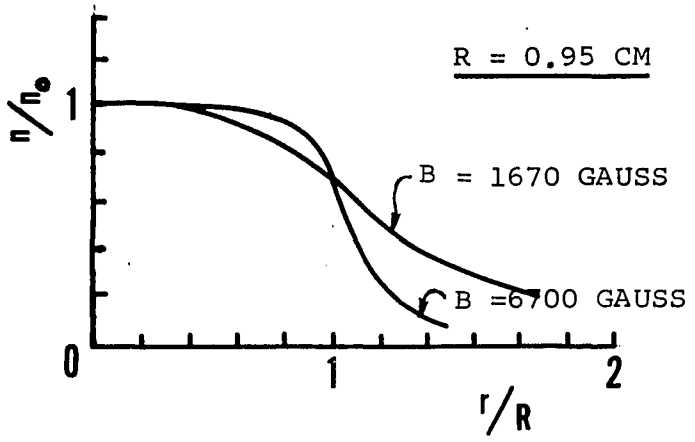

Figure 2.3 Calculated Radial Density Profiles

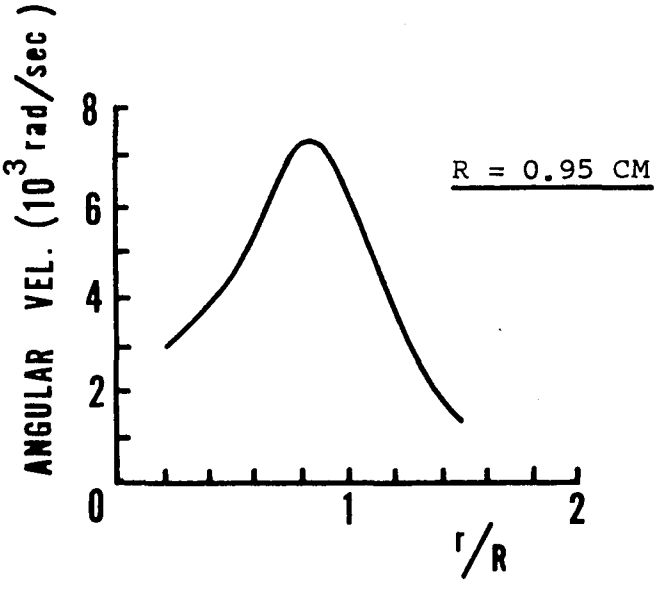

Figure 2.4 Calculated Angular Velocity due to Azimuthal Drift

thermal velocity occurs near the edge of the column.

2.1.2 The Construction of the Q-machine

The Q-machine is operated single-ended with the plasma generated at the hot end, where the plasma generator is situated, and collected at the cold end, both enclosed in a 4-3/4 in. (12 cm) I.D. non-magnetic stainless steel vacuum chamber. A low pressure in the order of 10^{-7} torr is maintained in the chamber. The chamber is 4 ft. 6 in. (140 cm) long and is provided with 1/4 in. O.D. cooling water tube banks along the exterior wall to keep the chamber wall at a low temperature (around 45^{o} F) for minimizing the background noise level in the experiment. The cooling water piping is arranged with dual systems having flow in alternate directions in adjacent tubes to ensure a uniform temperature at the chamber walls. Three 1-1/4 in. diameter ports (one top and two side ports) are provided at the mid-section of the vacuum chamber for the traversing of probes and for diffusion measurements and visual observation.

The plasma camera is positioned at the cold end of the chamber viewing the end cross-section of the plasma column. Descriptions of the plasma camera will be given in the next section. The flange for mounting of the plasma camera onto the chamber is provided with a holder with vacuum seals for the longitudinal Langmuir probe. The longitudinal probe can be rotated far from the column when not in use. Provision is also made to permit the measurement of the temperature of the ionizer by an optical pyrometer.

The magnetic field is in the axial direction pointing toward the plasma generator. It is provided by ten 7 in. (18 cm) I.D. Magnion Plasmaflux solenoid coils which are installed co-axially with the vacuum chamber and are so spaced to ensure uniform magnetic field strength along the length of the test section of the machine. The magnetic field strength can be controlled from 0 to 6000 gauss for sustained operation and to 10,000 gauss in short durations with an accuracy of 0.5% radial variation and 0.6% longitudinal variation in the test section.

At the plasma generator, the tungsten ionizer is maintained at about 2300 ^{o}K by electron bombardment from the hot filament. Free electrons are emitted from the hot ionizer plate by thermionic emission. The potassium neutrals are sprayed on the hot plate from the atomic beam oven. The flow of neutrals depends on the temperature of the oven. It is designated as the atomic beam mode of operation in contrast with the vapor pressure mode, with which excess potassium metal is introduced into the vacuum chamber and the amount of neutrals is controlled by the vapor pressure corresponding to the temperature of the chamber walls. Since the work function of tungsten (4.52 volts) is higher than the ionization potential of potassium (4.31 volts), the potassium neutrals sprayed onto the hot ionizer are ionized, hence producing plasma. The atomic beam oven is heated by a 0.009 in. diameter tungsten wire filament with variable current supply for proper neutral flux.

The ionizer is a circular tungsten plate of 1 in. (2.54 cm) diameter by 1/4 in. (0.64 cm) thick biased positive 1.8 to 2.0 kilo volts relative to the filament. The large thickness is necessary for uniform temperature distribution on the plate.

The filament is made of 0.012 in. diameter tungsten wire wound on ceramic pins in a boron nitride holder. The emission characteristic is in the space-charge limited regime following the Langmuir-Child Three-half law in the range of operation. This has the advantage that in the space-charge limited regime the temperature is a linear function of the energy input to the filament. Two concentric tentalum sleeve rings of 1-1/2 in. diameter and 2 in. diameter provide lateral shields of the filament against stray electrons.

Electrical connections for the plasma generator and the cooling water supply for the atomic beam oven are made through the stainless steel mounting flange for the plasma generator.

A tantalum aperture limiter is placed parallel to and at a distance of 3/16 in. from the ionizer. This aperture limiter, while it governs the size and shape of the plasma column, prevents stray electrons emitted by the filament from getting into the plasma column. Since the plasma column is well defined by the aperture limiter, which has lower values of work function and temperature than those of the ionizer, steep potential and density gradients exist at the edge of the column. This large potential gradient accounts for the radial electric field as discussed in Section 2.1.1. The density gradient is responsible for the universal instabilities which are

always present in the plasma produced in a Q-machine.

The plasma generator and its components are shown in Figs. 2.5 and 2.6.

While the most part of the experiment has been carried out with a plasma column of 3/4 in. (1.9 cm) diameter by 18 in. (46 cm) long, other column sizes are easily accommodated by adapting the desired size and shape of the aperture limiter.

2.2 High Speed Plasma Camera

The visualization of plasma motion is achieved by the use of a specially designed high speed plasma camera. It consists of a scintillator assembly and a Dynafax high speed framing camera with the necessary optical systems. The scintillator assembly was designed and built at The City College Magnetohydrodynamic Laboratory originally for single-frame picture operations[33]. Adaptions for high speed framing photography was done by modifications of the optics and high voltage power supply system.

A schematic diagram of the scintillator assembly is given in Fig. 2.7. The scintillator assembly is installed coaxially inside the vacuum chamber. O-ring seals are provided at the mounting flange and other instrumental connections. The assembly is constructed of non-magnetic materials, mainly copper and brass, and is chemically treated to give non-reflective surfaces. The plasma column terminates at a stainless steel grid screen, which is 50 percent transmissive with 1 mm grids. The

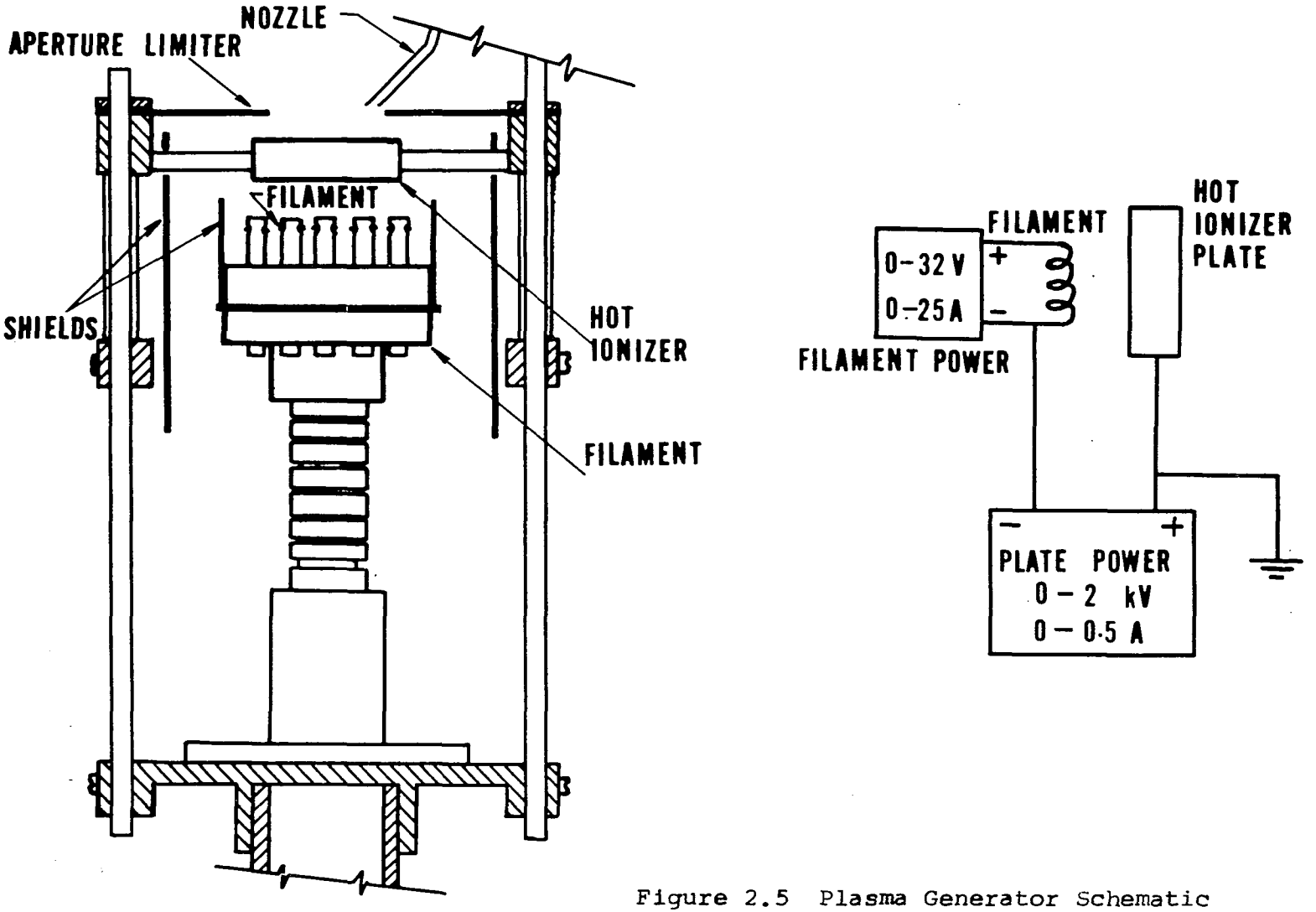

Figure 2.5 Plasma Generator Schematic

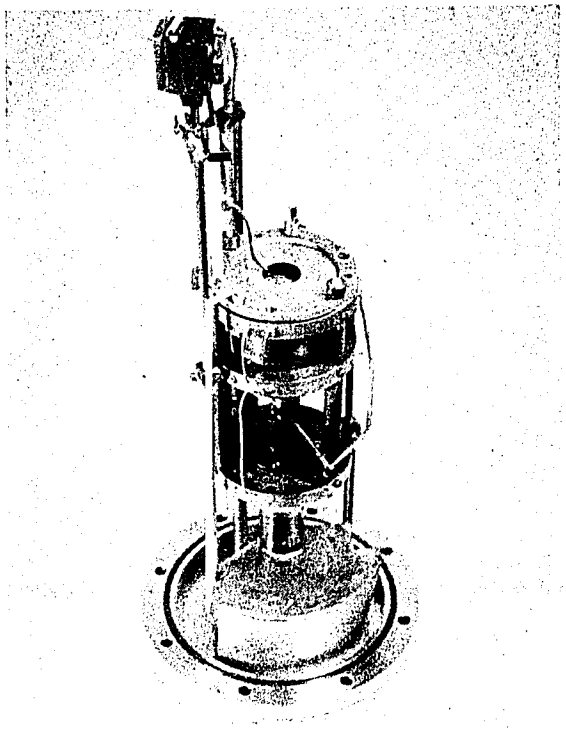

(a) Plasma Generator Viewed from above

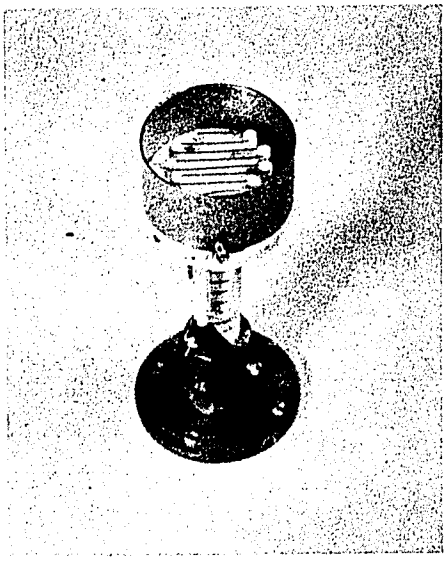

(b) Filament Holder

Figure 2.6 Plasma Generator and Filament Holder

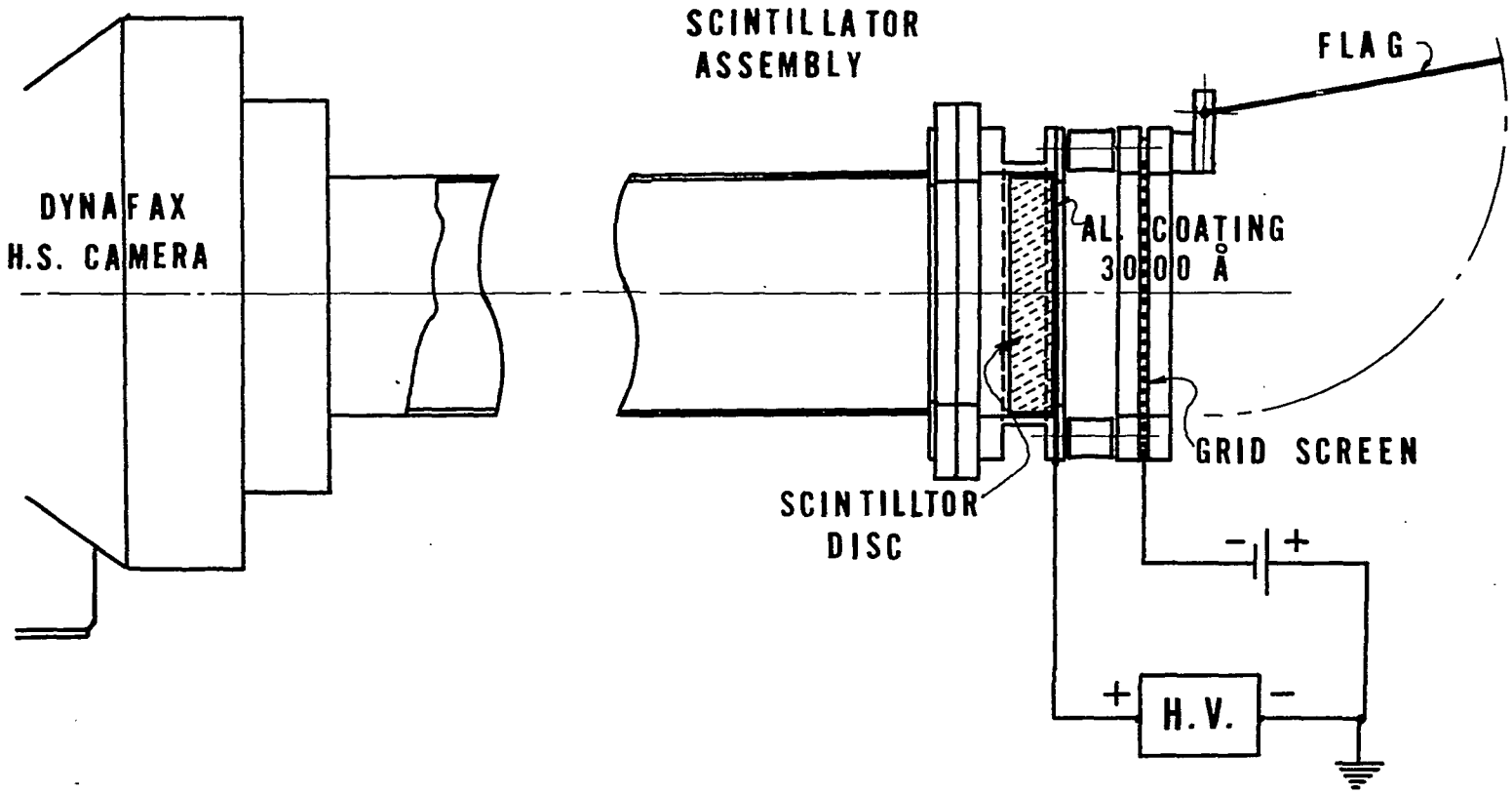

Figure 2.7 High Speed Plasma Camera Scintillator Assembly

scintillator disc, 3/4 in. from the grid screen, is 2-3/4 in. in diameter by 1/4 in. thick glass disc coated with type P11 phosphor, on which an aluminum coating of 3000 Angstrom thick is overlaid. The aluminum coating has dual purposes. It serves as a shield to cut off the light and ultraviolet radiation from the ionizer which can also cause scintillation, and as an electrode on which a positive high potential is applied. A movable plate, the "flag", may be swung down to isolate the scintillator assembly from the plasma column when the plasma camera is not in use.

The high speed camera is a Beckman-Whittley Dynafax Model 326.3 camera. It is of the rotating mirror and rotating drum type, constant speed, continuous writing framing camera. The images are of 16 mm size (0.300×0.410 in.) deposited alternatively in two rows on a 33-7/8 in. long 35 mm film strip. The maximum number of frames is 224. The framing speed is adjustable from 3000 to 25,600 pps (picture per second). Three interchangeable sets of aperture stops furnish a choice of shuttering speed ranging from 1.2 to 5 micro-seconds at the maximum framing speed. The frame separation (the time between two consecutive frames) is 50 micro-seconds at the maximum framing speed. Both the shuttering speed and the frame separation are linear functions of the framing speed.

The Dynafax camera is shown in Fig. 2.1 mounted on the Q-machine. The scintillator assembly is enclosed in the vacuum system and hence is not visible in the photograph.

2.3 The Langmuir Probes

A Langmuir probe is basically a small insulated metallic wire, an electrode, inserted into the plasma. The probe is attached to a power supply biased at various voltages positive or negative relative to the plasma. The current collected by the probe then provides information about the plasma. Under a wide range of conditions, provided the magnetic field is not very strong, the disturbance caused by the physical insertion of the probe in the plasma is localized, hence the presence of the probe does not affect the quantities measured.

2.3.1 The Construction of Langmuir Probes

The construction of the Langmuir probes used in this experiment is shown in Fig. 2.8. It consists of a 0.008 in. (0.203 mm) diameter tungsten wire enclosed in a 0.025 in. O.D. high density and high purity alumina tube. A 0.001 in. thick copper foil strip spirally wrapped around the alumina tube provides a shield for the probe to eliminate the spurous noises in detecting oscillations. The tungsten wire together with the inner alumina insulation and the copper shield is enclosed in an outer alumina tube of 0.057 in. O.D. The exposed tip of the tungsten wire is kept short (1 mm) for use in high magnetic fields. The inner insulating tube is recessed 0.5 mm to prevent short circuit between the tungsten wire and the copper shield which may develop as a result of conductive coating accumulated on the part exposed to plasma. If the inner tube is

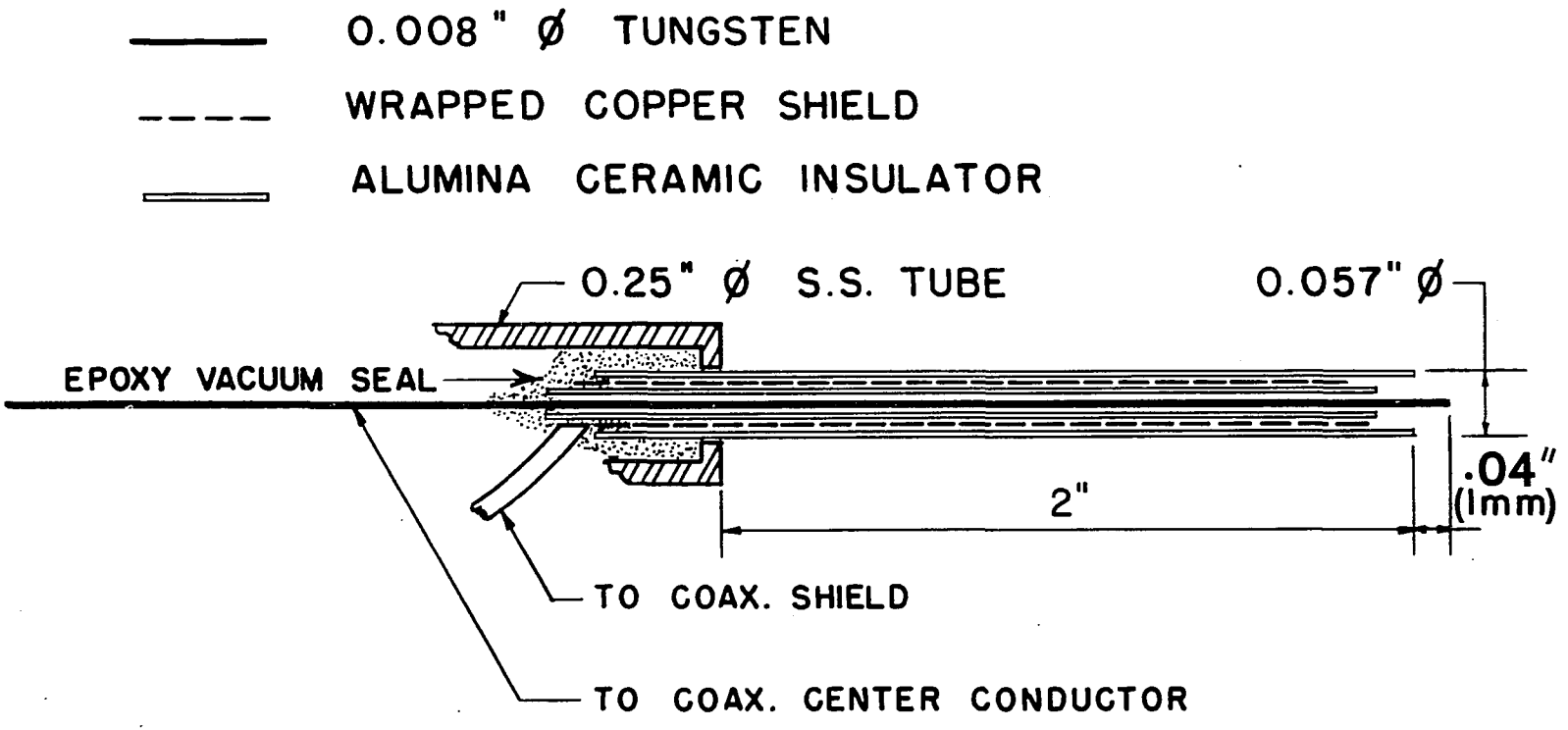

Figure 2-8 Construction of Langmuir Probe

set back too far with respect to the shield, arc may form between the tungsten wire and the shield because of plasma diffused into the space between them.

2.3.2 Types of Langmuir Probes Used

Four different types of Langmuir probes were used in the experiment. The probe tips are all of the same construction as described at the beginning of this section. The differences lie in the mounting of the probes, each suited for its particular applications.

Holders with vacuum seals are provided for the probes for mounting onto the vacuum chamber. The linear (radial) probe can be positioned at any of the three ports at the midsection of the chamber with the probe traversing radially with respect to the plasma column. The two-dimensional probe can also be mounted at one of the three ports. It can be traversed radially and rotated to a desired (r, θ) position. Both the radial and two-dimensional probes can be withdrawn into the holder with the probe clear of the chamber wall.

The probes are positioned by wall aligned traversing mechanisms with screw feeds. Linear potentiometers are provided on the traversing mechanisms for accurate positioning and for driving the x-y recorder.

The Langmuir probes used in this experiment are shown in Fig. 2.9.

i) Linear (radial) probe: This is the basic probe located at any of the three ports to measure the plasma radial density profile (by

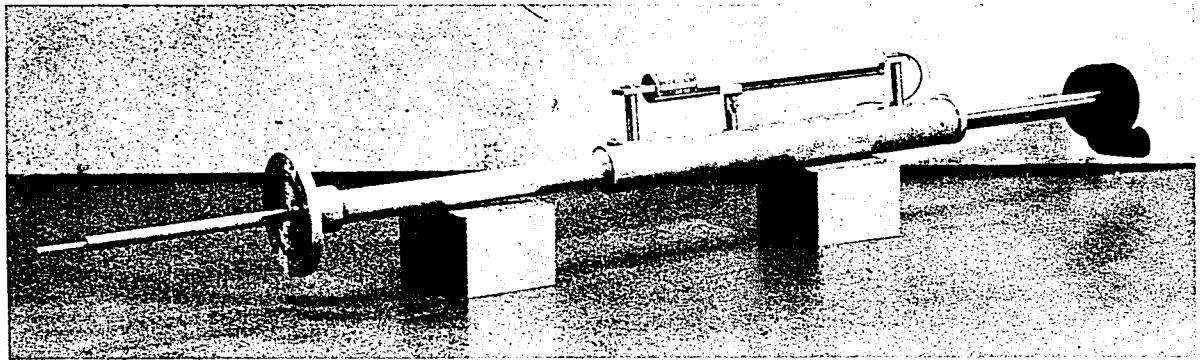

Radial Probe

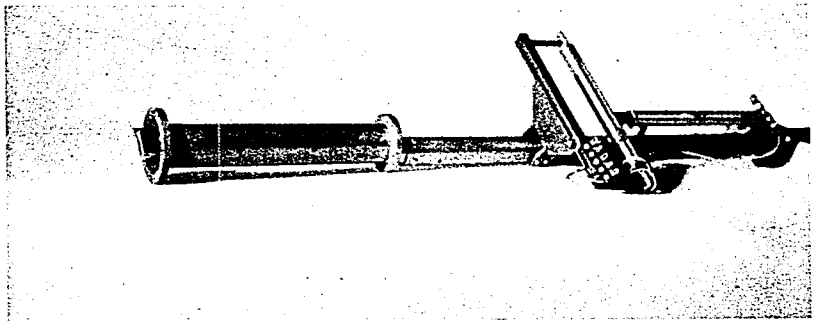

Two-dimensional (r,θ)
Probe

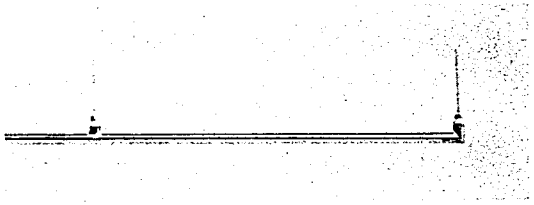

Double Longitudinal Probe

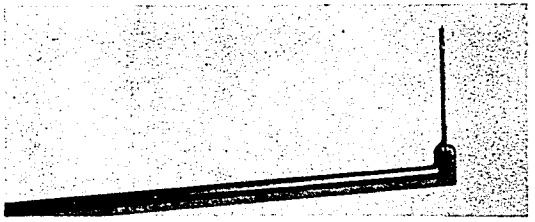

Single Longitudinal Probe

Figure 2.9 Langmuir Probes

measuring the saturation ion current), the floating potential curve, the probe characteristic, RMS value of density fluctuations and used as triggering probe for mode number measurements.

ii) Two-dimensional (r and θ) probe: When used in conjunction with the radial probe, the two-dimensional probe is capable to measure the mode number of the azimuthal component of the oscillations. It can also be used to check the symmetry of the density distribution of the plasma column.

iii) Single longitudinal probe: The probe was used to measure the longitudinal density gradient on the axis of the plasma column. When used with the radial probe as a trigger, it can also be used to measure the longitudinal wave number, k_z of the wave. This measurement is, however, difficult to make, as extra care is required in aligning the two probes on the same line of force of the confining magnetic field.

iv) Double longitudinal probe: This probe was used for k_z measurements of the longitudinal component of the wave. Great care has been exercised in the construction of the probe to ensure the accuracy of the dimensions and the alignment of the two probe tips in the vacuum chamber.

2.4 The Transverse Diffusion Collector

The transverse diffusion collector is a device to measure the transverse current flux of the plasma column, giving a direct measurement of the diffusion coefficient. A diagram of the diffusion collector showing its construction and circuit is given in Fig. 2.10. It consists of a set of parallel plates with a central plate sandwiched in between two interconnected outer plates. A gap of 1.5 mm is kept between the plates. The small gap is desirable for minimizing the effect of any longitudinal component of the current flux on the transverse diffusion data. The design of the diffusion collector is similar to that reported by Buchel'nikova et al. It is, however, floated electrically in the chamber in order to eliminate any effect on the potential due to its presence. The relatively small collection area is adapted also with the aim of reducing its influence on the plasma.

The diffusion collector is placed in the vacuum chamber with the plates perpendicular to the axis of the plasma column. While it can be traversed radially to any position, it is kept outside of the plasma column at a distance at least five times the column radius to eliminate possible interference to the motion of the plasma.

The principle of operation of the diffusion collector will be given in Section 3.5.

2.5 Auxiliary Equipment and Instrumentation

(a) Vacuum System

The vacuum chamber is maintained at a low residue pressure in

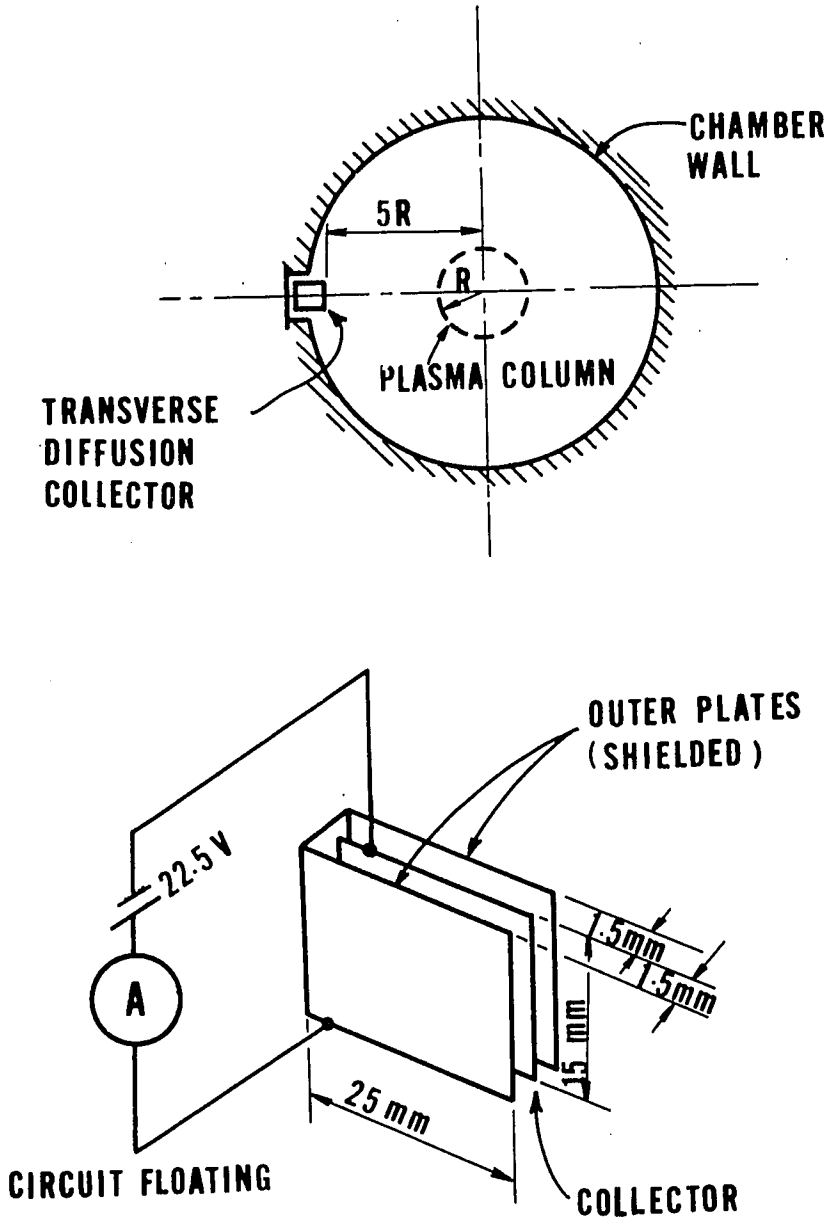

Figure 2.10 Transverse Diffusion Collector

the order of 10^{-7} to 10^{-8} torr by a vacuum pumping system consisting of a mechanical fore pump and a diffusion pump in series. The mechanical pump, or roughing pump is a two-stage Welch Duo-Seal vacuum pumb of 10 cu.ft. per minute at 0.1 microns capacity. The diffusion pump is a CVC (Consolidated Vacuum Corp.) 4 inch ultra-high vacuum pump with a water cooled chevron-ring baffle head to prevent oil vapor from the pumps entering into the vacuum chamber. The residue pressure in the vacuum chamber is monitored by a Veeco RG-30 Ionization Gauge with a combination two-station thermocouple gauge and an inverted nude Bayard-Albert type gauge (range 2×10^{-9} to 1 torr).

(b) Power Supplies

The power for the solenoids which furnish the longitudinal magnetic field is supplied by a Richardson-Allen rectifier with a maximum output of 200 kilowatts at 1000 amperes current.

Power supplies to the plasma generator filament, the ionizer and the potassium oven heating are all direct current regulated for 1% ripple to minimize the mechanical vibrations.

The external longitudinal electric field applied on the scintillator disc is supplied by a custom-built high voltage power supply system with a maximum output of 12 kilovolts at 2 milli amperes current. The high potential can be applied to the scintillator continuous or as a pulse of 1 microsecond duration.

(c) Oscilloscope and Spectrum Analyser

A Tektronix Type 555 Dual-Beam oscilloscope with Type 1A7 high-gain differential preamplifiers is used to monitor the ion current oscillations in the study of instabilities. The oscilloscope is coupled with a Tektronix Spectrum Analyser (Type 531A oscilloscope with Type 1L5 plug-in unit) to measure the plasma oscillations in the frequency domain giving instant display of the wave spectrum.

A Tektronix Type C-12 oscilloscope camera with Polaroid film back is provided to record the oscilloscope cathode ray tube and the spectrum analyser displays.

(d) Gaussmeter

The longitudinal magnetic field is measured by a Bell Gaussmeter, a precision magnetic flux measuring instrument using a Hall effect magnetic probe. The probe is of the axial type with high linearity and is temperature compensated for accurate measurement.

(e) Optical Pyrometer

A Leeds and Northrup optical pyrometer is used to measure the temperature of the hot ionizer. The pyrometer is of the disappearing filament type with null balance, lamp-current measuring circuit. It has three operating ranges to suit the application, each with $\pm$ 0.5% accuracy.

(f) X-Y Recorder

When measuring the Langmuir probe current and probe voltage by a electrometer, the outputs of the meter is fed to a Moseley 136A two-pen

X, Y_1, Y_2 recorder. With the chart recorder in use, the probe characteristic, the plasma density (saturation ion current) profile and the floating potential curves can be plotted instantly during the experiment.

(g) Electrometers

Keithley 601 and 601B Electrometers are used for measurements of plasma floating voltage, probe saturation ion current and the diffusion collector ion or electron current.

2.6 Summary

In this chapter a general description of the experimental apparatus and the diagnostic tools, i.e. the Langmuir probes, the high speed plasma camera and the diffusion collector has been given.

CHAPTER 3

DIAGNOSTIC TECHNIQUES

Langmuir probes have been used to determine the condition of the plasma, its density, electric potentials and electron temperature, and to detect the existence of instabilities as well as the properties of such instabilities. A high speed photographic technique using the plasma camera has been developed and applied to the experiment. This photographic technique provides measurements of both spatial and temporal distributions of the plasma, hence it greatly facilitates the study of the characters and time evolution of the plasma instabilities, furnishing more complete information of the observed phenomena. Diffusion of plasma across the magnetic field is related closely to the instability present in the plasma and is important. It was determined by direct measurement of the transverse plasma flux using the transverse diffusion collector. In the following sections the theory, operating principle and procedures of the major diagnostic techniques used in the experiment are presented.

3.1 General Discussion on Theory of Langmuir Probes

While experimentally the Langmuir probes are simple in construction and convenient to use, the theory of probes is rather complicated and difficult even with the simple case of cylindrical or spherical probes in a collisionless plasma without magnetic field. The difficulty arises mainly from the fact that probes are boundaries in the plasma which they measure

and near the boundaries the equations governing the motion of the plasma change their characters. The condition of quasi-neutrality which is fulfilled in the body of plasma is not valid near the boundaries. The exact knowledge of the density, potentials and other plasma parameters at the boundaries is lacking. Chen[34] gives a rather complete review on the theory of probes, in which important analyses by Langmuir[35], Bohm[36], Lam[37] and others are discussed.

Since the probe is biased at a potential different to that of the surrounding plasma, a thin layer, or sheath can form. Inside the sheath ion and electron densities can differ, hence large electric fields will be sustained. If the sheath is assumed very thin, it can be approximated that almost all the potential change occurs inside the sheath. At the sheath edge the potential is practically the same as that in the body of the plasma, and the condition of quasi-neutrality holds. All particles that enter the sheath are collected by the probe. Simple relation between the current collected at the probe and the plasma density and temperatures can be established if the velocity distribution of the repelled species is assumed to be Maxwellian.

Depending on the bias voltage of the probe with respect to the plasma, the thickness of the sheath may not be small. Then the thin sheath approximation no longer holds and the finite size of the sheath has to be considered. Particles that enter the sheath now may or may not be collected depending on the energy and angular momentum of the individual

particles. Therefore, the orbital motions of the particles are important.

The imposing of the sheath surrounding the probe is, however, rather artificial. As it can be demonstrated the potential at the sheath edge differs from that of the plasma far away, i.e. the potential "penetrates" the sheath. This is important if the colder species, usually ions, is collected at the probe.

The effects of collision are to be considered if the plasma is dense, i.e. the mean free path, λ is not much greater than the radius of the probe, r_p, or the Debye length, λ_D. In the collisional case the probe current is affected by the potential profile in the sheath region. The velocity distribution at the sheath edge will be different to that of the undisturbed plasma.

In the presence of magnetic field the Larmor radius effects in the plasma are important and the Larmor radius, r_L replaces λ as the governing length parameter. Due to the difference in the magnitudes of the ion and electron Larmor radii the effects of the magnetic field on the collections of ion and electron current are different. Anisotropy exists in the plasma motion as electrons and ions are hindered by the magnetic field in the transverse direction but not in the direction along the field lines. If the magnetic field is very strong, thermal equilibrium may not be assumed isotropic and all probes resemble a plane probe, as the collection of current is significant only in the direction along the magnetic field. The current collected depends, therefore, on the production of plasma in the entire region, rather than on the local properties.

Despite all the difficulties and shortcomings of the theory of probes in general, simple but adequate theory exists under the conditions of this experiment, and the Langmuir probe is a valuable diagnostic tool with which reliable information of the plasma can be obtained. In the following sections the construction and theories of the Langmuir probe applied to the present experiment will be presented, starting with the cylindrical probe in a collisionless plasma without magnetic field. The determination of plasma density, temperature and potentials of the plasma, the effects of the size of the sheath at the probe, the orbital motion of electrons and ions in the sheath, and effects of the magnetic field are then discussed.

3.2 Probe Theory of Collisionless Plasma without Magnetic Field

Most work on the theory of Langmuir probes has been carried out for the simple case where collisions and magnetic fields are negligible. With the concept of the sheath at the probe and the assumptions of known potential profile in the sheath region and quasi-neutrality at the sheath edge, local measurements made by the probe can adequately yield information of the plasma as a whole.

(a) The Probe Characteristic

The plasma density, electron temperature and electric potentials can be obtained from the plot of the probe current against the probe voltage, i.e. the probe characteristic. A typical probe characteristic in

a collisionless plasma in the absence of the magnetic field is given in Fig. 3.1. The probe characteristic is obtained by measuring the probe current while changing the bias voltage on the probe. Here the electron current to the probe is plotted against the probe voltage with respect to an arbitrary reference point. At the point V_s, the space potential, the probe is at the same potential as the plasma. There is no electric field at the probe, and electrons and ions migrate to the probe only because of their thermal velocities. Current collected is predominantly electrons because of their high mobility. If the probe voltage is biased positive relative to the plasma, electrons are accelerated to the probe and ions are repelled. Near the probe surface there is an excess of negative charge. This layer of charge, the sheath, is usually very thin, of the order of the Debye length λ_D. Outside of the sheath there is very little electric field and the plasma is not disturbed. The electron current portion of the curve is relatively flat, since the area of the sheath has only a slight increase when the bias voltage is increased. The portion A of the curve is called the region of saturation electron current.

When the probe is made negative relative to the plasma voltage, electrons are repelled and ions are accelerated to the probe. In region B the electron current falls as the probe voltage is decreased, and this region is called the transition region of the characteristic. At the point, V_f, the floating potential, the probe draws no net current. An insulated probe tip inserted into a plasma assumes this potential.

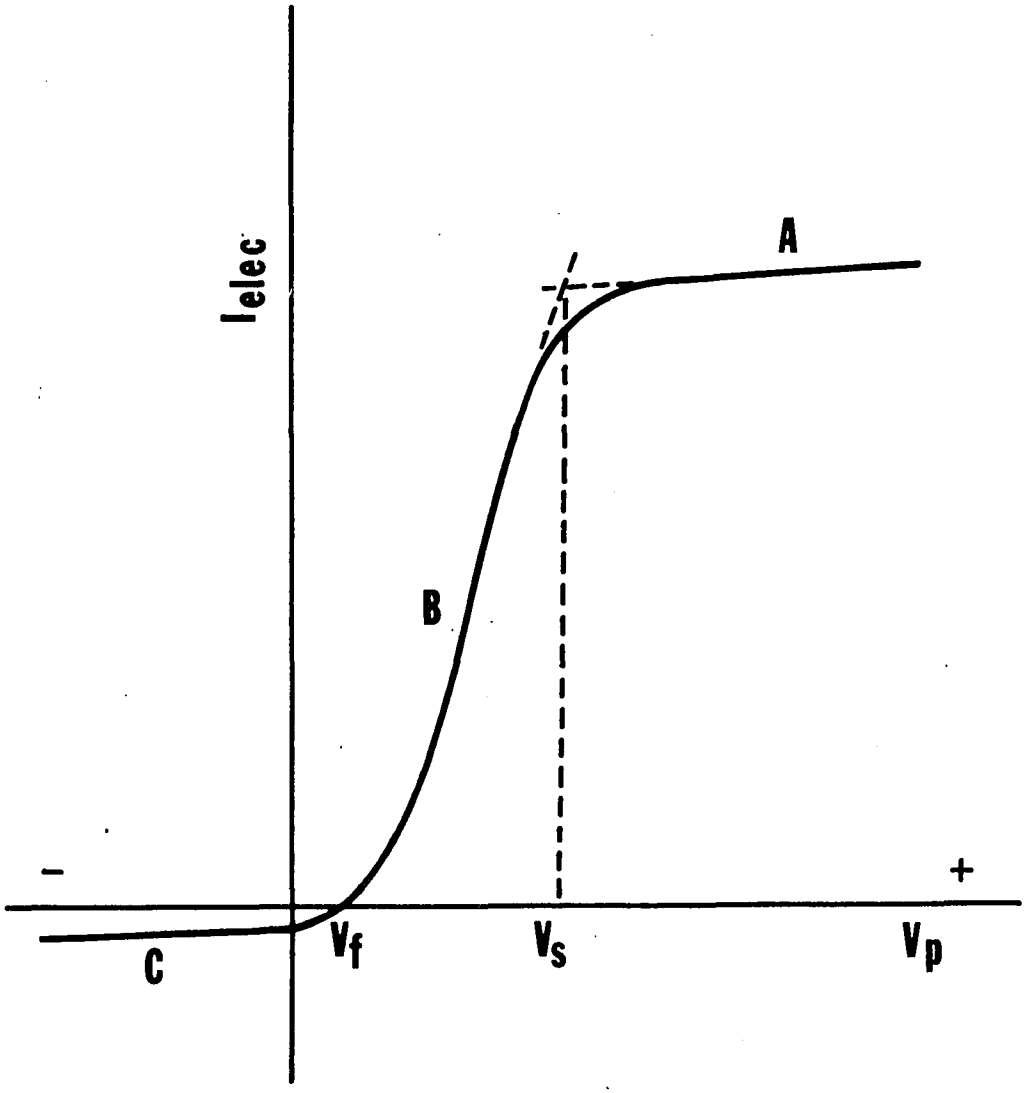

Figure 3.1 Typical Probe Current-Voltage Characteristic

At high negative voltage at the probe, all electrons are repelled and ion sheath forms and the probe draws saturation ion current. This is the region of saturation ion current, corresponding to part C of the characteristic.

(b) The Determination of Plasma Parameters

The potential of the plasma, or the space potential, V_s and the floating potential, V_f can be found readily from the probe characteristic. V_f is located at the point I = 0 on the current-voltage or C-V characteristic curve, where no net current is drawn to the probe. V_s is found at the intersection of the tangent lines of regions A and B of the C-V curve, where the electrons experience a change from an attractive to a repelling electric field. It will be shown later that the location of V_s is not quite certain if a strong magnetic field is present.

The electron temperature, T_e is computed from the transition region, or part B of the probe characteristic. In this region the probe is biased negatively to the plasma. The bias voltage is moderate and the probe, then, collects electrons which move to the probe against a repelling field. With the electron distribution in thermal equilibrium part B of the probe characteristic is exponential, i.e.

$$I \sim \exp\left(-\frac{eV}{kT_e}\right)$$

If one plots ℓn I against V, the slope gives the value of e/kT_e, from which the electron temperature kT_e can be computed.

(c) The Thin Sheath Case

If the sheath of radius s is thin and the mean free path is large as compared to the probe radius, i.e., $(s - r_p) \ll r_p$ and $\lambda \gg r_p$, the potential variation is limited to within the sheath and all particles that enter the sheath are collected. The collection of current is space-charge limited, related to the applied voltage at the probe with respect to the plasma. With the probe at a positive potential and assumed perfectly absorbing for electrons and perfectly reflecting for ions, the velocity distribution of the electrons near the sheath edge is essentially Maxwellian. This is because of the relatively high mobility of electrons.

In general the current collected by the probe is

$$I = A_s \, j_r \tag{3.1}$$

where I is the current collection, A_s is the area of the sheath, and j_r is the random current density crossing a unit area in one direction.

For electrons with Maxwellian distribution,

$$j_r = \frac{1}{4} n \bar{v}_e = \frac{n}{2} \sqrt{\frac{2 k T_e}{\pi m_e}} \tag{3.2}$$

where $\bar{v}_e$ is the average velocity of electrons and $\bar{v}_e = \frac{2}{\sqrt{\pi}} \sqrt{\frac{2 k T_e}{m_e}}$. The factor 1/4 comes from a product of two 1/2's. The first 1/2 is because at the sheath only one-half of the density is toward the probe, and the other is the average of the direction cosine over a hemisphere enclosing the probe.

Hence the electron current is given by

$$I_e = \frac{A_s}{2} n \sqrt{\frac{2kT_e}{\pi m_e}} \tag{3.3}$$

If the area of the sheath and the electron temperature are known, the plasma density, n can be computed with the measured saturation electron current. As a first approximation, for a thin sheath, A_s can be replaced by the surface area of the probe, A_p. It then gives

$$I_e = \frac{A_p}{2} n \sqrt{\frac{2kT_e}{\pi m_e}} \tag{3.4}$$

Equation (3.4) is not valid for the collection of ion current as the assumption of Maxwellian distribution at the sheath edge does not hold due to their mobility.

For more accurate calculations, the sheath area, A_s has to be used. The result of an analysis by Langmuir and Blodgett is cited here. Based upon calculations of the space-charge limited emission from the sheath edge to the probe surface, the electron current to the probe surface is, in the cylindrical geometry,

$$j = \frac{1}{9\pi} \left(\frac{2}{em}\right)^{\frac{1}{2}} \frac{|V_p - V_s|}{r_p^2 \beta_1^2} \left(1 + \frac{2.66}{\sqrt{\frac{e(V_p - V_s)}{kT_e}}}\right) \tag{3.5}$$

where V_p and V_s are the potentials at the probe and at the sheath respectively, and

$$\beta_1 = \frac{s}{r_p} - 0.4 \frac{s^2}{r_p^2} + \ldots\ldots$$

At the sheath edge assume that $V_s = 0$. Then

$$j = j_r$$

and the radius of the sheath, s can be calculated.

(d) The Thick Sheath Case

If the sheath at the probe is thick, i.e. $s > r_p$, not all the particles of the plasma which enter the sheath reach the probe, depending on the energy and angular momentum of individual particles. Hence the orbital motions are to be considered. In the analysis of the thick sheath case the probe current is assumed independent of the distribution of potential in the sheath, V(r), as only the final values of the energy and angular momentum are of concern.

With the aid of Fig. 3.2 consider the orbit of a particle approaching the probe. From the conservation of energy and angular momentum, we have

$$\tfrac{1}{2} m v_o^2 = \tfrac{1}{2} m v_p^2 + e V_p \qquad (3.6)$$

$$v_o d = v_p r_p \qquad (3.7)$$

Where the subscript p and o refer to quantities at the closest approach with $r_c = r_p$ and at the impact parameter d respectively. From Eq.(3.6)

$$v_p = \sqrt{v_o^2 - \frac{2}{m} e V_p}$$

Substituting into Eq. (3.7), we have

$$d = r_p \sqrt{1 - \frac{e V_p}{\tfrac{1}{2} m v_o^2}}$$

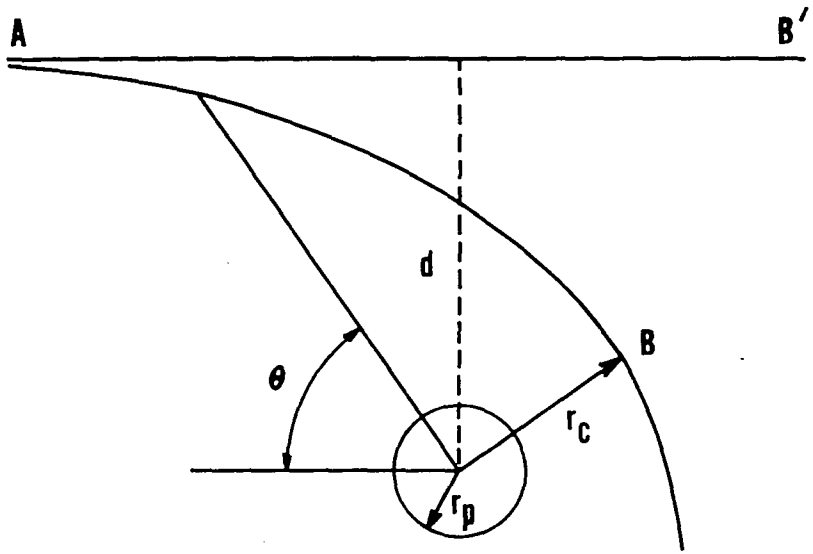

AB': direction of motion of the particle before it is deviated

d : collision or impact parameter

ABC : path of the particle under an attractive field of the probe

r_c : distance of closest approach

Figure 3.2 Orbit of a Particle Approaching the Probe

Noting that at r = d

$$\tfrac{1}{2} m v_o^2 = - e V_s$$

The minus sign is due to the attractive force field at the probe.

Substitute for v_o, we have

$$d = r_p \sqrt{1 + \frac{V_p}{V_s}} \tag{3.8}$$

All particles with an approach smaller than d will reach the probe and be collected. Therefore, d is the effective collecting radius. Using d in place of r_p for the computation of the collecting area in Eq. (3.3), for cylindrical probes the probe current is given by

$$I_e = r_p \, \ell n \sqrt{\frac{2\pi k T_e}{m_e}} \sqrt{1 + \frac{V_p}{V_s}} \tag{3.9}$$

where ℓ is the length of the probe.

It should be noted that in the analysis the distribution of energy at the sheath edge is not considered and the particles are assumed to have the same energy, i.e. isotropic and mono-energetic.

Taking into consideration the velocity distribution at the sheath edge, Langmuir and Mott-Smith, with the assumption of Maxwellian distribution for the electrons, give a somewhat different result

$$I_e = A_p \, j_r \frac{2}{\sqrt{\pi}} \sqrt{1 - \frac{e V_p}{k T_e}}$$

$$= r_p \, \ell n \sqrt{\frac{2\pi k T_e}{m_e}} \frac{2}{\sqrt{\pi}} \sqrt{1 - \frac{e V_p}{k T_e}} \tag{3.10}$$

(e) Dependence of Electron Temperature in Ion Collection

With the probe at a highly negative potential to collect ions, electrons are repelled by the probe and they remain in thermal equilibrium. Since the electrons are mobile and have kinetic energy, they can enter the sheath a short distance against the repelling electric fields, or alternatively speaking, they permit some residue potential penetrating the plasma.

This residue potential causes an increase of ion current collection at the probe. At the sheath with the residue potential V, the average velocity of the ions is

$$\bar{v}_i = \sqrt{\frac{2}{m_i}} \sqrt{\frac{kT_i}{3} + eV}$$

The factor of 1/3 is due to random thermal motions; approximately one-third of their thermal energy will be directed normal to the sheath.

At the sheath, $n_i \cong n_e$ and $n_e = n_o \exp\left(-\frac{eV}{kT_e}\right)$

Thus

$$j_i = n_i \bar{v}_i = n_o \exp\left(-\frac{eV}{kT_e}\right) \sqrt{\frac{2}{m_i}} \sqrt{\frac{kT_i}{3} + eV}$$

For maximum j_i, differentiate j_i with respect to V and set $\frac{dj_i}{dV} = 0$

$$\frac{dj_i}{dV} = n_o \sqrt{\frac{2}{m_i}} \left[-\frac{e}{kT_e} \exp\left(-\frac{eV}{kT_e}\right) \sqrt{\frac{kT_i}{3} + eV} \right.$$

$$\left. + \exp\left(-\frac{eV}{kT_e}\right) \frac{e}{2} \frac{1}{\sqrt{\frac{kT_i}{3} + eV}} \right] = 0$$

Hence

$$(j_i)_{max} = n_o \sqrt{\frac{kT_e}{m_i}} \exp\left(-\frac{1}{2} + \frac{T_i}{3T_e}\right) \qquad (3.11)$$

If $kT_e > kT_i$, $(j_i)_{max}$ occurs at $V = \frac{1}{2}\frac{kT_e}{e}$.

Bohm et al have demonstrated that the ion sheath is stable only when $V \geq \frac{kT_e}{2e}$ and ions must have an energy greater than $\frac{1}{2}kT_e$ at the sheath edge in order to penetrate it. With this rather crude analysis the ion current is given as

$$I_i = 0.43 A_p n \sqrt{\frac{2kT_e}{m_i}}, \qquad \left(\frac{kT_i}{kT_e} = 0.01\right)$$

$$I_i = 0.50 A_p n \sqrt{\frac{2kT_e}{m_i}}, \qquad \left(\frac{kT_i}{kT_e} = 0.5\right)$$

In a more accurate analysis taking into account the potential shape in the sheath, they give

$$I_i = 0.40 A_p n \sqrt{\frac{2kT_e}{m_i}} \qquad \left(\frac{kT_i}{kT_e} = 0.01\right) \quad (3.12)$$

$$I_i = 0.38 A_p n \sqrt{\frac{2kT_e}{m_i}} \qquad \left(\frac{kT_i}{kT_e} = 0.5\right) \quad (3.13)$$

It has been shown that the ion current is insensitive to the ion temperature and the collection of ion current depends on the electron temperature rather than the ion temperature.

Compare Eq. (3.13) with Eq. (3.4), the ratio of electron current to ion current is in the order of $\sqrt{\frac{m_i}{m_e}}$. For potassium it is approximately 100.

(f) Lam's Theory of Ion Current Collection

Lam presents a theoretical analysis of the Langmuir probe in a quiescent, collisionless plasma considering the practical case of large probe size to Debye length ratio. The electric potential distribution in the

sheath surrounding the probe is taken into account.

The plasma density n can be determined from a single measurement of the ion saturation current from the equations

$$- \frac{V_p}{(e I_i r_p)^{2/3}} = \left(\frac{2 m_i}{e}\right)^{1/3} \tau^{2/3} G(\tau) \tag{3.14}$$

$$\tau = \frac{I_i}{I_B} \tag{3.15}$$

$$I_B \cong 1.9 r_p n \sqrt{\frac{2k T_e}{m_i}} \tag{3.16}$$

where I_B is essentially the probe current predicted by Bohm. The relation between $\tau^{2/3} G(\tau)$ and τ is given in Fig. 3.3 using Lam's numerical results. With the measured ion saturation current, I_i, $\tau^{2/3} G(\tau)$ can be calculated from Eq. (3.14) and the corresponding value of τ is found from Fig. 3.3. With the known τ, I_B and then the plasma density, n can be obtained from Eqs. (3.15) and (3.16). The plasma density calculated by Lam's theory is about 10 to 20 percent higher than that by Bohm's theory for the range of the present experiment.

3.3 Probe Theory in the Presence of Magnetic Fields

In the presence of strong magnetic fields the factors affecting the probe characteristic are complex and the theory of Langmuir probes is rather crude and incomplete. However, if the magnetic field is not very strong, such that the ion Larmor radius is still larger than the probe radius, as in the case of the present experiment, the probe theory based upon the

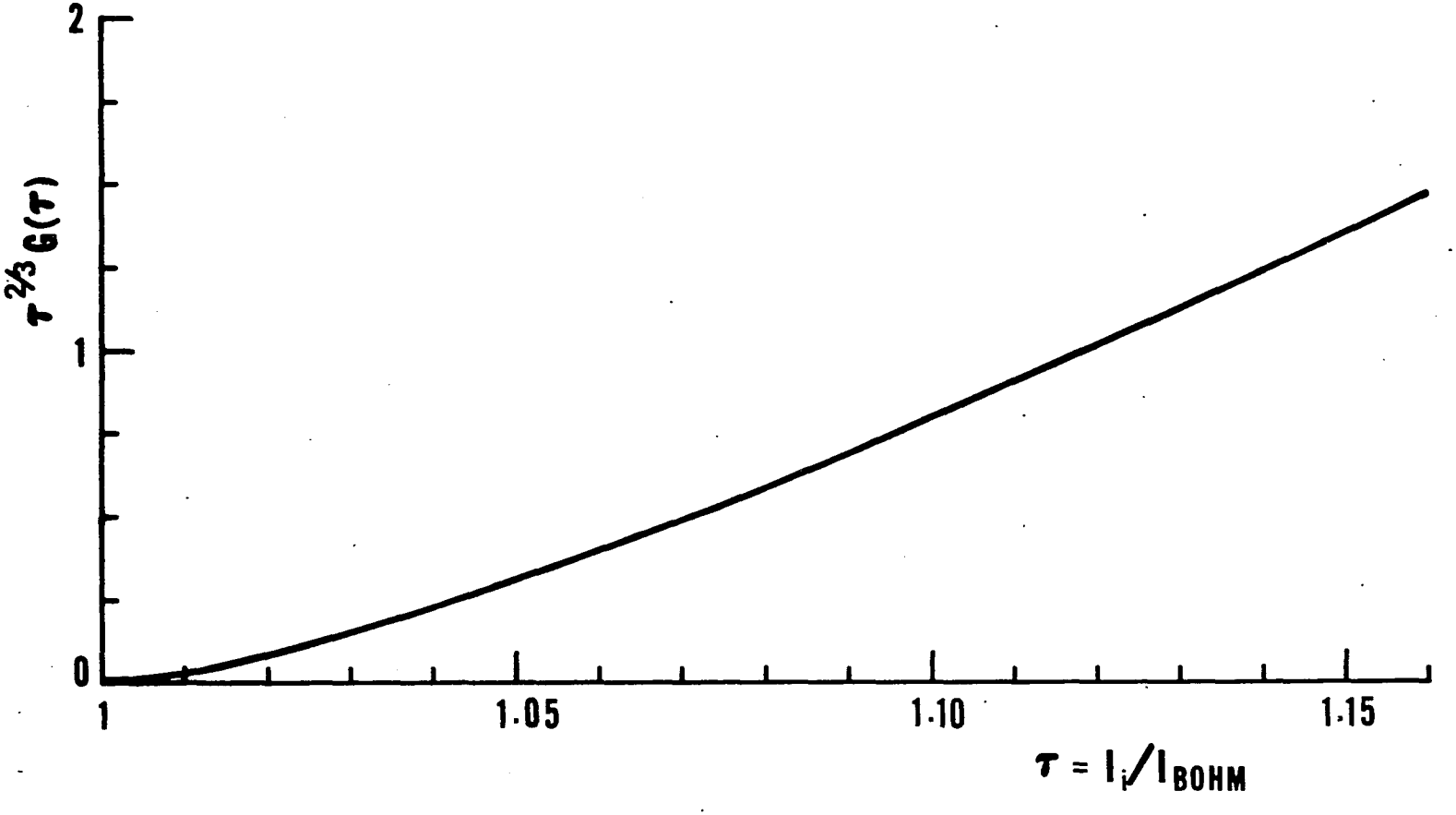

Figure 3.3 Function $\tau^{2/3} G(\tau)$ for Cylindrical Probes

collection of ion current is still adequate.

(a) Effects of the Magnetic Fields

In a magnetic field electrons and ions are constrained to gyrate about the magnetic field lines. Their motions cross the magnetic field lines are limited to the Larmor radii, but not along the field. This introduces anisotropy. The effective mean free path is now reduced to the Larmor radius as electrons or ions can only travel transversely this far without a collision.

Electrons have much smaller Larmor radius than that of ions and the effect of the magnetic field on them is more severe. As the electron Larmor radius is of the order of 10^{-3} cm even in a moderate field of 1000 gauss, it is at least one order of magnitude smaller than the radius of the probe (10^{-2} cm). The usual assumption of $\lambda \gg r_p$ no longer holds and the theory based on the electron current collection cannot be considered collisionless. The theory of electron current collection in a collisionless plasma presented in Section 3.2 is then not valid in the presence of the magnetic field. This can be seen from the marked reduction of electron current collection at the probe and the changes in the probe characteristic.

(b) The Probe Characteristic of Plasma in a Magnetic Field

Figure 3.4 is the probe characteristic obtained at a magnetic field of 800 gauss. When compared with the probe characteristic without magnetic fields (Fig. 3.1), first to be noted is the absence of electron

saturation in Fig. 3.4. The electron current continues to increase with voltage without reaching saturation, due to the increase of the length of electron collection region along the magnetic field with the voltage.

Next to be noted is the reduction of the magnitude of the electron current. The ratio of the electron current to the saturation ion current is now between 10 and 20, as compared to 100 in the case of collisionless plasma without the magnetic field. This reduction in electron current is believed to be due to the lower diffusion rate of electrons from the constraint of motion across the magnetic field.

The third to be noted is the fluctuations in electron current in region A of the probe characteristic. The fluctuations in electron current reflect fluctuations in plasma density at the probe. The mechanism of the fluctuations in the electron current has not been studied except being touched upon by Demetriates and Doughman[38] on their study of Langmuir probe in turbulent plasmas.

The determination of V_s now is somewhat difficult due to the disappearing of the sharp "knee" between part A and part B of the probe characteristic.

(c) Electron Temperature

In the presence of the magnetic field, part B or the transition region of the probe characteristic is exponential only at the lower portion of the curve close to V_f. In this portion the presence of the magnetic field

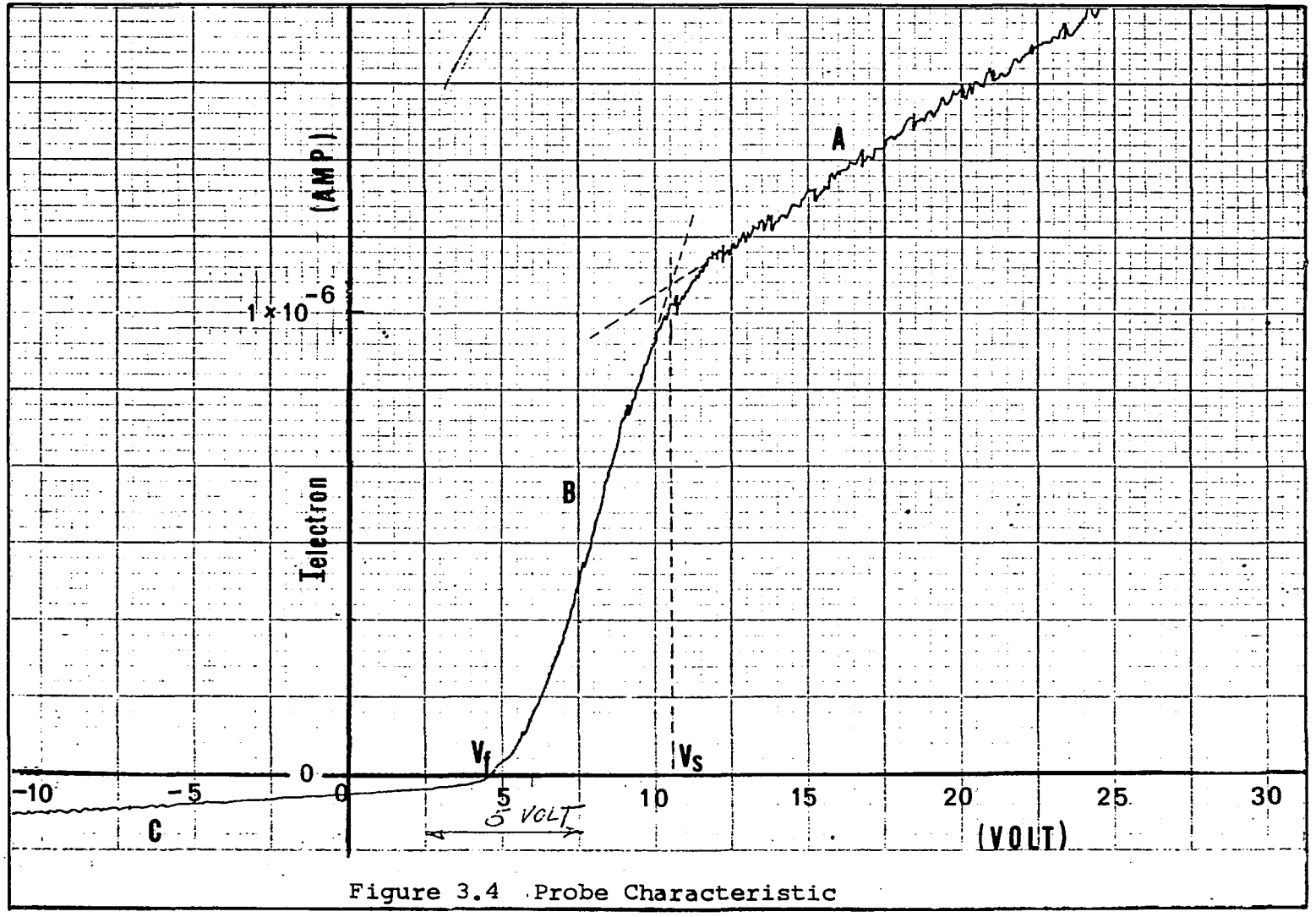

Figure 3.4 Probe Characteristic

does not seem to change the state of equilibrium of the plasma at the sheath edge. In principle the electron temperature can still be determined from the transition region of the probe characteristic. However, the accuracy of the electron temperature computed in this manner is no longer reliable.

(d) Electron Current Collection

The theory of spherical Langmuir probes in a strong magnetic field has been studied analytically by Sanmartin[39]. Electrical potential distribution in the sheath is taken into account and the potential is found not confined to the sheath. Numerical results are given for the current collected at the probe for various magnetic fields relating the electron current to the quantity, $n\sqrt{\frac{kT_e}{m_e}}$. They are valid, however, only for very low positive to negative potentials, thus not good for the saturation electron current collection.

(e) Saturation Ion Current

Under the conditions that the ion Larmor radius is considerably larger than the probe radius and the sheath is small as compared with the probe the effects of magnetic field on the saturation ion current can be neglected. The plasma density then can be computed from the saturation ion current using the probe theory for collisionless plasma without magnetic field as discussed in the preceding sections.

In the recent work of Sanmartin the same conclusion has been reached for a quiescent, fully ionized plasma in a strong magnetic field.

In the present experiment with the magnetic field ranging from 500 to 6,000 gauss, the ion Larmor radius is in the range of 1 to 0.1 cm respectively, while the radius of the probe is approximately 0.01 cm. The thickness of the sheath at the probe is in the order of the Dabye length, or 10^{-3} cm. Therefore, the above requirements are satisfied and the plasma density is determined from the saturation ion current using Bohm's or Lam theory given in Section 3.2 (e) and (f).

Wade[40] has checked the validity of Langmuir probe measurements in the experiment of cesium plasma in a Q-machine over a range of magnetic field from 300 to 1,500 gauss. The plasma density computed from the saturation ion current measured by double probes is compared with the microwave plasma density measurement with an agreement within 30 percent. The electron temperature obtained from the probe measurements show 10 to 20 percent agreement with that obtained by the optical pyrometer.

(f) Measurement of Oscillations

The measurement of plasma oscillations is one of the most important applications of Langmuir probes, since such measurements make full use of the spatial resolution of probes and are not subjected to the errors in absolute calibration of the probe current. However, the speed of response of a probe is important to the phenomena under study.

The electrons, due to their high mobility, react almost instantaneously to a changing field, but the ions move rather slowly in comparison. Since the maximum velocity of the ions is of the order $v_i = (\frac{kT}{m_i})^{\frac{1}{2}}$ and they

must travel a distance of the order of $\lambda_D = (\frac{kT}{4\pi ne^2})^{\frac{1}{2}}$ to form a new sheath, the maximum frequency response of ions would be expected to be of the order of the ion plasma frequency, $\omega_{pi} = \sqrt{\frac{4\pi ne^2}{m_i}}$. The maximum frequency response of electrons is of the order of the electron plasma frequency. The frequency response of Langmuir probes, therefore, is much faster than that required for the experiment of studying the low frequency (5 to 30 kHz) oscillations in the Q-machine.

Ion density oscillations are observed by biasing the probe to collect ion current and let the current pass through a 1 kilo ohm resistor. The AC signals are displayed on the oscilloscope and on the spectrum analyzer.

Basic circuit for probe measurements of current and voltage is shown in Fig. 3.5. For probe current measurement, switch S is in "a" position, connecting the battery. The current is given by meter V_1 and the probe voltage is read by meter V_2. For floating potential measurement switch is in "b" position, isolating the battery. The floating potential is given by meter V_2.

3.4 The High Speed Photographic Technique

The principle of the plasma camera is not dissimilar to that of a cathode ray tube. With the electrons streaming to the grid screen at their thermal velocities, an applied high potential on the aluminum coating of

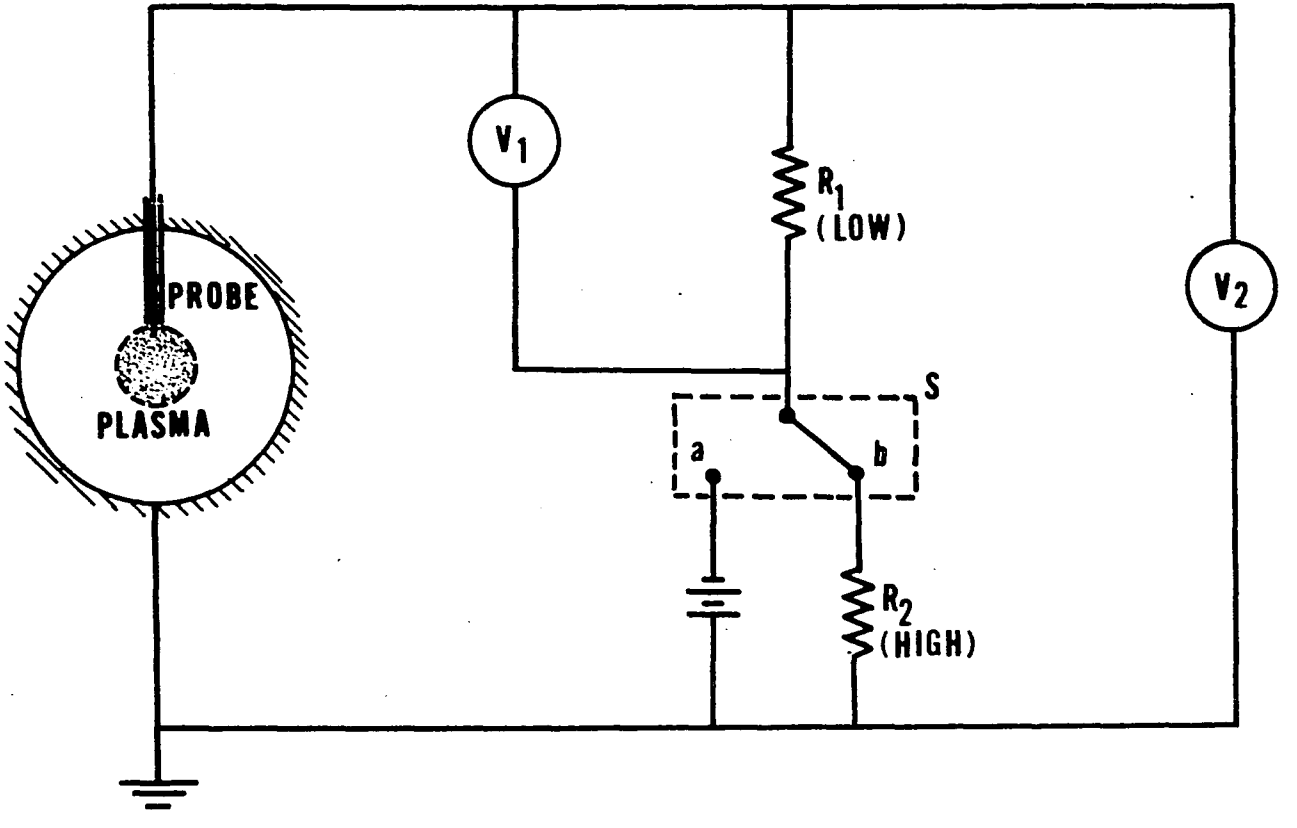

Figure 3.5 Basic Circuit for Probe Measurements

the scintillator accelerates the electrons between the grid screen and the scintillator disc to move toward the disc. When sufficiently high positive potential is applied on the aluminum coating the accelerated electrons will have high enough energy to penetrate the aluminum and strike the phosphor coating causing luminescence which is then photographed by the high speed camera. A minimum potential of 8 kilo volts is necessary for proper scintillation, of which approximately 3 kilo volts is required for penetrating the aluminum coating.

Since the operation of the plasma camera is by acceleration of the electrons in the plasma to strike the scintillator and cause luminescence, the scintillator is exposed to the plasma through the 50% transmissive grid. Owing to the high temperature (2300 ^{o}K) of the plasma, the scintillator has to be protected from excessive heat and radiation from the plasma. The operating procedure, therefore, is such that the scintillator is exposed to the plasma only when the high speed photographs and other data are taken. Normally the flag (the copper plate) is kept down in front of the plasma camera, thus isolating it from the plasma.

At the scintillator, where end recombination of electrons and ions occurs, a thin coating of potassium may develop after the plasma camera has been used for a short period of time. For the purpose of ensuring consistency of the test results, a scintillator, once found with noticeable potassium deposit, is to be replaced.

While high magnitudes of the applied electric potential and current at the scintillator are desirable for scintillation of high intensity, the applied potential is limited to 12 kilo volts and the current to 2 ma for proper operation of the plasma camera. Higher energy applied to the scintillator exceeding the above-stated limits may cause saturation of phosphor-scintillation or damage to the aluminum and phosphor coatings due to the excess heat and radiation from the plasma. The design of the scintillator for proper operation in the experiment is aided by experimentation of various types of phosphors in combination with the aluminum coating of various thickness. This will be discussed further in Section 4.6.

The selection of the Dynafax framing camera is for its applicability to the problem under investigation. The Dynafax high speed camera is particularly suitable for the study of the low frequency helical mode instability of the potassium plasma in a Q-machine for its constancy of framing speed, adequate shuttering speed and frame separation, wide selection of films and simplicity in operation[41]. The linear relationship between the frame separation and the framing speed greatly facilitates the analysis of the photographic data and their correlation to the experimental results obtained by Langmuir probes.

In preliminary investigations of the problem, a single frame plasma camera was also employed using the same scintillator assembly but with a Graflex camera and Polaroid film back. A one-to-one image to object ratio is obtained with a 360 mm focal length lens as shown in Fig. 3.6.

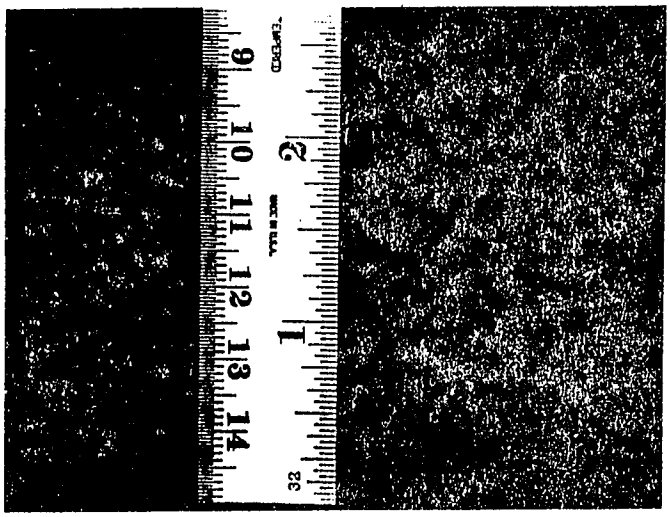

FIGURE 3.6 SINGLE FRAME PLASMA CAMERA PICTURE SHOWING ONE TO ONE IMAGE TO OBJECT RATIO

3.5 Measurements of Diffusion of Plasma Across the Magnetic Field

Diffusion of plasma across the magnetic field was computed from the transverse plasma flux, $j_\perp$ and the radial density gradient, dn/dr according to the relation

$$D = \frac{j_\perp}{dn/dr} \tag{3.17}$$

where D is the transverse diffusion coefficient. The transverse plasma flux was measured directly by the use of the transverse diffusion collector as described in Section 2.4, while the plasma density gradient was determined by the Langmuir probe.

To measure the transverse current flux, a potential is applied between the collector plates. The applied potential is sufficiently high to cause a complete charge separation of the plasma entering the space between the plates due to the diffusive motion. This results in a current flow in the measuring circuit, rendering the value of the transverse plasma flux, $j_\perp$.

Three diffusion flux collectors have been constructed and tested. Collectors A and B are of similar design, differing only in the width and the gap between the collector plates, which governs the quantity of plasma flux entering the collector. Collector C consists of only two plates between which a voltage is applied. The principle of collection of all collectors is the same.

Figure 3.7 presents the voltage and current characteristics of the collectors. Three regions exist in the curves. They are, however, not

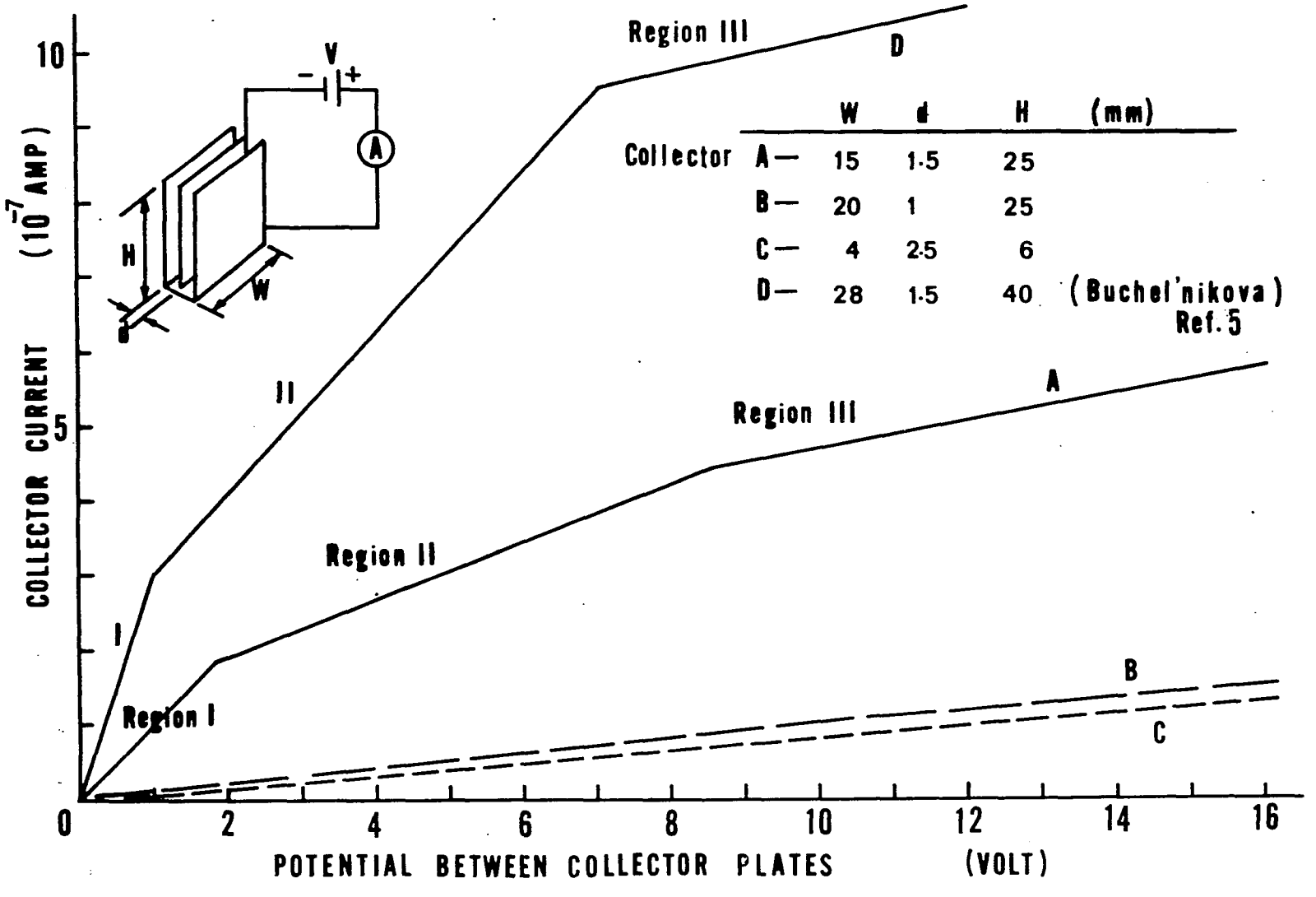

Figure 3.7 Diffusion Collector Current-Voltage Characteristic

clearly defined for collectors B and C, for which the magnitude of current is rather low. In region I, the effect of the applied potential extends only to the neighborhood of the surface of the plate and a thin sheath is formed, positive or negative depending on its polarity of the applied voltage. In region II, as the potential difference increases, the thickness of the sheath grows, and the current increases as the volume in which charge separation takes place increases. Complete charge separation of ions and electrons has not been achieved as the sheath of one plate does not extend fully into that of the opposite plate. In region III, the potential between the collector plates is sufficiently high and the sheaths overlap. There is complete charge separation of ions and electrons in the plasma flux entering the collector. The current measured is the saturation ion or electron current depending on the polarity of the biasing voltage of the collector plate.

A plot of collector current per unit area normal to the transverse plasma flux against the biasing voltage between the plates is given in Fig. 3.8. In both Figs. 3.7 and 3.8 the data by Buchel'nikova et al are included for comparison.

Collector A was used in the experiment throughout. Collector B and C were not used due to their low current collection. Furthermore, collector C behaved more like a double probe than a diffusion collector because of its relative large gap between the two small collector plates.

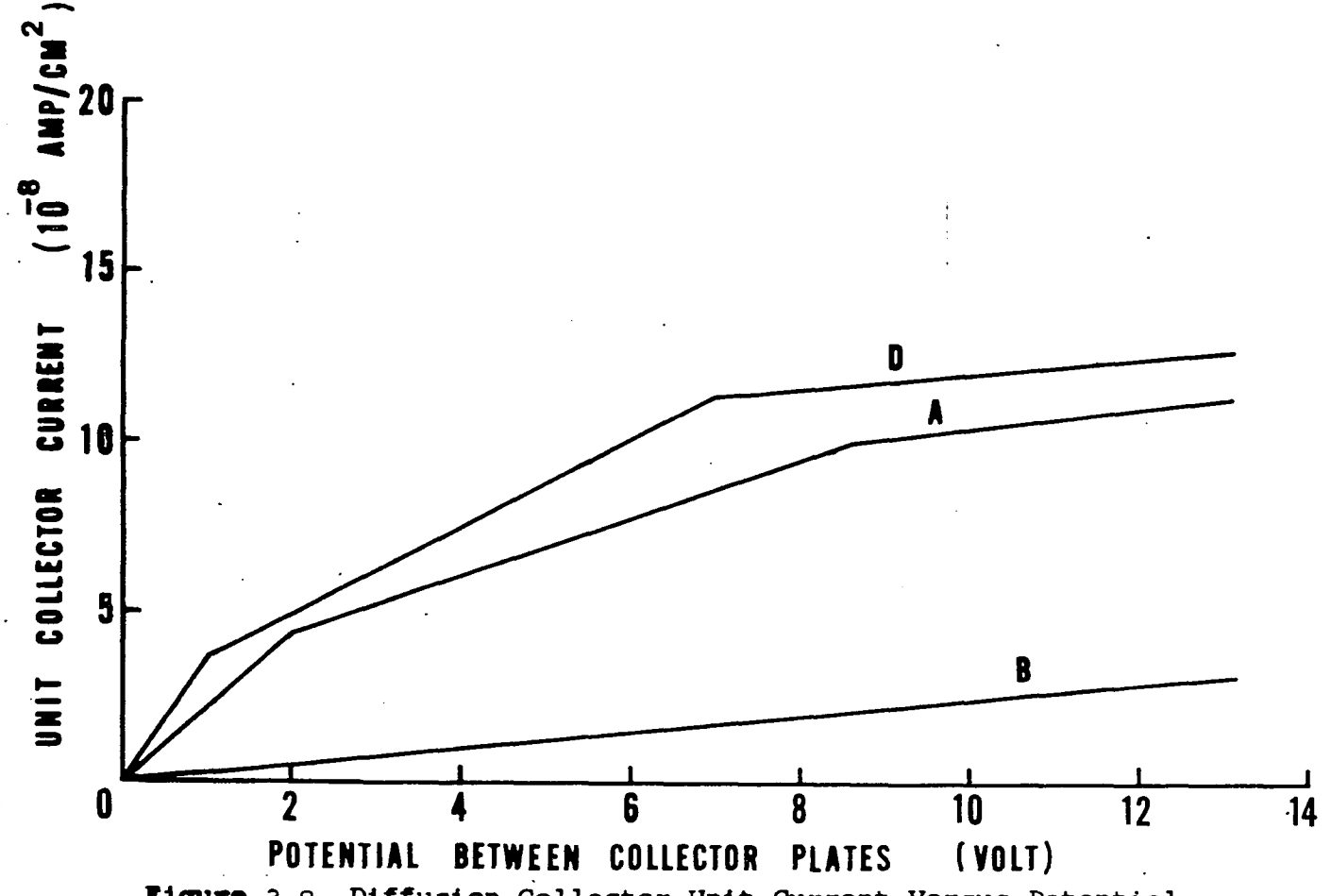

Figure 3.8 Diffusion Collector Unit Current Versus Potential
(**See** Figure 3.5 for dimensions of collectors A,B and D)

CHAPTER 4

CALIBRATION OF EQUIPMENT AND PREPARATORY EXPERIMENT

The goal of the experiment is to determine the presence of the helical instability in a highly ionized potassium plasma and to study its parametric dependence and enhanced diffusion resulted from the instability.

For positive identification and study of the helical instability, separating it from other types of instabilities which may occur in a potassium plasma, calibration of the experimental apparatus and preparation for proper test conditions are important.

4.1 Plasma Column

In the experiment before each run a check on the plasma column shape was made by taking the density profiles and floating potential curves in the horizontal and vertical directions at moderate magnetic fields. This is to ensure the consistency and compatibility of the experimental results from various test runs. Even with all the controllable parameters kept the same, the plasma column may vary due to the shifting of the position of the spray of potassium neutrals, the aging of the cathode filament, or the out-of-alignment of the ionizer plate from quick heating and cooling due to repeated start-up and shut-down of the Q-machine. Under such circumstances experimental runs were halted. Only after obtaining the desired plasma column shape experimental runs were carried out and data collected.

Typical plasma density and floating potential curves are shown in Fig. 4.1. The slight asymmetry of the density profile outside the column is attributed to the influence of the probe which is traversed across the column.

4.2 Longitudinal Magnetic Field

The magnetic field strength of the Magnion solenoid coils was calibrated and the variations of field strength along and across the vacuum chamber were determined by using a Bell axial type Gaussmeter. Calibration covered the whole experimental range from 500 to 6000 gauss. Axial variation along the length of the test section was measured within $\pm 0.6\%$ while the variation across the test chamber was within $\pm 0.5\%$. They are better than the manufacturer's claims. Figures 4.2 and 4.3 present the data sheet for a field strength of 3,500 gauss obtained during the calibration.

4.3 Sheath Condition at the Ionizer Plate

In the study of low frequency oscillations in a highly ionized plasma the property of the sheath formed on the surface of the hot ionizer plate is important. While the condition of quasi-neutrality holds in the body of the plasma, inside the sheath the plasma is not neutral. It may be ion- or electron-rich depending on the balance between ions and electrons at the ionizer plate. In the presence of an ion sheath flute, ion-acoustic and drift instabilities may occur. The drift instability, however, may not develop in the presence of an electron sheath due to the Simon short-circuit effect[42].

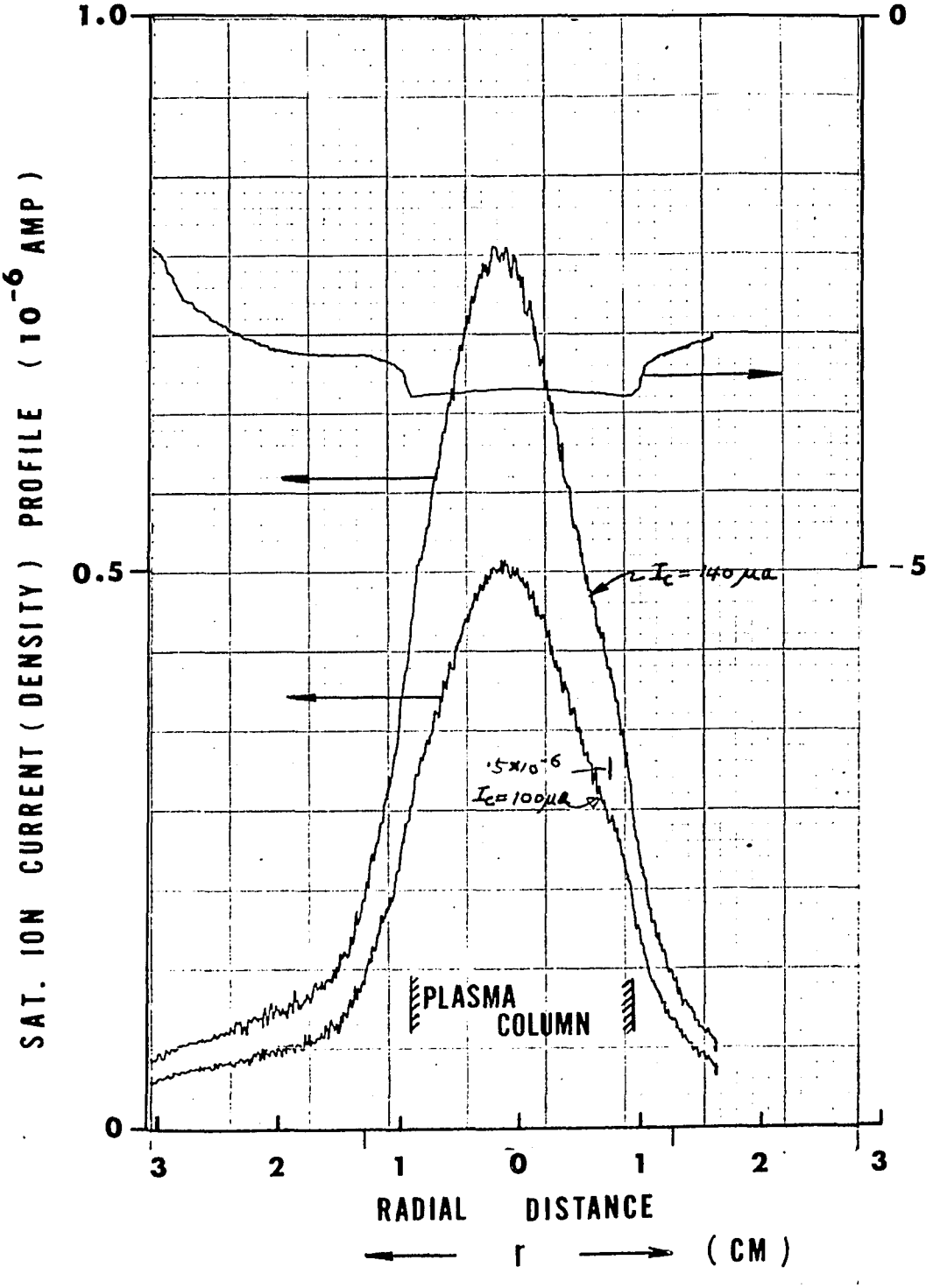

Figure 4.1 Density Profile and Floating Potential Curve

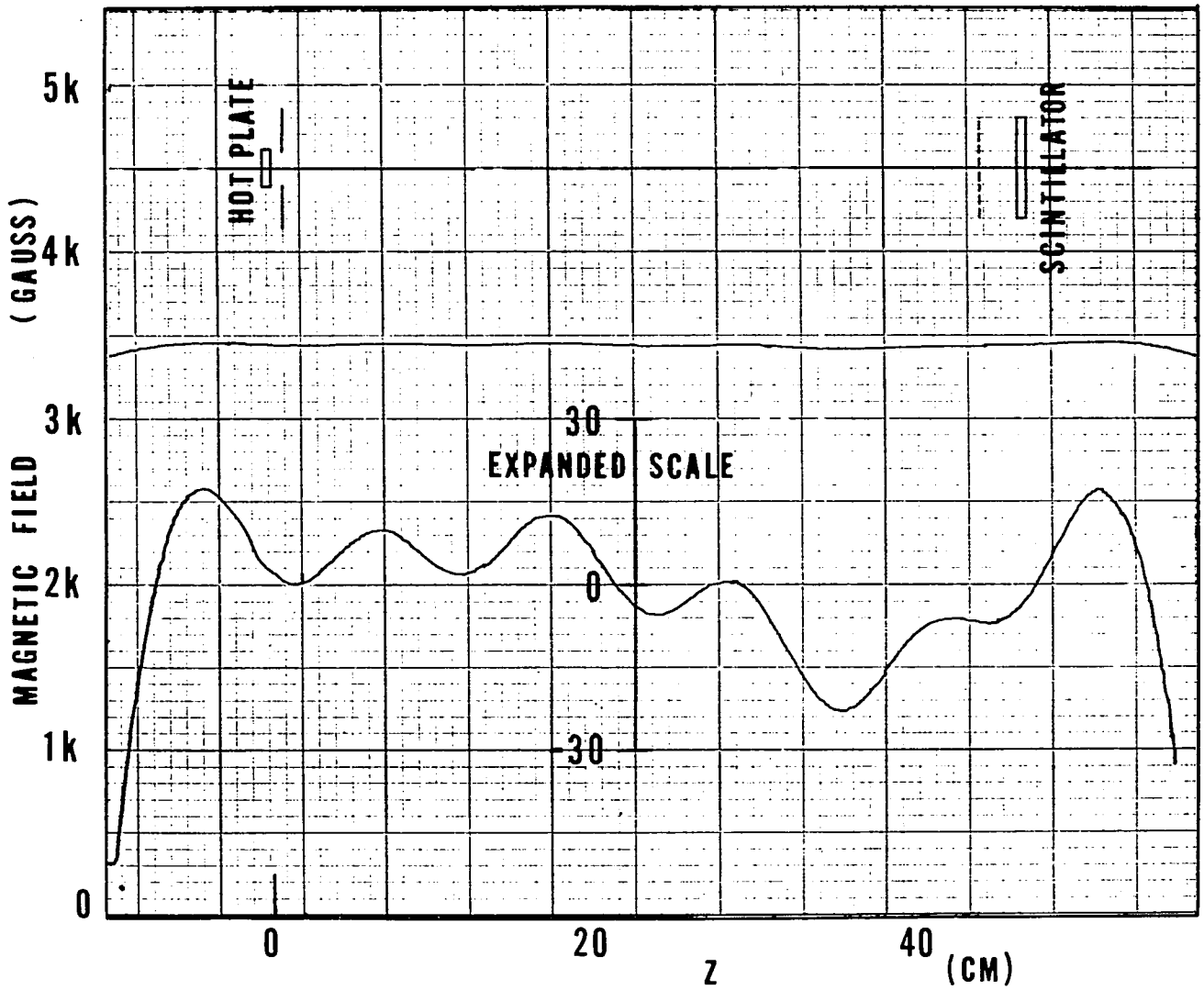

Figure 4.2 Calibration of Magnetic Field Along the Axis of the Test Section

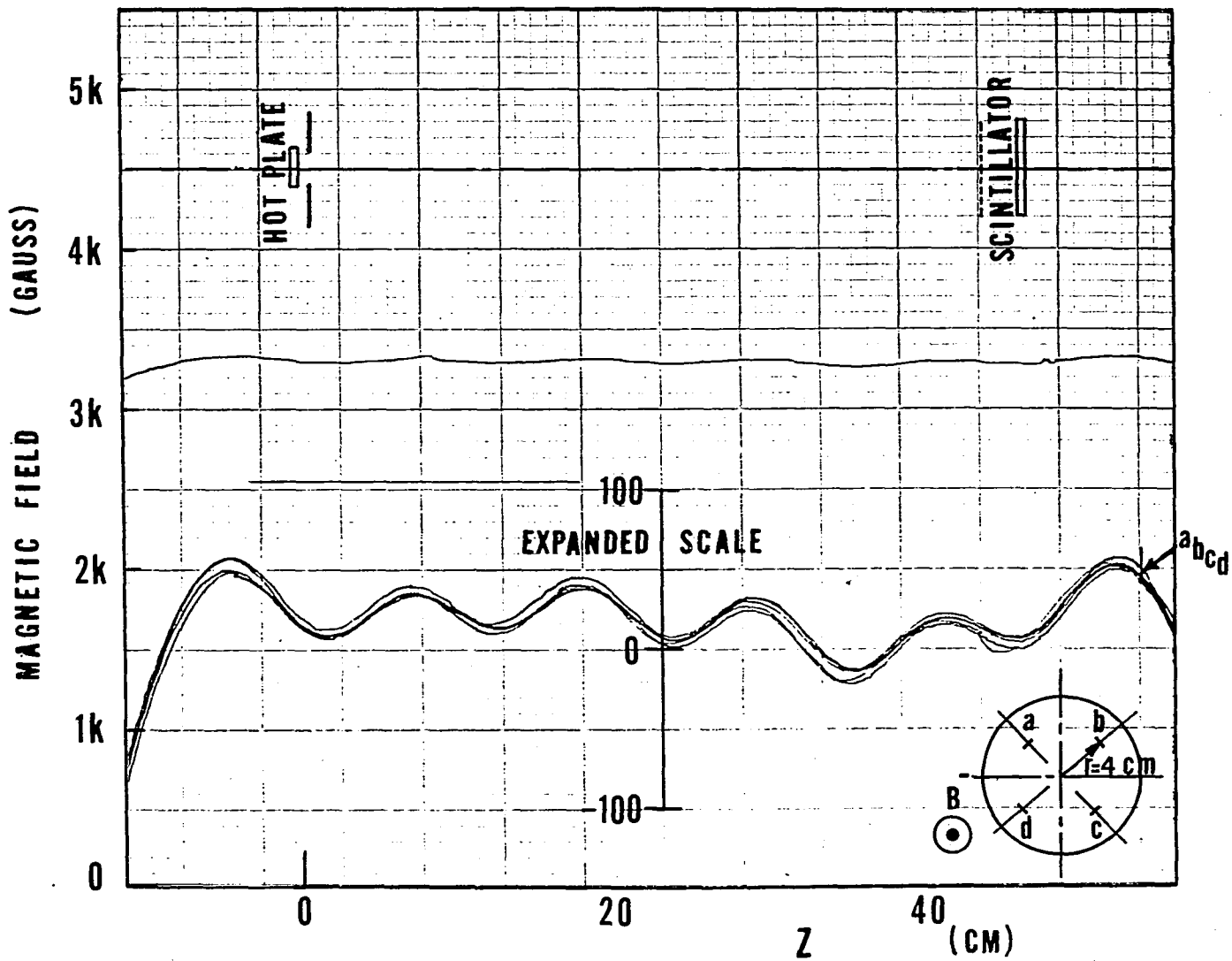

Figure 4.3 Calibration of Magnetic Field Parallel to the Axis of the Test Section

In the range of the experiment an ion sheath existed in all cases. The evidence of the ion sheath is presented in Fig. 4.4. It was determined at constant neutral flux by varying the power input to the ionizer and measuring (i) the plasma density and (ii) the floating potential at the axis of the column. The increase of plasma density corresponding to an increase in power input to the ionizer indicates the existence of an ion sheath. In this case excess ions are in the sheath, hence higher electron emission from the ionizer plate due to the increased power input will raise the density. The floating potential will be lower as the plasma contains more electrons due to higher electron emission from the ionizer. This continues to hold true until the electron sheath is formed. Then further increase in power to the ionizer will not bring an increase in density or decrease in floating potential as the plasma density is now limited by the quantity of neutral flux.

4.4 Ionizer Plate Temperature Variation

Temperature readings at the center and along the periphery of the plasma column were taken by using a Leed and Northrup optical pyrometer. The variation of the ionizer temperature are within $\pm 10^{\circ}$K, which amounts to a variation of about $\pm$ 0.5%. Effects of temperature gradient of this magnitude is insignificant in the experiment.

4.5 Diffusion Collector

The collector was positioned with the plates perpendicular to the

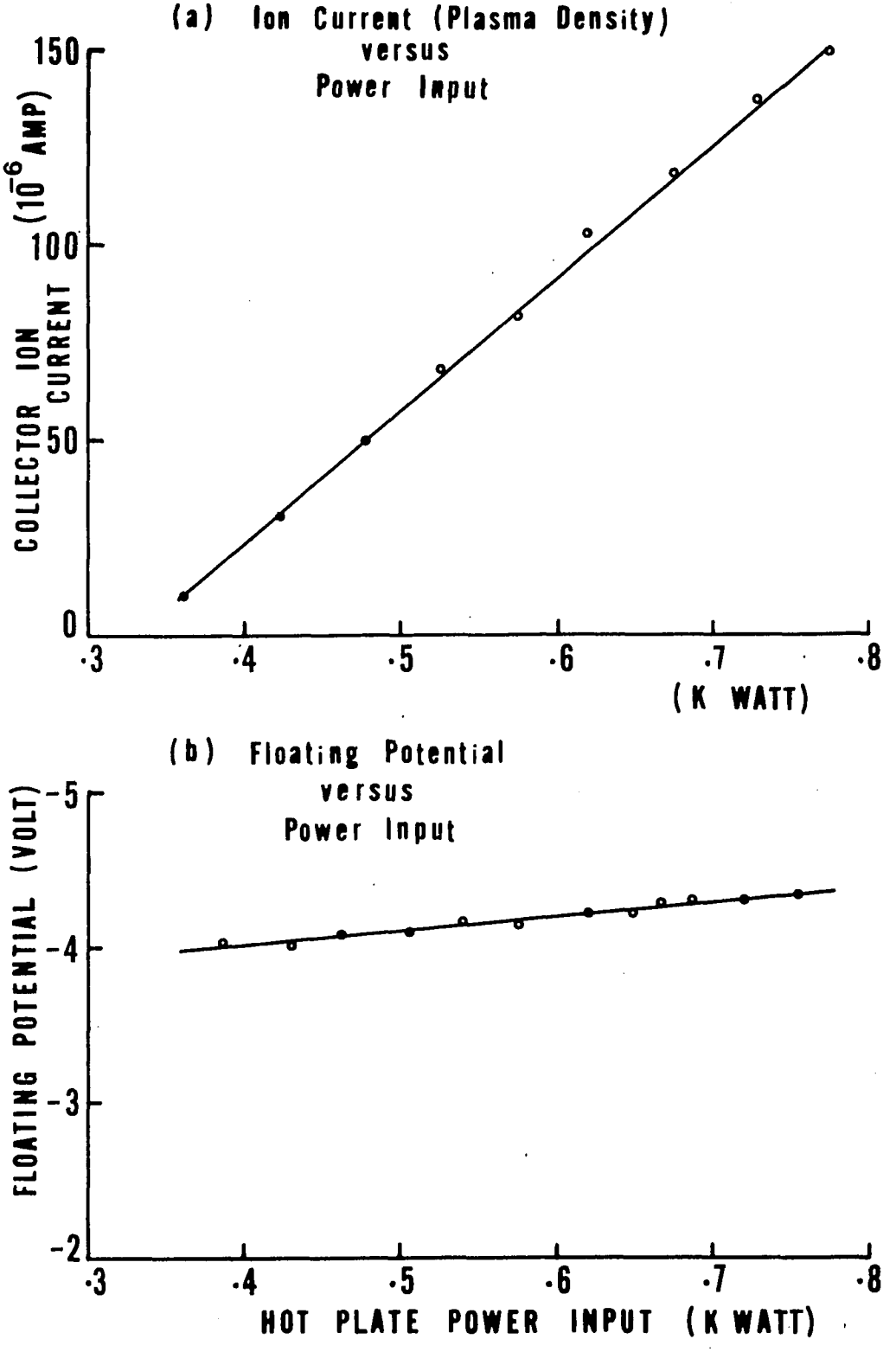

Figure 4.4 Sheath Condition at the Hot Ionizer Plate, B = 850 gauss

axis of the plasma column with its tip at a distance of 1-7/8 in. from the axis, i.e. 5 times of the column radius. A potential of 22.5 volts is applied between the collector plates to ensure a complete charge separation of the plasma flux entering the collector. The presence of the diffusion collector was shown to have no effect on the column shape or wave properties of the plasma.

The collector A (15 mm by 25 mm collector with 1.5 mm gaps between plates) was tested with its outer plates floating or grounded. Readings of both cases followed the same pattern except that when grounded higher current was collected. Floated circuit was used for minimizing the effect of the presence of the collector on the plasma column.

4.6 High Speed Camera, Scintillators and Films

As the photographs of the cylinderical plasma geometry have no fixed frame of reference inside the vacuum chamber, test film strips were made by photographing objects outside of the Q-machine to ascertain the orientation of plasma camera photographs. All photographs presented in this work give the true picture of plasma motion viewed toward the hot ionizer plate.

Type P1, P11 and P15 phosphors were tested for the coating of the scintillators with an aluminum overlay ranging from 3000 to 5000 angstroms thick. These scintillators were constructed to a specification aimed to give a sharp and fast-responsed image. The selection of phosphors was

made by their applicability to this experiment. Table I gives the decay characteristics of the three types of phosphor[43].

Table I

Decay Characteristics of Phosphors

Phosphor Type	Color of Luminescence	Decay Time To 50%	Decay Time To 10%	Voltage Required	Classification
P 1	Yellowish green	7.5 msec	24.5 msec	3 KV	Medium
P 11	Blue	8 μsec	34 μsec	3 KV	Medium Short
P 15	Green	0.25μsec	2.8μsec	3 KV	Short

In the preliminary runs the scintillator with type P 1 phosphor gave plasma camera pictures of high intensity but it lacked proper definition and contrast in registering density oscillations due to its relatively long decay time as compared with the period of azimuthal oscillations of the order of 200 microseconds. Scintillators with type P 15 phosphor gave a desirable decay time but had insufficient intensity of image even with the most sensitive film. Thicker aluminum coating, while providing better shield for the phosphor, required higher energy for the electrons to penetrate, thus gave a less luminous image for the applied electric potential. In order to obtain best scintillations for the experiment, a compromise between high intensity and short decay time and the selection of an optimum thickness of the aluminum coating had to be made. Consequently scintillators with type

P 11 phosphor and 3000 Angstroms thick aluminum coating were chosen for use in the experiment.

Kodak high speed recording film No. 2485 was used for the experiment. This film has a relative CRT (Cathode Ray Tube) speed of 10,000 for type P 11 phosphor photography which is the highest among all high speed recording films available in the market. Other films tested in the preliminary experiment are Kodak Linograph recording, Kodak 2484 Pan and GAF Hyscan films.

4.7 Summary

Calibration of the longitudinal magnetic field strength, determination of the hot ionizer plate temperature variation and sheath condition and the preparatory experimentation of the high speed plasma camera scintillators have been presented. Preparations for proper test conditions of the plasma column are also described.

CHAPTER 5

EXPERIMENTAL RESULTS

Plasma without the external longitudinal electric field ($E_z = 0$) was first investigated. The plasma density and potential profiles, properties of the wave and diffusion were determined at constant magnetic fields under steady state conditions. Then the case with the longitudinal electric field was studied following similar procedures. Effects of various parameters on the plasma were deduced from experimental runs holding all parameters constant except the ones in question.

5.1 Plasma in the Absence of Longitudinal Electric Field

In the absence of the longitudinal electric field low frequency waves were observed at low and moderate magnetic fields. The plasma density profiles are generally symmetrical with large density gradient near the edge of the column. The shape of floating potential profiles is an inverted plateau with a large drop of potential at the location corresponding to the maximum density gradient. The density and potential profiles are similar to those as shown in Fig. 4.1.

(a) Properties of Waves

At a magnetic field from 500 to 2000 gauss the waves observed were coherent with a predominated mode at 10 to 30 kH_z. Above 2000 gauss the waves gradually lost their coherency and multi-mode waves

existed in the mist of high background noise. Completely turbulent spectrum, however, was not observed as noisy low frequency waves of 10 to 15 kH_z persisted at magnetic fields up to 6000 gauss. The propagation of the low frequency waves was azimuthal, having no radial of longitudinal components as indicated by the measurements of the azimuthal, radial and longitudinal phase shifts of the oscillations respectively. Variations in plasma density, temperature and the magnetic field affected only the amplitude and frequency of oscillations, with no change on other properties of the wave. The wave was thus identified as of the flute mode similar to that observed by Kent, Jen and Chen in experiments conducted in the same Q-machine as the present experiment.

(b) Transverse Diffusion

The diffusion of plasma across the magnetic field was determined from direct measurements of the transverse plasma flux collected at the diffusion collector. Collector A as outlined in Section 3.5 (15 mm wide by 25 mm deep with 1.5 mm gaps between collector plates) was used. The applied potential of 22.5 volts is sufficient for complete charge separation of the plasma flux which enters the collector.

Figure 5.1 shows the diffusion coefficient obtained for various magnetic fields. It indicates that in the absence of the longitudinal electric field the transverse diffusion of plasma is proportional to B^{-2} for ranges of magnetic field from 500 to 1000 gauss and from 2000 to 6000 gauss.

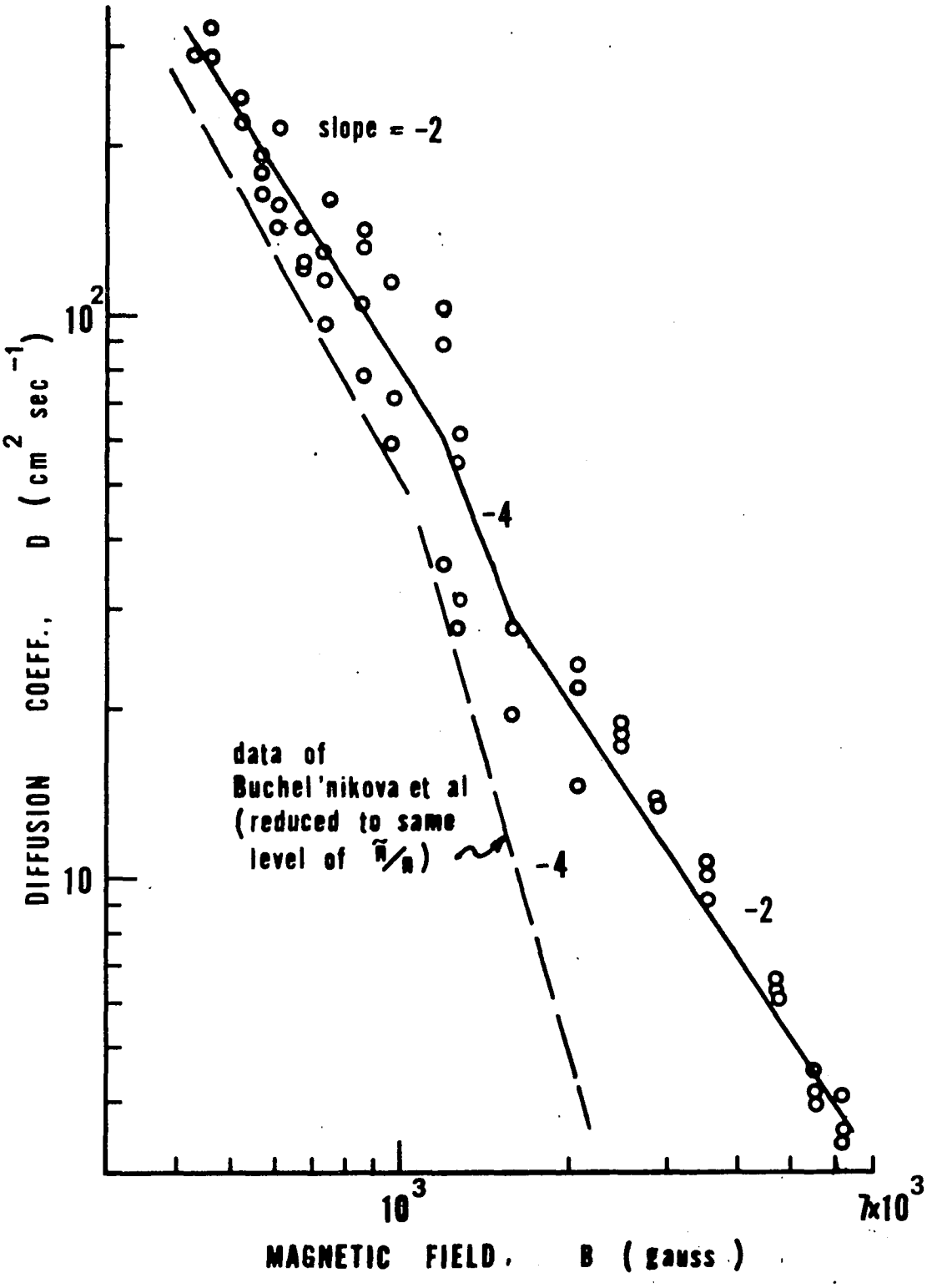

FIGURE 5.1 DIFFUSION COEFFICIENT IN THE ABSENCE OF LONGITUDINAL ELECTRIC FIELD

The magnitude is, however, higher than the value of the classical diffusion. There appears a small region between 1000 to 2000 gauss, in which the diffusion is approximately proportional to B^{-4}.

The diffusion coefficient obtained in the experiment in the absence of the longitudinal electric field verifies the theoretical prediction of $D \sim B^{-2}$ for plasma produced in a Q-machine and subsequent experimental results on "D versus B" relationship in potassium and cesium plasmas[44]. It also agrees closely with the experimental observation of Buchel'nikova et al of a potassium plasma in the presence of the drift instability up to 2000 gauss. The diffusion coefficient above 2000 gauss is not given in their results.

(c) Visualization of the Plasma Column

Visualization of the plasma column without the constant longitudinal electric field was done by using the single frame plasma camera as discussed in Section 3.4. With a high voltage pulse of the order of one microsecond applied on the scintillator, electrons of the plasma in the space between the grid screen and the scintillator were accelerated toward the scintillator and produced luminescence. As the effect of the short pulse of electric field does not extend to the body of the plasma, the luminescence presents the true visualization of the plasma motion. The column was shown to maintain its symmetry in density distribution independent of the magnetic field except the density variation at the edge of the column,

which is in conformity with the theoretical prediction and Langmuir probe measurements of the flute mode instability. Figure 5.2 is a typical single frame plasma camera photograph of the column. The frequency spectrum of the flute oscillations under the same conditions is also given.

5.2 Plasma in the Presence of Longitudinal Electric Field - General Remarks

The properties of the wave observed in the plasma with an external electric field and current flow in the axial direction differed little from those of the case without the axial electric field when the confining magnetic field was below 700 gauss. Above 700 gauss, however, the wave behaved differently. The existence of a longitudinal wave component ($k_z \neq 0$) was detected by the Langmuir probe measurements, indicating that the instability is of a type different from the flute mode ($k_z = 0$). With an increasing magnetic field the longitudinal wave length decreased while a low frequency mode at a frequency of about 5 kH_z was excited. The wave was highly coherent against a relatively quiescent background at a magnetic field up to 3000 gauss. Above 3000 gauss the wave lost coherency and gradually approached a turbulent state.

In the range of magnetic field (700 to 3000 gauss) enhanced diffusion was observed. There appeared a critical magnetic field, B_c at about 700 gauss, at which the diffusion process underwent an abrupt change. At $B < B_c$ the diffusion rate was classical. At $B > B_c$ the diffusion became anomalous.

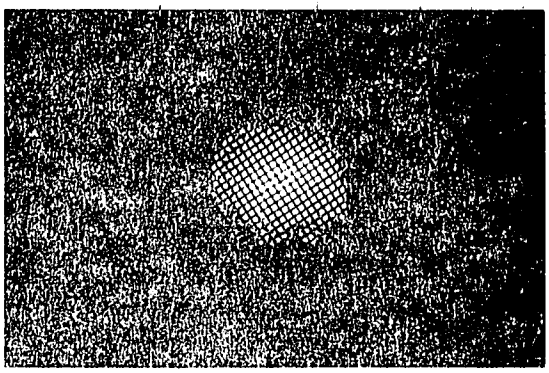

PLASMA COLUMN

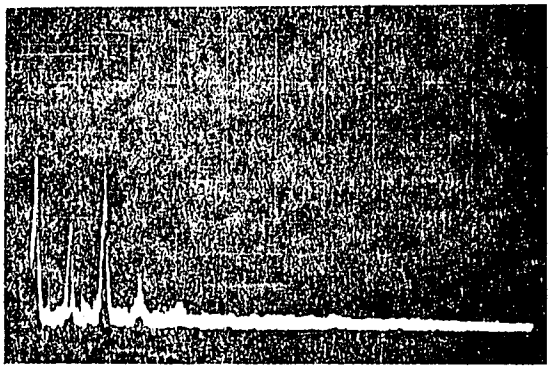

FIGURE 5.2 SINGLE FRAME PHOTOGRAPH OF THE PLASMA COLUMN WITHOUT THE LONGITUDINAL ELECTRIC FIELD

Evident from the observed wave properties, which contain a significant longitudinal component, and the anomalous diffusion above the critical magnetic field, the instability is believed to be of the helical mode similar to that observed in partially ionized plasmas of the positive column.

Table II is a summary of the conditions under which the experiment was performed. The results of the experiment will be discussed in the subsequent sections.

Table II Experimental Conditions

Plasma:	column diameter	3/4 in. (1.9 cm.)
	column length	18 in. (46 cm.)
	density	1 to 5 $\times 10^{10}$ cm^{-3}
	temperature	2300 ^{o}K
	degree of ionization	up to 92%
	(particle/magnetic pressure), β	$\cong 10^{-7}$
	chamber residue pressure	10^{-7} torr
	longitudinal magnetic field	500 to 6,000 gauss
Diffusion Collector:	dimension, (w $\times$ H) $\times$ d	(15 mm $\times$ 25 mm) $\times$ 1.5 mm
	voltage between plates	22.5 volts
	radial distance	5 times column radius
	saturation current	10^{-8} to 10^{-7} amperes
	High Speed Plasma Camera	
Scintillator:	phosphor	Type P 11
	aluminum coating	3000 Angstrom Thick
	high voltage	8 to 12 Kilo volts
	electron current	0 to 2 milliamp.
	grid screen bias	positive 10 to 15 volts
Dynafax Camera:	framing speed	5000 to 25,000 pps
	frame spearation	40 to 200 microsec.
	shuttering speed	5 to 25.6 microsec.
	film	Kodak No. 2485 (35 mm)
Langmuir Probes:	probe tip	tungsten wire 0.2 mm dia by 1 mm exposed length
	inner shield	0.7 mm dia by 5 cm long alumina ceramic
	outer shield	1.4 mm dia by 5 cm long alumina ceramic
	ground shield	0.025 mm thick copper foil (wrapping the inner shield)

5.3 Anomalous Diffusion

Figure 5.3 presents the diffusion coefficient obtained by using the diffusion collector and the radial density gradient of the plasma with the method as obtained in Section 3.5.

The diffusion process changes its character at B_c just below 700 gauss. In contrast to nearly classical diffusion below 700 gauss, the diffusion above B_c is anomalous. It increases abruptly with an increasing magnetic field up to 1000 gauss.

Above the critical magnetic field, B_c, the transverse diffusion includes, in separate ranges of B field, contributions from coherent and incoherent waves. In the range from 1000 to 3000 gauss where large amplitude coherent waves are present, the diffusion coefficient varies with B^{-1}, similar to the Bohm diffusion but with approximately one order lower magnitude. Above 3000 gauss, where incoherent waves dominate, the diffusion follows a B^{-2} proportionality. It should be remarked that both the B^{-1} and B^{-2} laws have been derived by Tchen[47,48,49] in the theoretical studies of turbulent diffusion of a plasma across the magnetic field.

The diffusion measurements presented in Fig. 5.3 was obtained under steady state conditions with a constant longitudinal electric field (12 kv) and electric current ($\geq$ 0.4 ma). When the electric current was kept at a minimum ($<$ 0.1 ma) the magnitude of diffusion was relatively lower. Anomalous diffusion still occurred above the same critical magnetic field (Fig. 5.4). The effect of the electric current is evident when comparing Fig. 5.3 with Fig. 5.4. Higher axial current corresponds to a sharper rise in diffusion above B_c.

It should be noted that the sudden change of the diffusion rate at the critical magnetic field indicates the occurrence of an instability which has not been observed in a Q-machine. The instability is determined by the

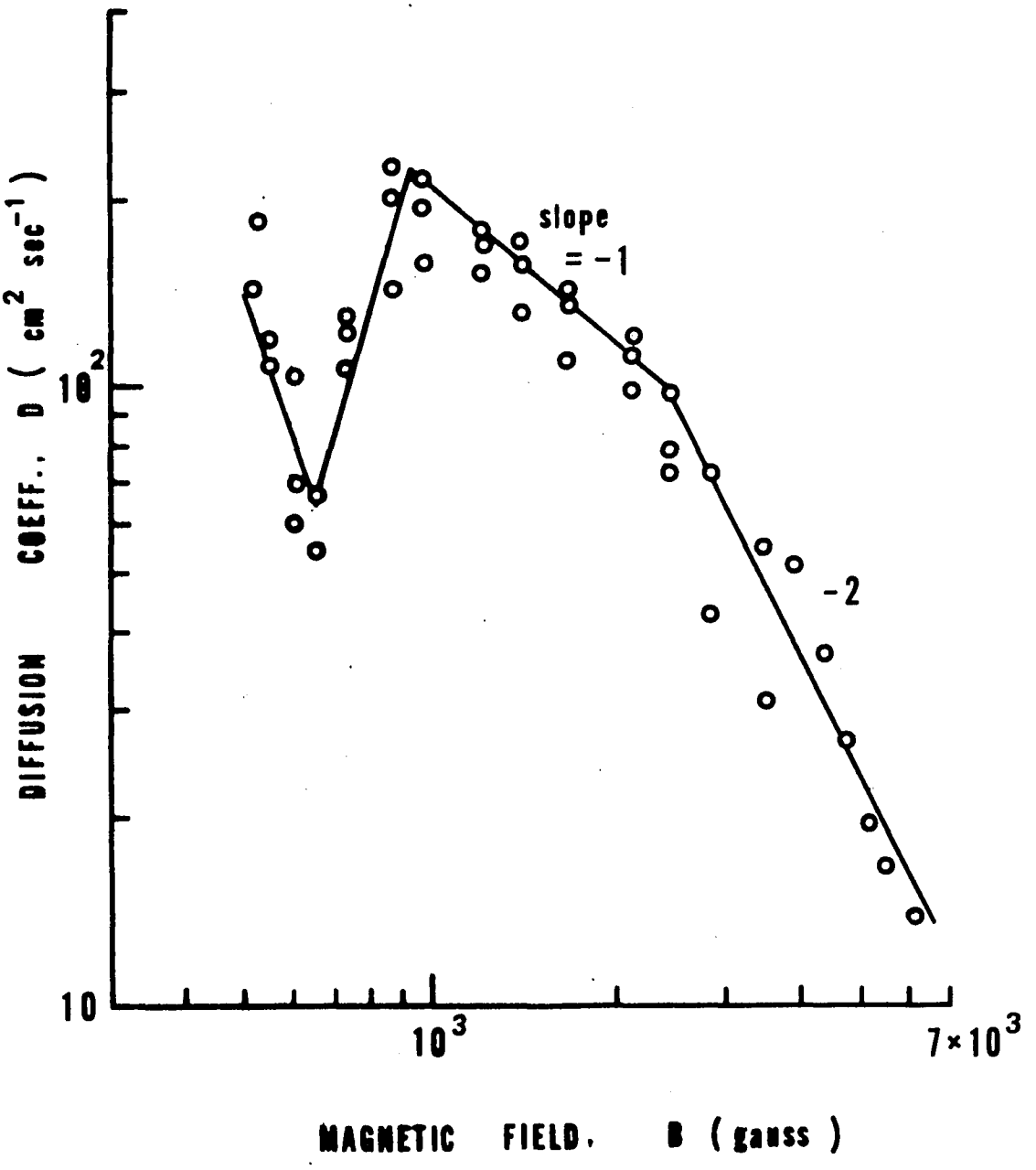

FIGURE 5.3 DIFFUSION COEFFICIENT VERSUS MAGNETIC FIELD - WITH LONGITUDINAL ELECTRIC FIELD

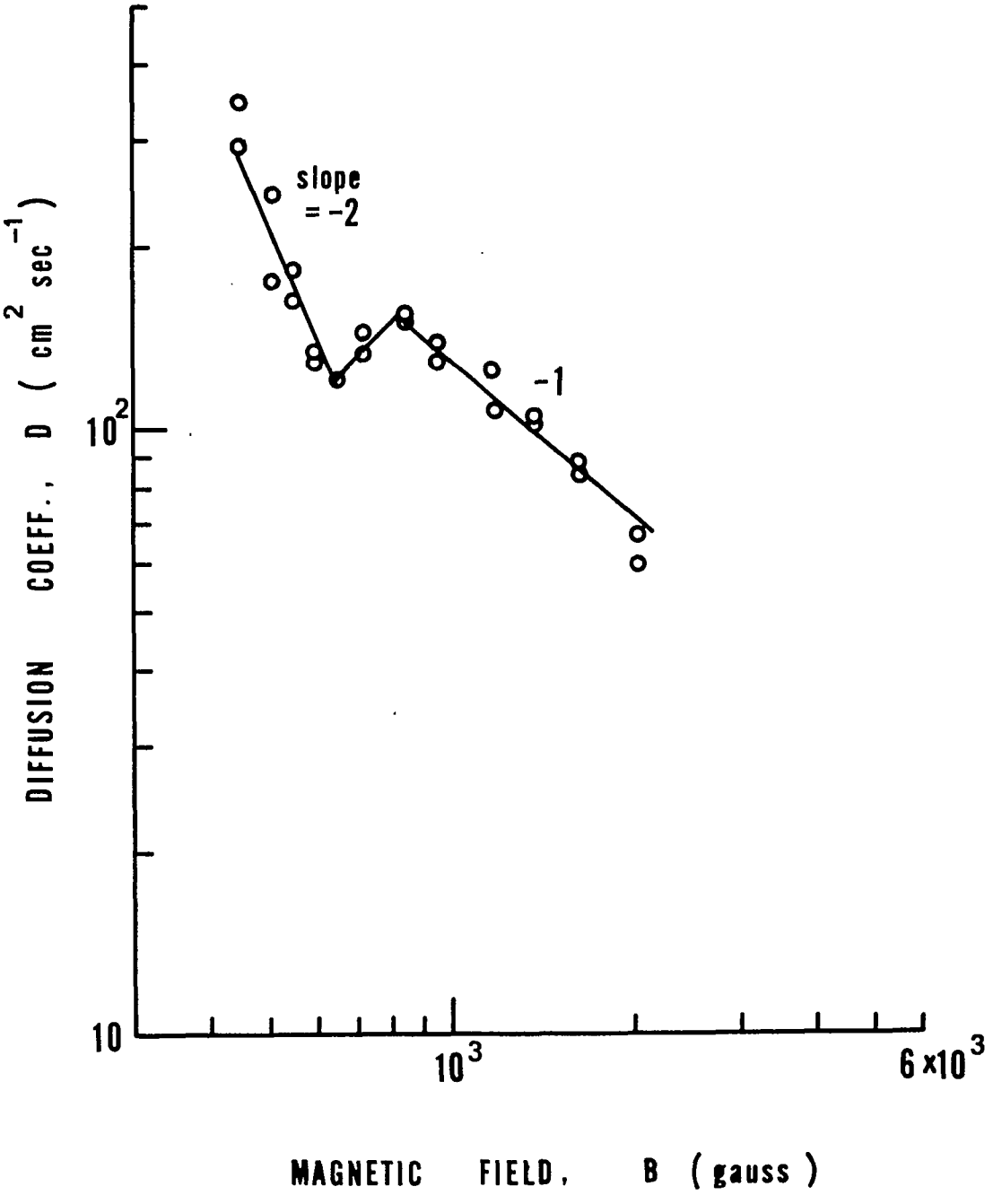

FIGURE 5.4 DIFFUSION COEFFICIENT VERSUS MAGNETIC FIELD - LOW LONGITUDINAL ELECTRIC CURRENT

Langmuir probe measurements of the wave properties and verified by the high speed photography in the following sections.

5.4 Azimuthal Propagation of the Wave

The azimuthal component of the wave was measured by the use of the two-dimensional and the linear (radial) Langmuir probes located in the same z-plane at an angle θ apart and at the same radial distance from the axis. The linear probe was used as a trigger probe while the two-dimensional probe was positioned to attain any desired angle θ between the two probes. The magnitude of the phase-shift between the displays of the AC signals of the two probes on the dual-beam oscilloscope depends on the angle θ and the mode number, m of the wave.

The direction of azimuthal propagation of the wave was first determined. This was done by varying the angle between the two probes with fixed trigger probe and observing the change in the phase-shift on the oscilloscope displays. A decrease (or increase) in θ accompanied by a decrease (or increase) in phase-shift indicates that the propagation of the wave is in the direction of the movement of the moving probe. Otherwise the wave is travelling in the opposite direction. The azimuthal propagation of the wave was shown to be in the direction of electron diamagnetic waves, i.e. in the clockwise direction when viewing in the direction of the magnetic field.

The mode numbers were determined by measuring the phase-shift between the signals of the two probes with a predetermined θ. The azimuthal phase velocity is $2\pi r/m\tau$ where τ is the period of the wave and the phase velocity measured by the phase shift is $r\theta/t$ where t is time scale of the phase shift on the dual-beam oscilloscope. The mode number is hence given by $m = 2\pi t/\theta\tau$.

Mode numbers two and three were observed for low and moderate magnetic fields ($B \leq 1600$ gauss) and mode one was observed at higher magnetic fields. At magnetic fields above 3000 gauss mode number measurements became difficult due to the distorted wave form and high noise level on the oscilloscope displays. Figure 5.5 shows the measurement of mode one at a magnetic field of 2000 gauss.

The correctness of the determination of the mode numbers was checked by taking at least two different θ's for each mode number measurement. This is to overcome the uncertainty due to the fact that on the oscilloscope displays a phase-shift of 1/4-wave length and that of 1-1/4 wave length are not differentiable. Detail methods for the determination of the azimuthal mode number are given in the Appendix.

5.5 Radial Propagation

No radial propagation of the wave was observed in the experiment. Two Langmuir probes were aligned at the same θ-position. With one probe held stationary while the other traversed radially, no phase shift was

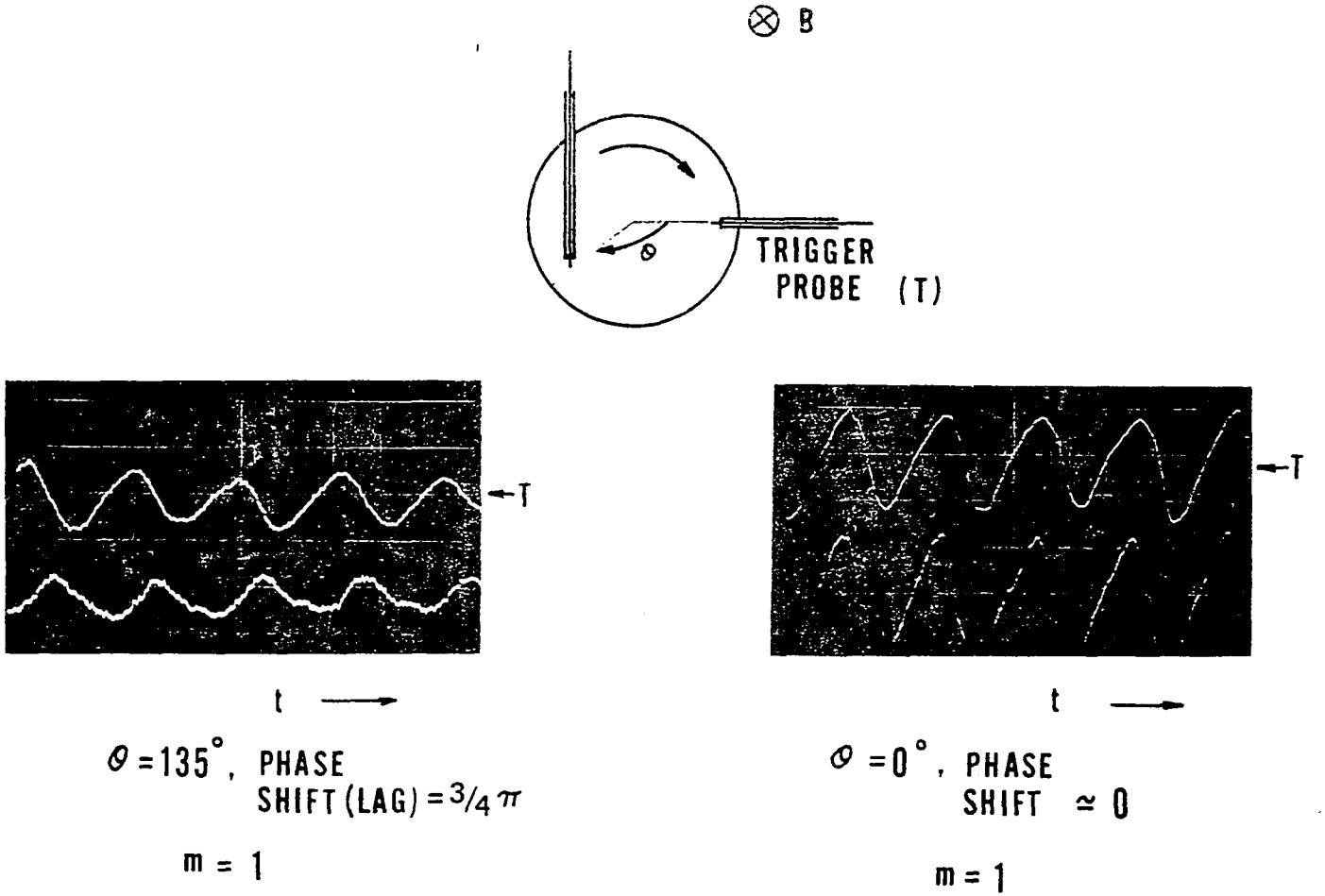

$\phi = 135°$, PHASE SHIFT (LAG) $= 3/4\,\pi$

m = 1

$\phi = 0°$, PHASE SHIFT $\simeq 0$

m = 1

Figure 5.5 Mode Number Measurement

observed on the oscilloscope dual-beam displays. Only changes in the amplitude of the wave was detected by the moving probe. Figure 5.6 presents the variation of the wave amplitude as the Langmuir probe traversed radially across the plasma column. It not only verified that the wave did not propagate radially but also confirmed that the oscillations were predominant near the edge of the plasma column, as predicted by the theory of Q-machine plasmas (Kent, Jen and Chen).

5.6 Longitudinal Propagation

Measurements of longitudinal propagation of the wave are similar to that for the azimuthal mode numbers except that the two probes are placed at a known distance z apart. The longitudinal probes were used. The longitudinal component of the phase velocity was measured by $(v_{ph})_z = z/t$. From the relation $(v_{ph})_z = \lambda_z/\tau$, the longitudinal wave length $\lambda_z = z\tau/t$ was calculated. (t and τ are defined in the preceding section.) The longitudinal wave number k_z was calculated by equating the phase velocity ω/k_z to the velocity measured by z/t, giving $k_z = \omega t/z$. Figure 5.7 gives the measurements of the longitudinal wave length for magnetic fields above the critical value B_c.

Tables III lists the longitudinal wave lengths at various magnetic fields.

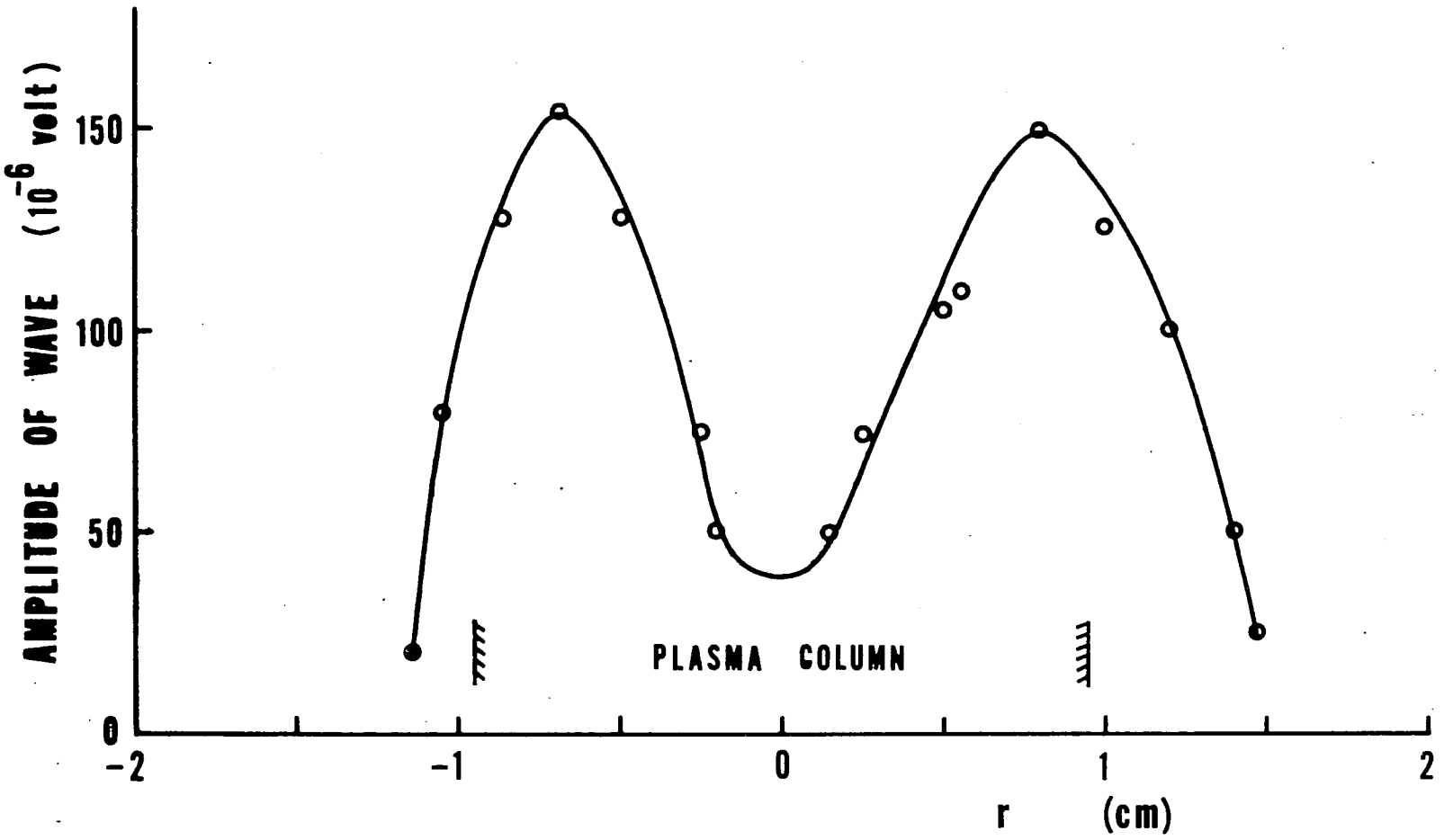

FIGURE 5.6 RADIAL DISTRIBUTION OF THE AMPLITUDE OF WAVES

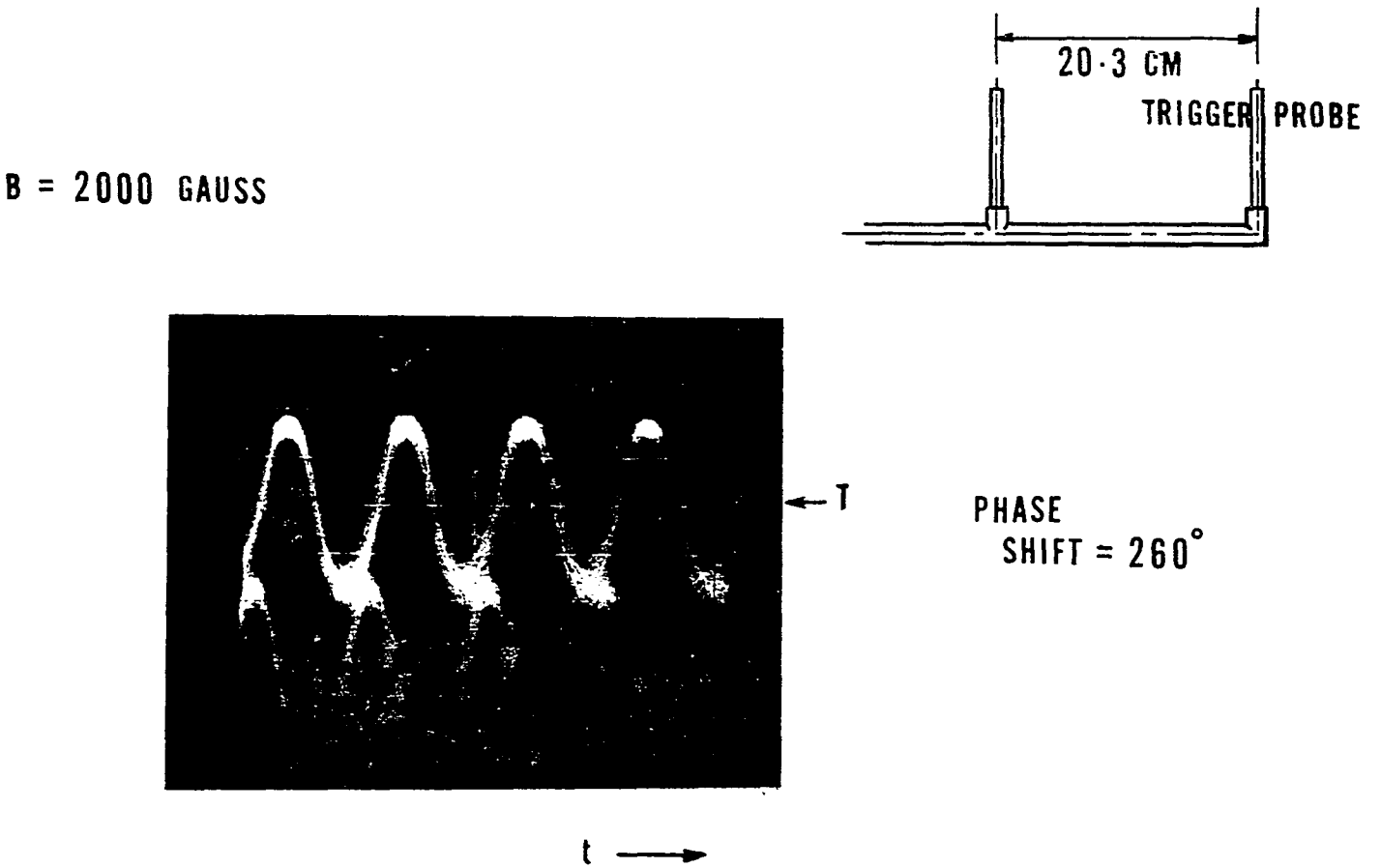

Figure 5.7 Measurement of Longitudinal Propagation of Wave

Table III

Longitudinal Wave Length

Magnetic Field (gauss)	500	600	700	850	950	1200	1600	2000	2400
Ratio λ_z/L	∞* ($\overset{*}{>}$ 20L)	∞*	10.6	7	5.5	2.5	1.6	0.6	0.5

L = length of plasma column = 18 in. (46 cm.)

z = distance between probes = 8 in. (20.3 cm.)

At strong magnetic fields, B $\geq$ 2800 gauss, the determination of λ_z becomes unreliable as the wave form is so distorted due to the interactions between different modes that accurate measurements of the phase shift between the two longitudinal probes are no longer possible.

It should be noted that the longitudinal components of the wave is significant and the longitudinal wave length is short as compared to the length of plasma column. This, when viewed together with the azimuthal propagation of the wave, indicates that the instability observed appears to be of the helical mode. Further affirmation to this conclusion is attained by the use of the high speed photographic technique.

5.7 Visualization of Helical Instability

The visualization of the helical instability, its onset, evolution, growth and finally its development into a turbulent state have been carried out by the use of the high speed plasma camera. The sequential plasma camera pictures recorded the fast changing motion of the plasma. They presented not only the instantaneous spatial distribution of the density, but also the time scale of the plasma motion from which information was obtained for the verification of the helical mode instability, its properties and its development in an increasing magnetic field.

With this photographic technique it was found that at low magnetic fields (500 to 700 gauss) the plasma column maintained its circular shape and symmetry. The oscillation of plasma was not significantly recognizable in the plasma camera pictures which are shown in Figs. 5.8 to 5.10. The amplitude of the wave is relatively low.

At a magnetic field just above the critical magnetic field (800 to 1200 gauss), the density oscillation became evident, while the amplitude of the wave increased indicating that instability had set in. The plasma column lost, to some degree, its axial symmetry, however, the existence of helicity in the plasma column could not be determined from the photographs. In Figs. 5.11 to 5.13 the plasma density oscillations are clearly visible.

When the magnetic field is much above the critical value the helical form of the plasma column became apparent. At magnetic field

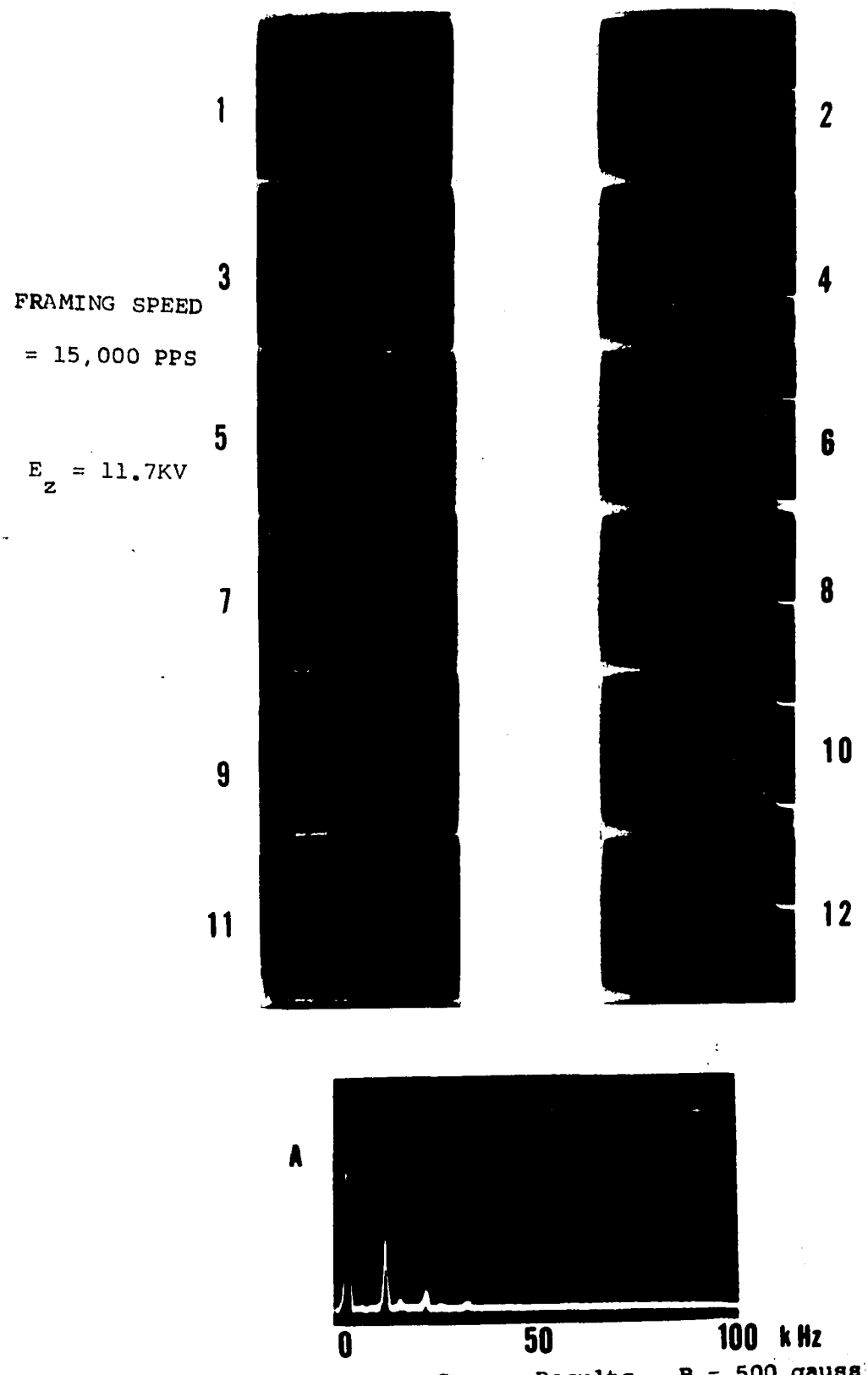

Figure 5.8 High Speed Plasma Camera Results, B = 500 gauss

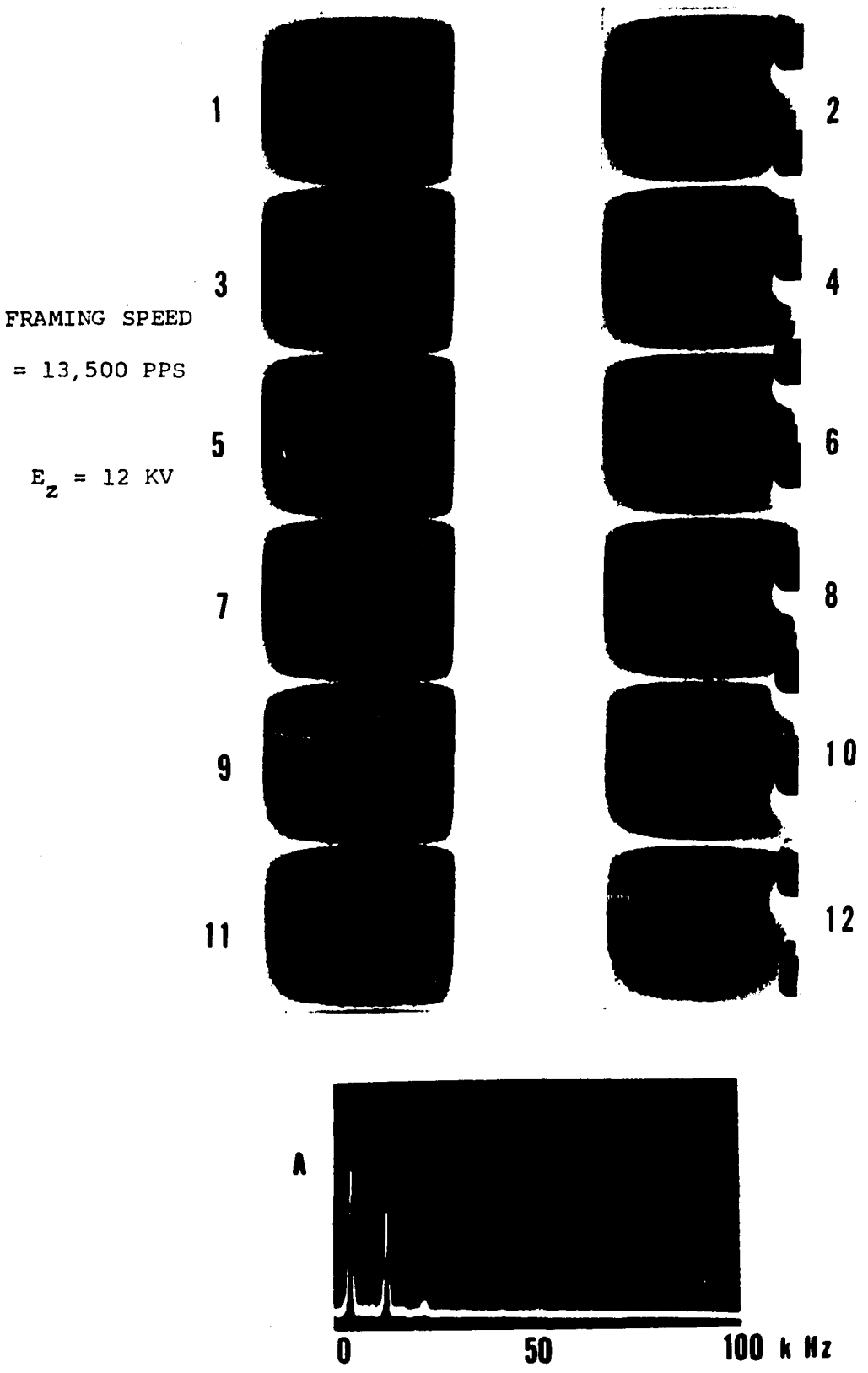

Figure 5.9 High Speed Plasma Camera Results, B = 600 gauss

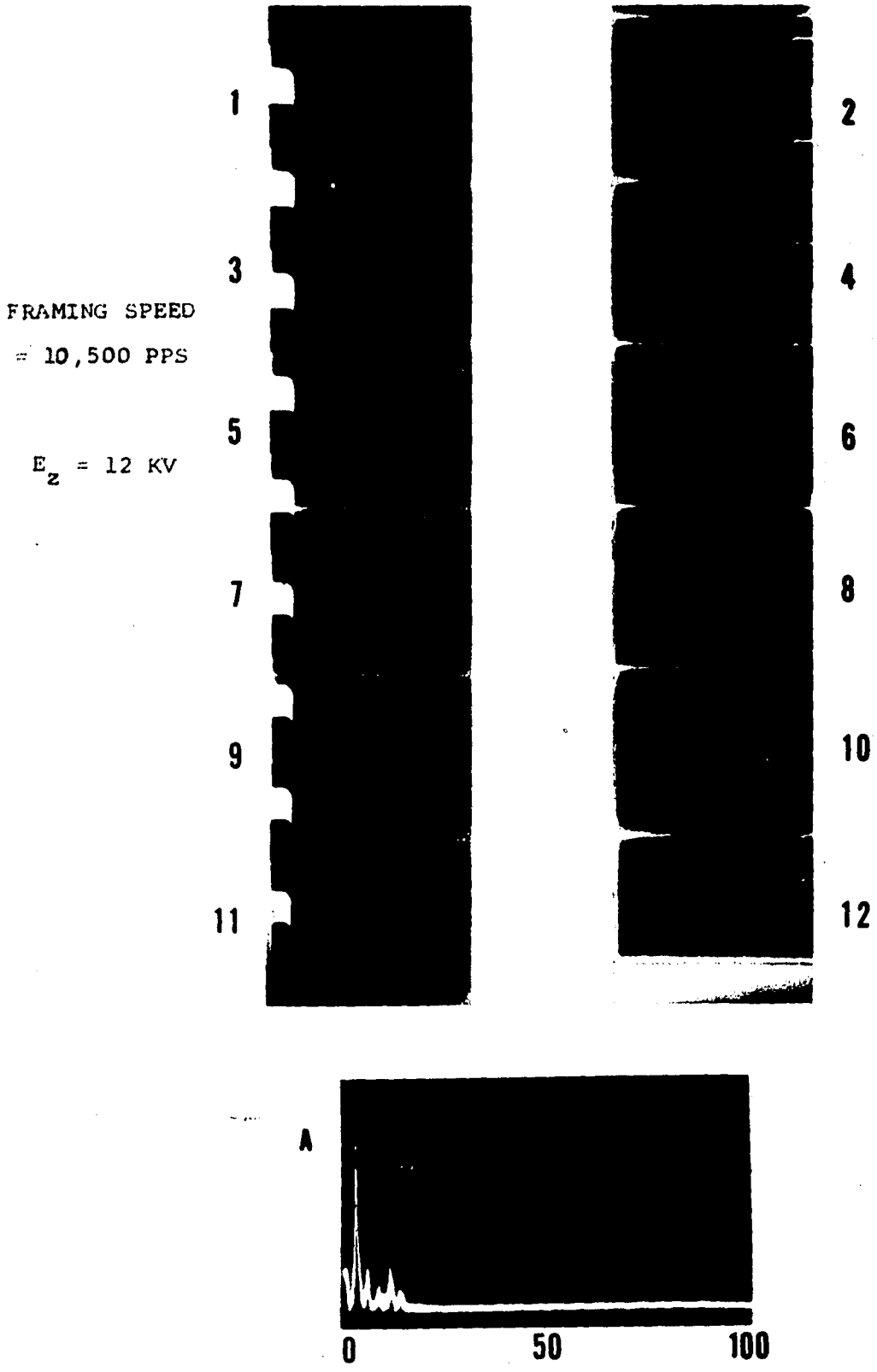

Figure 5.10 High Speed Plasma Camera Results, B = 700 gauss

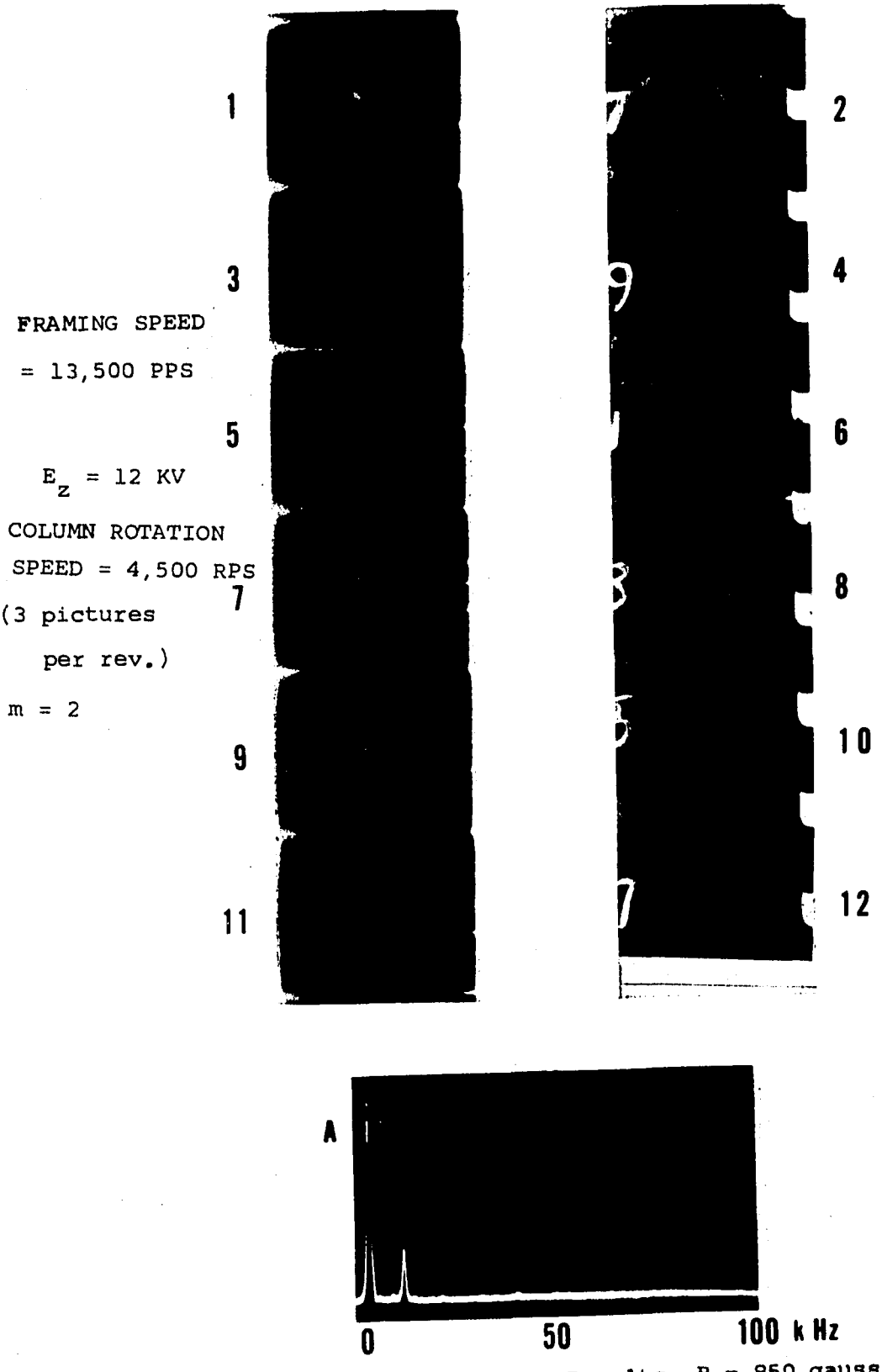

Figure 5.11 High Speed Plasma Camera Results, B = 850 gauss

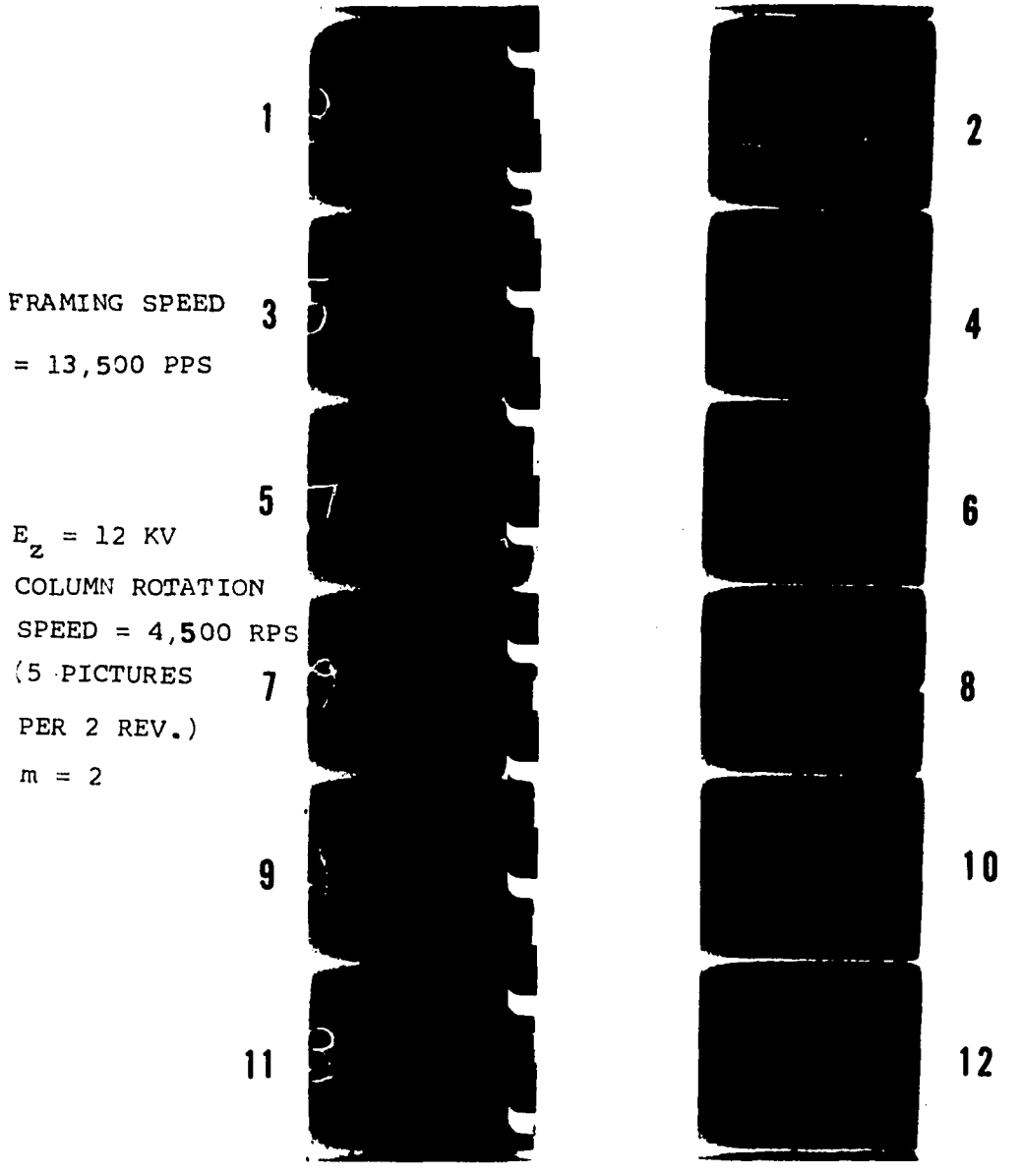

Figure 5.12 High Speed Plasma Camera Results, B = 950 gauss

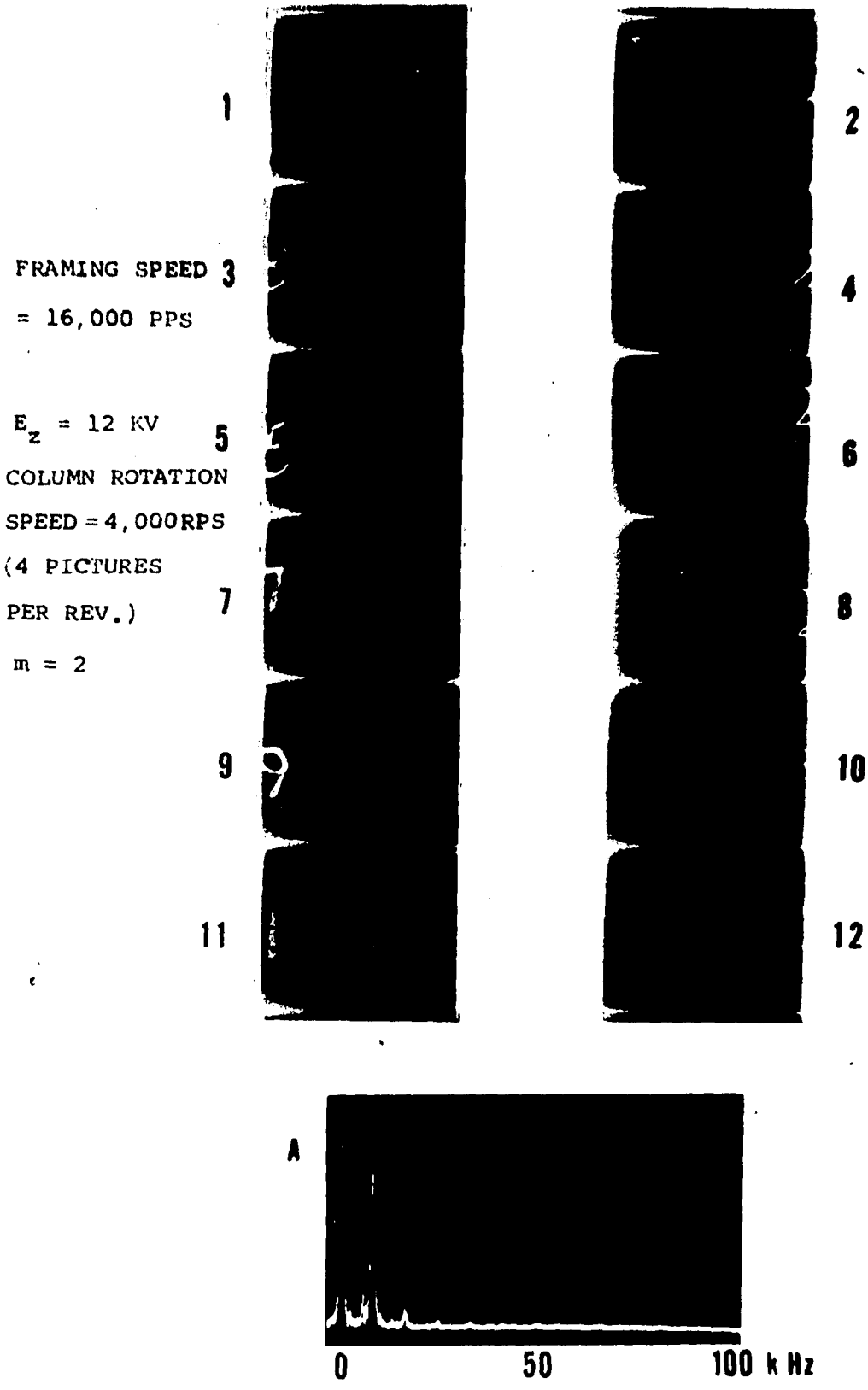

Figure 5.13 High Speed Plasma Camera Results, B = 1200 gauss

ranging from 1600 to 2800 gauss, the column was highly asymmetrical and the off-set of the axis was appreciable indicating a helical column. Meanwhile, the wave spectrum showed a low frequency and high amplitude display. Figures 5.14 to 5.17 present the plasma camera photographs showing the plasma with the instability appearing to be of the helical mode. In the phtographs only the parts of high plasma density were recorded, as sufficient energy for adequate scintillation was not attained in the low density portion of the column.

The instability in the plasma grew with increasing magnetic field and finally developed into a state of turbulence at 5000 gauss. The density distribution of the plasma column changed erratically and the helical-form oscillations were no longer recognizable. The plasma camera photographs showed randomly changed shapes of the plasma column with no fixed pattern or sequence as indicated in Fig. 5.21. Figures 5.18 to 5.20 show photographs of the plasma column changing from helical form to turbulence.

5.8 The Evaluation of Helical Instability

After the helical instability has been excited, an increase of the magnetic field up to approximately 1000 gauss causes the instability to grow and the diffusion to enhance. Further increase in the magnetic field from 1000 to 3000 gauss is accompanied by an increase of the amplitude of the wave. In this range the azimuthal propagation of the wave changes from a frequency of about 9 kHz and mode two (m = 2) to about 5 k Hz of a

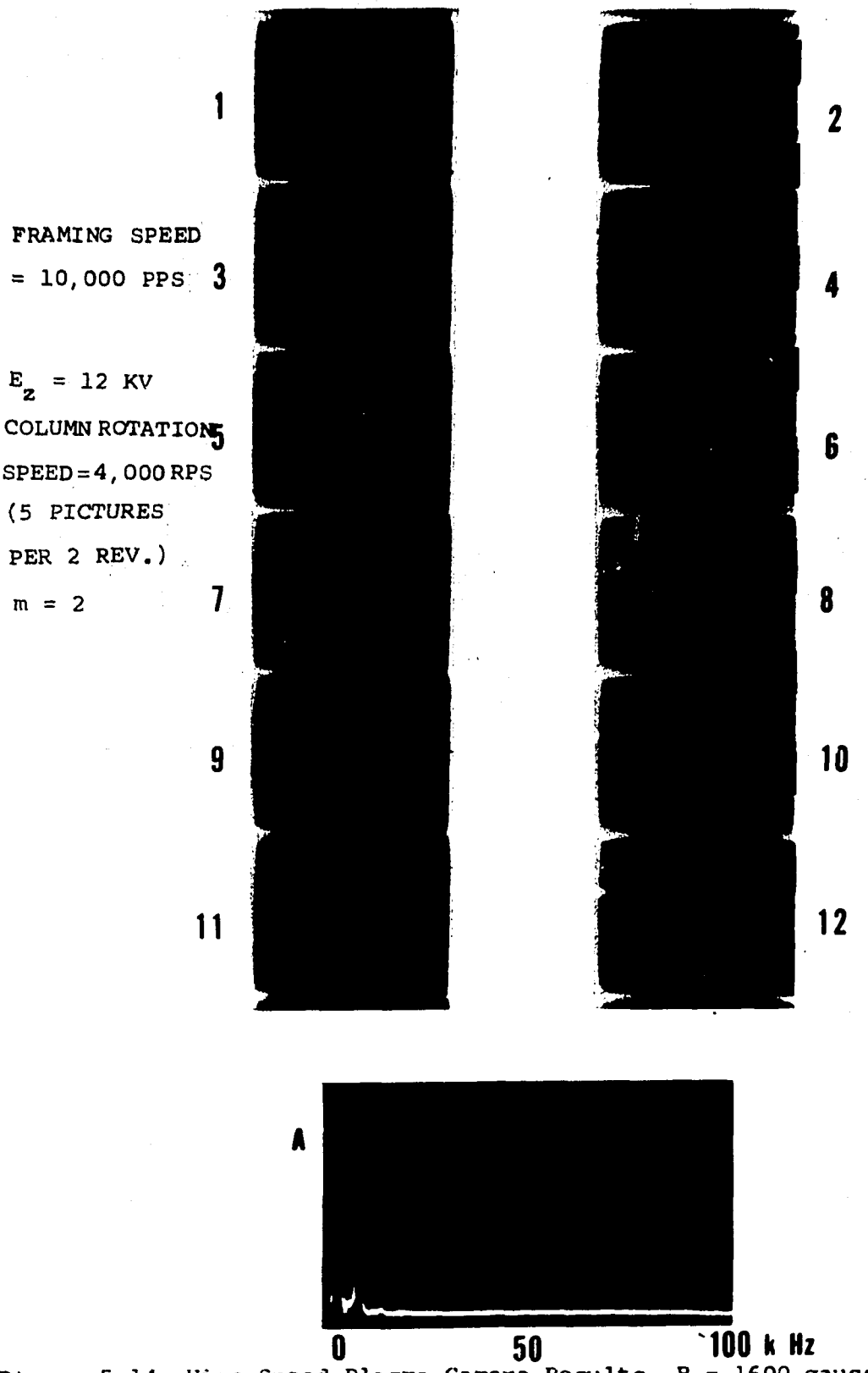

Figure 5.14 Hign Speed Plasma Camera Results, B = 1600 gauss

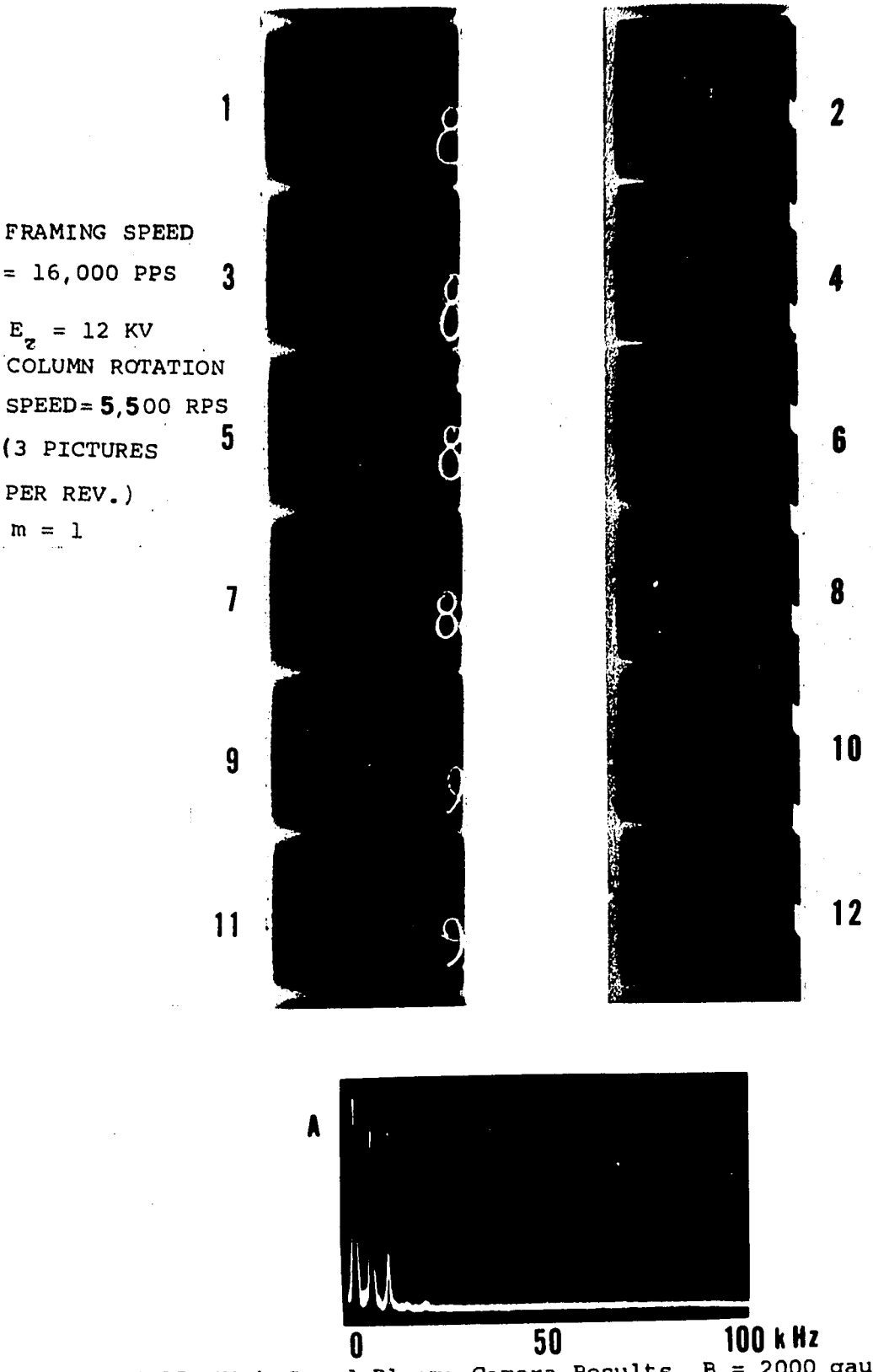

Figure 5.15 High Speed Plasma Camera Results, B = 2000 gauss

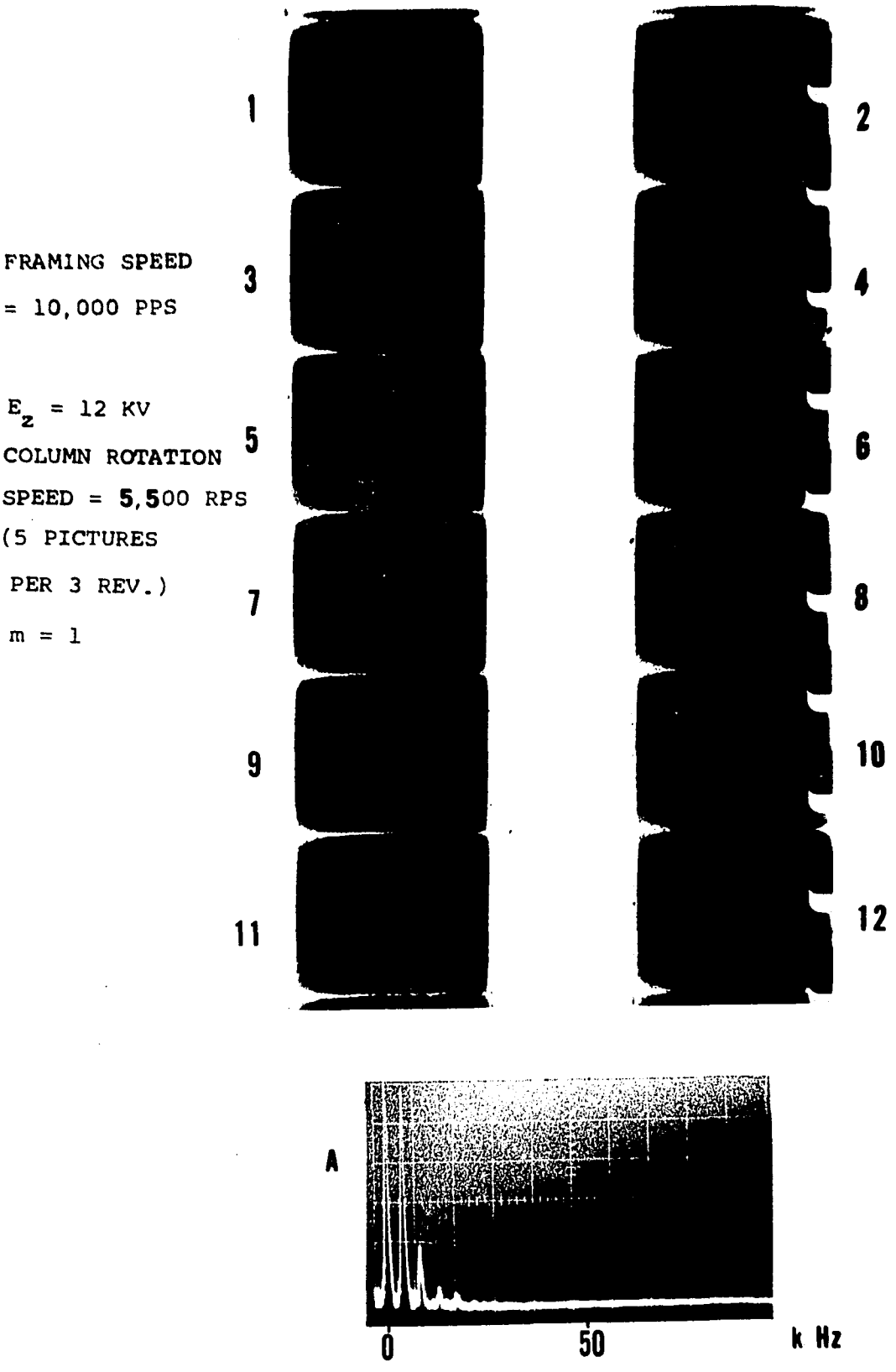

Figure 5.16 High Speed Plasma Camera Results, B = 2400 gauss

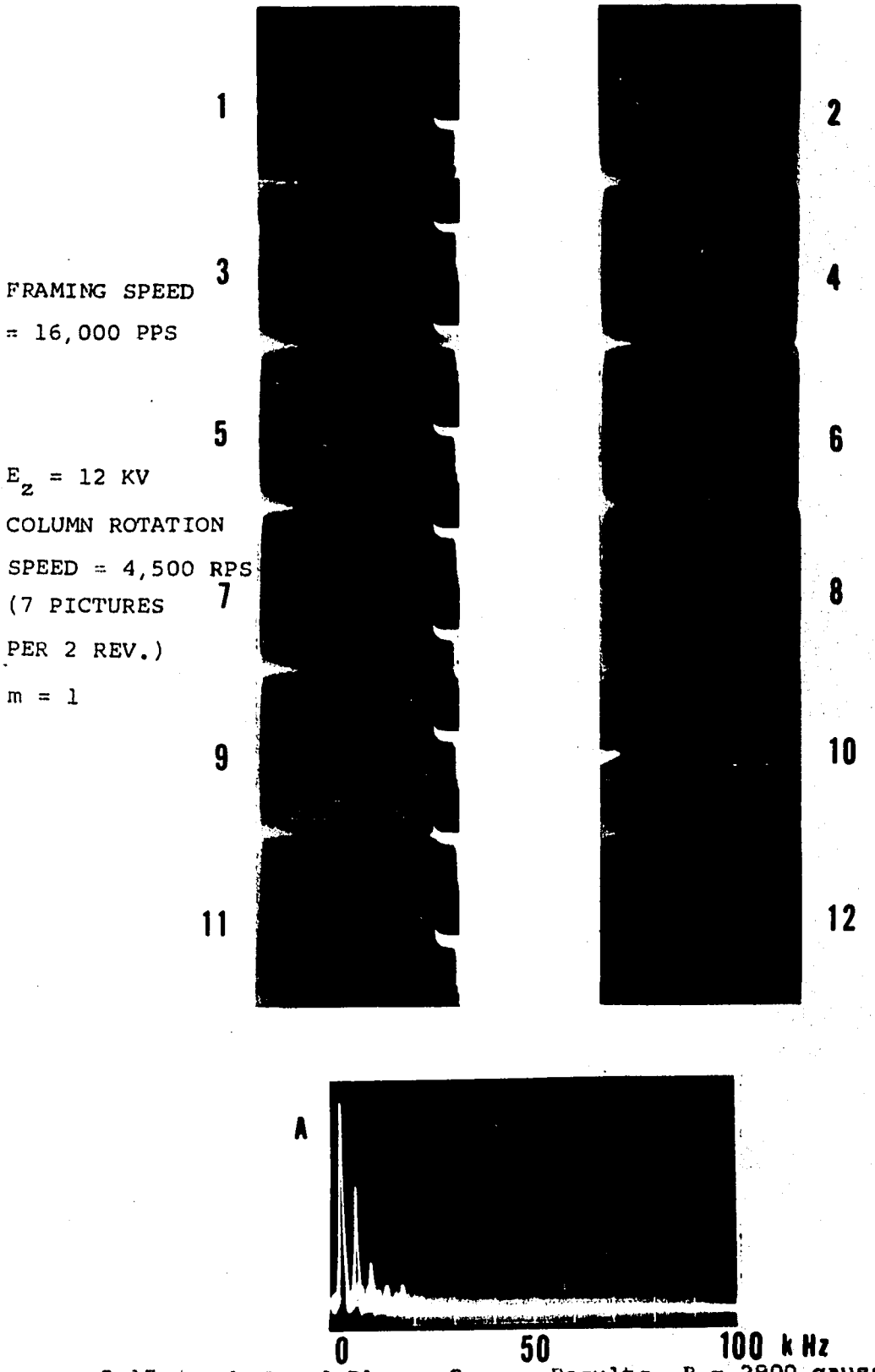

Figure 5.17 High Speed Plasma Camera Results, B = 2800 gauss

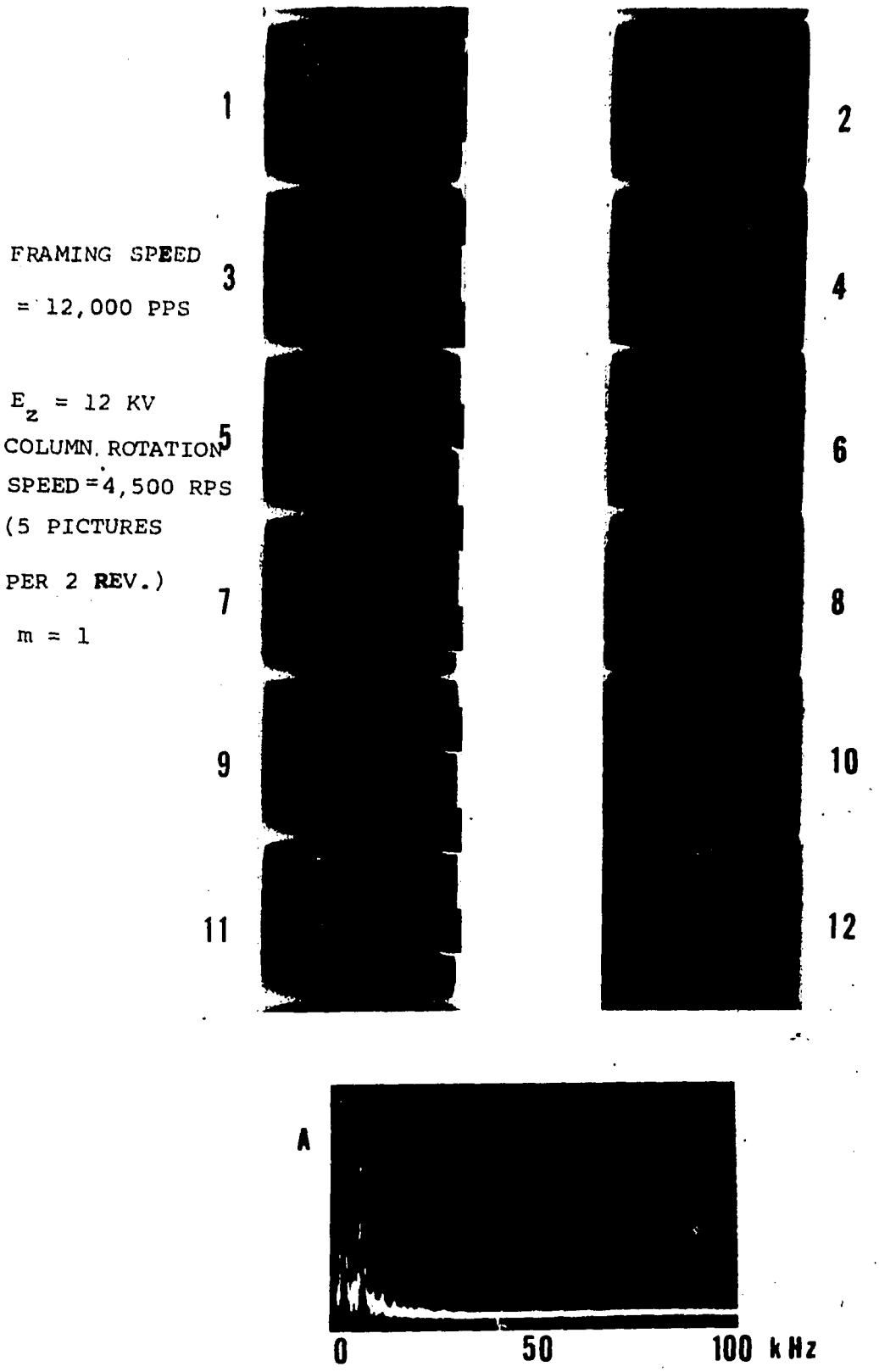

Figure 5.18 High Speed Plasma Camera Results, B = 3450 gauss

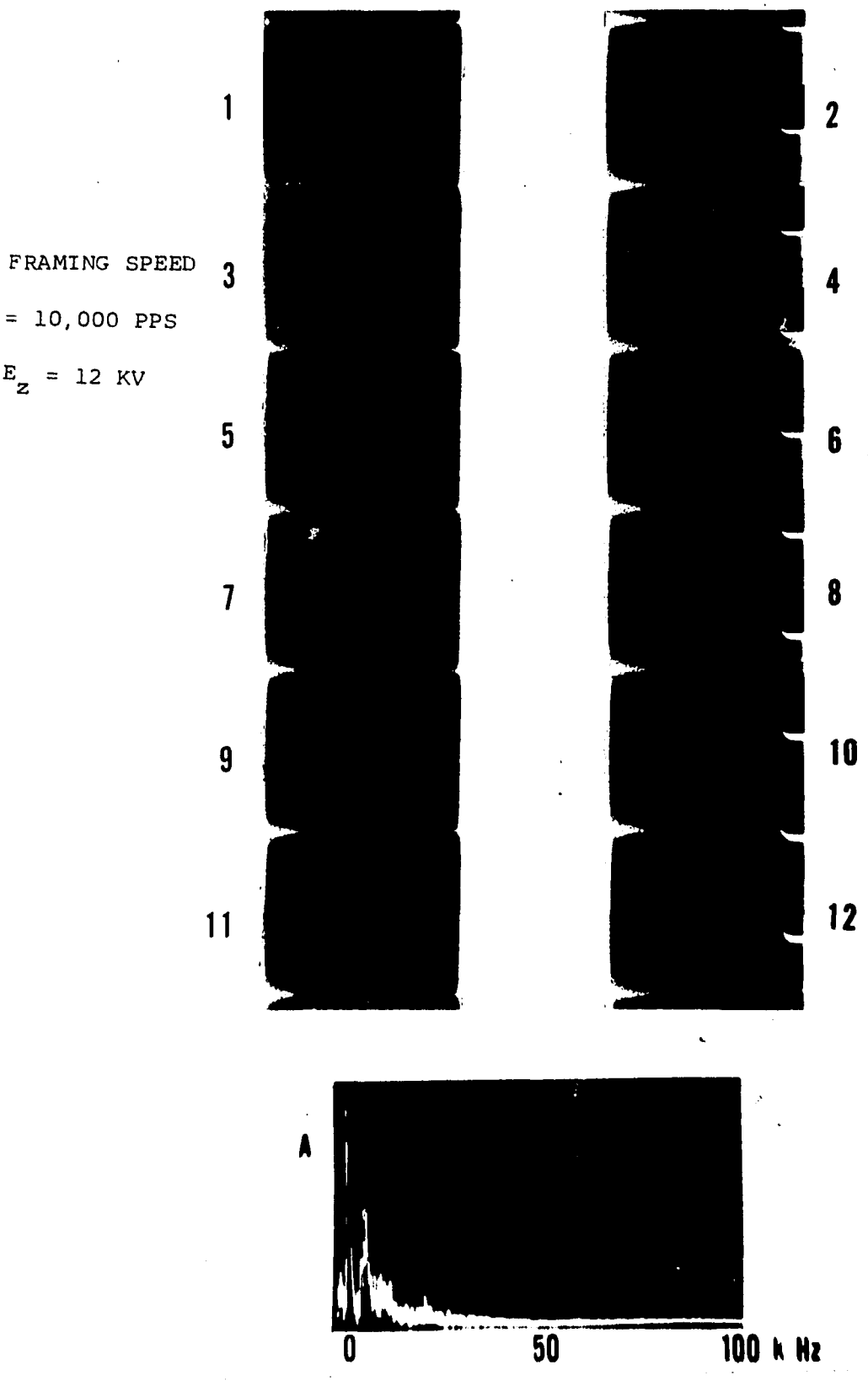

Figure 5.19 High Speed Plasma Camera Results, B = 3850 gauss

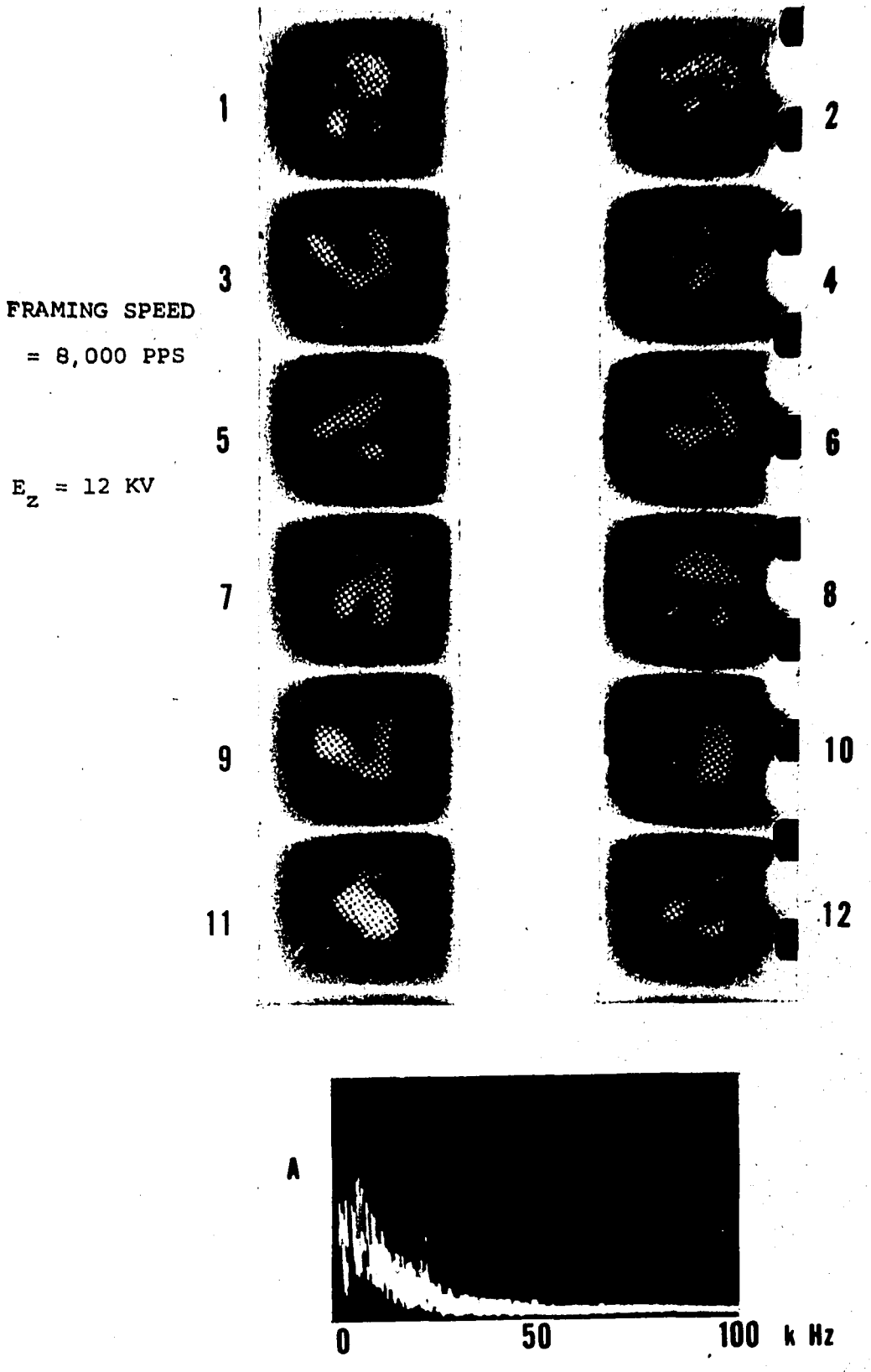

Figure 5.20 High Speed Plasma Camera Results, B = 4350 gauss

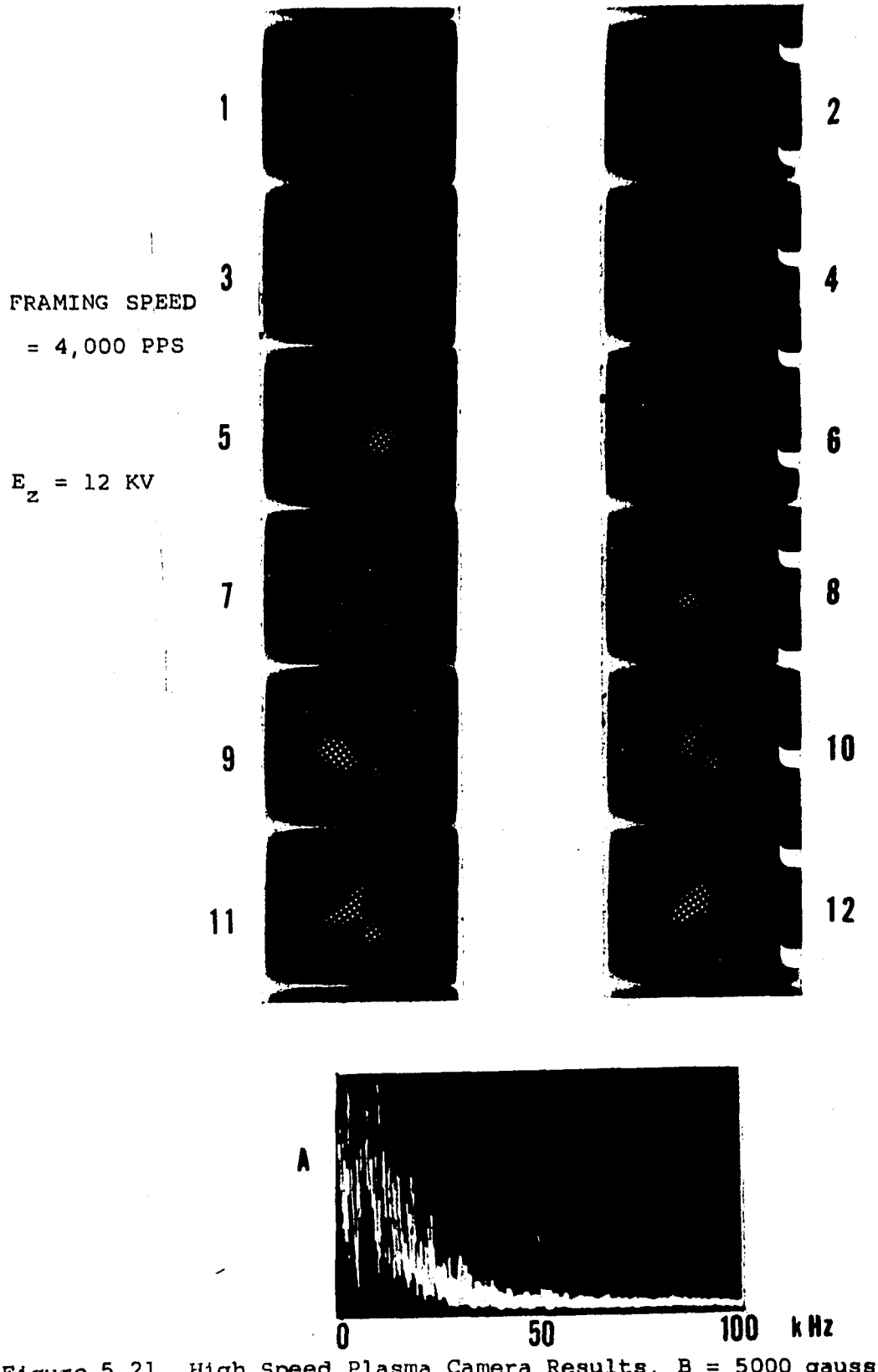

Figure 5.21 High Speed Plasma Camera Results, B = 5000 gauss

lower mode number (m = 1), while the longitudinal wave length is decreased rapidly to about one-half of the length of the column. In effect a fully developed helical instability has occurred in the column. A high density portion in the form of a left-handed helix exists which rotates azimuthally and drifts longitudinally from the hot ionizer to the cold end of the machine.

The correspondence between the frequency of density oscillation calculated from the high speed photograph framing speed and that measured by the Langmuir probe is good. Table IV presents the close agreement between the wave frequencies obtained by the two different diagnostic techniques.

When the magnetic field is raised above 3000 gauss, the helicity of the wave starts to break down due to the turbulence which is excited under the strong magnetic field. With further increase of the magnetic field the helical instability gradually develops into turbulence (Fig. 5.22). It is important to point out that the experimental observations of the development of a highly ionized potassium plasma from the helical instability into plasma turbulence verifies Kadomtsev's theory on the helical instability of a positive column.

Figure 5.23 shows the variation of the amplitude of the waves as a function of the magnetic field.

TABLE IV Correspondence of Wave Frequency by High Speed Photographic Technique and by Langmuir Probe Method

Magnetic Field, B (gauss)	Data by High Speed Photographic Technique						Langmuir Probe
	Framing Speed (pps)*	Frame Separ. (10^{-6} sec)	Cycle or Recurrence of Pictures: Frames / Rev**	Cycle or Recurrence of Pictures: μ sec / Rev**	Period of Wave (μ sec)	Frequency of wave (H_z)	Frequency of Wave (H_z)
850	13,500	74	3	223	115(m=2)	8,700	9,000
950	13,500	74	5/2	185	93(m=2)	10,600	9,000
1200	16,000	62.5	4	250	125(m=2)	8,000	8,000
1600	10,000	100	5/2	250	125(m=2)	8,000	7,400
2000	16,000	62.5	3	188	188(m=1)	5,300	5,500
2400	10,000	100	5/3	167	167(m=1)	5,950	5,500
2800	16,000	62.5	7/2	218	218(m=1)	4,700	4,500
3450	12,000	83.3	5/2	208	208(m=1)	4,800	4,500

*pps - pictures per second

**Rev - column revolution

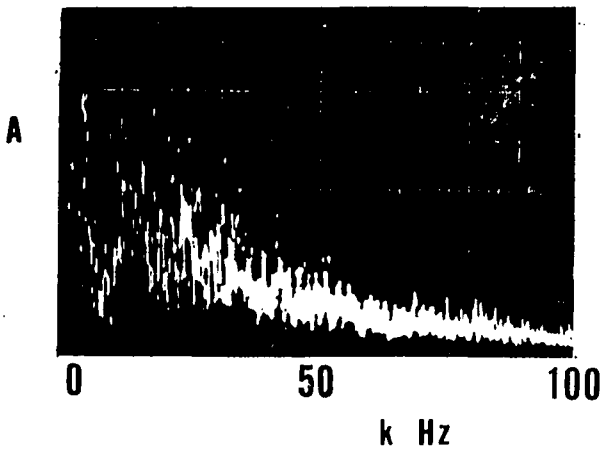

Figure 5.22 Turbulent Wave Spectrum

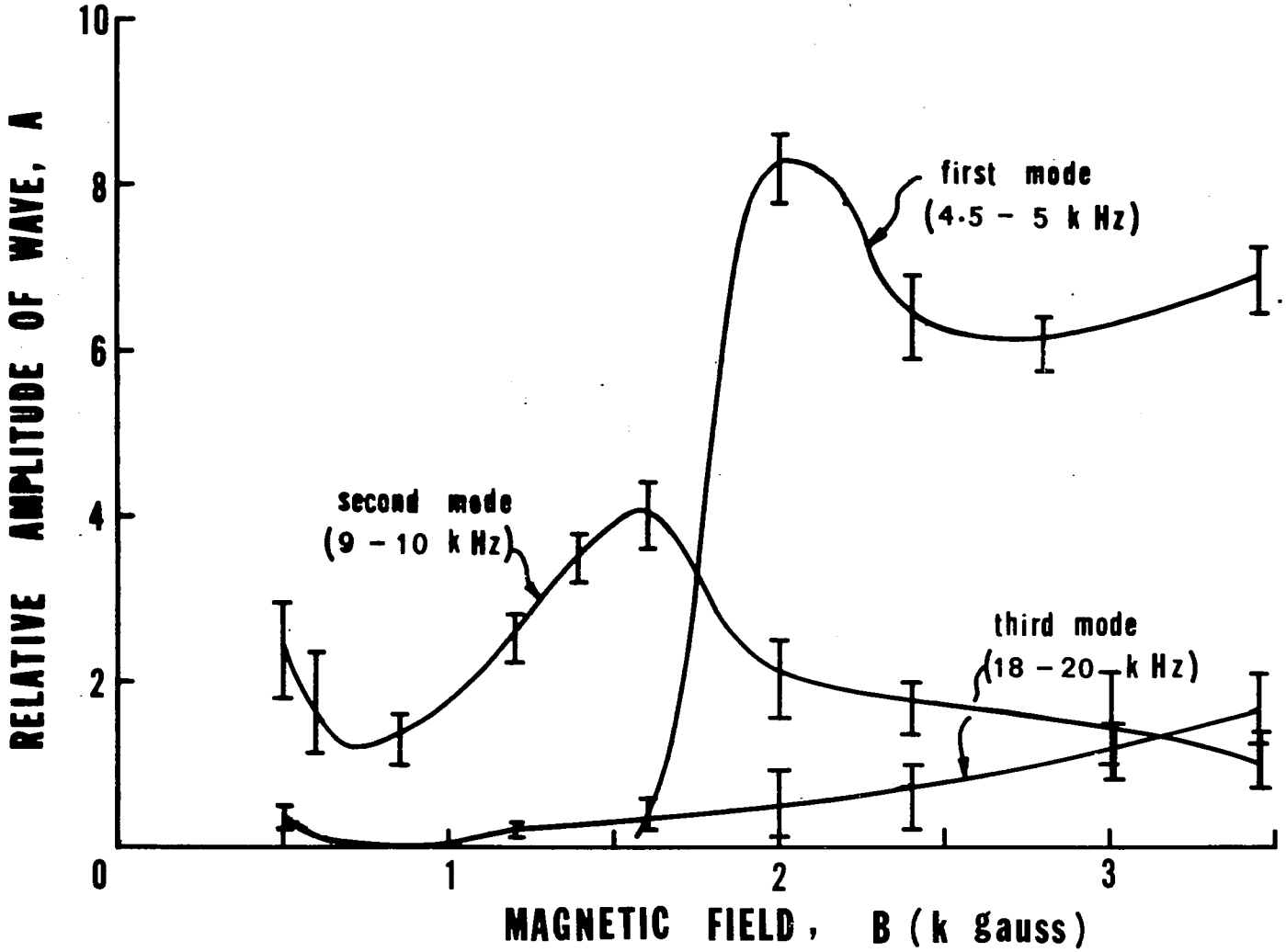

FIGURE 5.23 AMPLITUDE OF WAVES AS A FUNCTION OF THE MAGNETIC FIELD

5.9 Evidence of Non-linear Effects

The rapid increase in the amplitude of the wave above the critical magnetic field is due to the linear growth of the helical instability. The increase is leveled off approximately at B = 2000 gauss. The limitation of the fast linear growth of instability is believed due to non-linear interactions among various modes which become more predominent at high magnetic fields. This non-linear effect provides a damping on the growth of the instability. The oscillations displayed on the oscilloscope in the experiment, when shown with a large time-scale, indicated the non-linear behavior of the instability. In Fig. 5.24 the growth and damping of the waves in the unstable plasma at high magnetic fields are apparent. A time scale of 0.6 millisec. was noted between the excitation and quenching of the waves, which is long as compared with the time interval covered by the high speed plasma camera scanning. As a result the non-linear effects was registered. The variation in intensity of the plasma camera photographs at high magnetic field has demonstrated this non-linear damping effect (Figs. 5.16 and 5.17).

5.10 Effects of Other Parameters

(a) Pressure: The residue pressure in the Q-machine is not an accurately controllable parameter. However, over the range of pressure of 10^{-6} to 10^{-7} torr in the experiment the effect of pressure on the helical instability was shown to be insignificant. This is contrary to the case of the

(B = 2 k gauss)

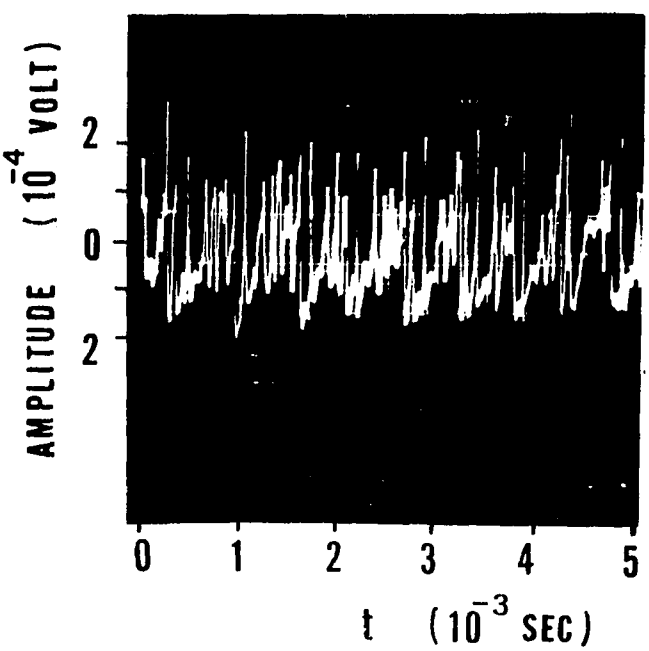

Figure 5.24 Non-linear Damping of Waves

weakly ionized gas discharge where the ionization process is by collisions between emitted electrons and neutral atoms and thus has strong dependence on the system pressure.

(b) The grid screen: In the bulk of the experiment the plasma column was terminated at the grid screen of the plasma camera scintillator assembly. The grid screen was biased to control the quantity of axial electron current flow when the positive high potential was applied onto the scintillator. For the purpose of checking whether the applied high potential extended into the main body of plasma, a second grid screen was placed between the first screen and the scintillator. The added grid screen was of the same construction as the first one and was connected electrically to ground. This arrangement assured the termination of the plasma at the first grid screen, hence subjecting no influence from the applied high potential. With the added second screen no significant change was observed in the properties of the helical instability except that the plasma camera photographs had very low intensity as well as contrast. The result of poor photographs was expected as under similar operating conditions the quantity of electrons accelerated to the scintillator was reduced nearly by half by the hindering of the additional screen.

(c) The flag: The question of whether the flag, when swung open, would create an asymmetrical field affecting the conditions of the plasma

was checked by performing experimental runs with the flag removed. No change in wave properties was observed.

(d) Plasma parameters: Variations in plasma density, temperature and the applied longitudinal electric field in the range of the experiment did not have any significant effect on the characters of the instability.

5.11 Summary

The observed abrupt change in diffusion at the critical magnetic field pointed out the presence of an instability. Langmuir probe measurements of the properties of various components of the wave established the identification of the helical mode instability at magnetic fields above the critical field strength. The instability was characterized by a rotating helix whose frequency and pitch (longitudinal wave length) have been determined. High speed plasma camera photographs further ascertained the helical characters of the instability. The sequential photographs also provided the time evolution of the instability in addition to the instantaneous density distributions of the plasma.

The helical instability grew with increasing magnetic field above B_c while nonlinear effects limited the growth of the instability. The plasma finally developed into a turbulent state. Good agreement was obtained between the results by probe measurements and those by the high speed photographic technique.

In the next chapter an analysis and conclusion of the experimental results will be presented.

CHAPTER 6

ANALYSIS AND CONCLUSION

In the range of the experiment the particle number density, $n = 10^{10} - 10^{11}$ cm^{-3}, the temperature $T = 2300\,^{o}K$, the observed frequencies, $\omega \approx 10$ k Hz, the calculated self-collision time[45] for the electrons, t_{ce} is of the order of 10^{-7} sec., the condition of $\omega t_{ce} << 1$ is easily satisfied. For the ions, ωt_{ci} is of the order of unity. The motion of electrons can be treated as a fluid in studying their motion along the magnetic field, and the motion of ions is primarily transverse to the magnetic field. Since the condition $\omega << \omega c_i$ is satisfied, the plasma is to be considered in the collision dominant regime. The discussions to follow pertain only to the collisional plasmas.

6.1 Discussion on the Identification of the Helical Instability

As stated in Section 5.6 the observed phenomenon in the experiment has been identified as the helical mode instability by both the Langmuir probe method and the high speed photographic technique. However, a highly ionized, non-uniform plasma in a magnetic field, such as the surfacely ionized potassium plasma under investigation, is inherently subject to instabilities leading to low frequency oscillations ($\omega << \omega_c$)[46]. The helical instability as well as the drift and flute instabilities all fall in this group. The driving mechanisms may be density gradient, the tempera-

ture gradient or electric current flow in the plasma, potential gradient, electric resistivity, the curvature of the confining magnetic field, or any combination of these factors.

Since the oscillations arising from the helical, the drift and the flute instabilities are in the same frequency range and of similar characters (i.e. azimuthal waves with zero or finite longitudinal wave number, k_z), and they may be present concurrently, the identification of the helical instability, separating it from other possible instabilities, deserves further attention.

First the density gradient driven drift instability is considered, for in this experiment the density gradient is significant and localized near the edge of the plasma column. The drift instability is characterized by (i) the correspondence of its phase velocity, v_{ph} to the diamagnetic drift, v_d due to the interaction between the density gradient and the magnetic field, (ii) large longitudinal wave length as compared with the column length, and (iii) the parametric dependence of the wave properties on the magnetic field. More specifically it is summarized, for the drift waves as follows:

(i) The azimuthal propagation is in the direction and of the order of the electron diamagnetic drift, v_d, where

$$v_d = - \frac{kT}{eB} \frac{\nabla n}{n}$$

A relation, $v_{ph} = \frac{1}{2} v_d$ is predicted by linear theories for the

maximum growth rate of the drift instability and is verified by experimental observations for collisional plasmas.

(ii) The longitudinal wave is a standing wave with a wave length, $\lambda_z \geq 2L$.

(iii) Waves of higher modes have high growth rate and are expected to occur at high magnetic fields, $m = 1$ mode has the lowest growth rate and is not usually observed in experiments.

In the present experiment linear correspondence between v_{ph} and v_d is not found. The azimuthal phase velocity of the observed oscillation, as shown in Fig. 6.1, does not have significant dependence on the magnetic field. The v_{ph} and v_d relation changes from $v_{ph} < v_d$ for $B \leq 700$ gauss to $v_{ph} \approx v_d$ for $700 < B \leq 1600$ gauss, and to $v_{ph} > v_d$ for $B > 1600$ gauss. This is in conflict with the character of the drift wave (i) above. The longitudinal wave length, λ_z measured in the experiment varies from an extremely large value ($\lambda_z \geq 20L$) at $B < 700$ gauss to a length of approximately $0.5L$ at $B = 2400$ gauss. The short λ_z cannot satisfy the requirement of (ii) above of the drift waves. The observation of $m = 1$ mode at $B \geq 2000$ gauss, while $m = 2$ mode at lower B further substantiates the conclusion that the drift wave is not observed in the experiment at $B \geq 1600$ gauss.

Secondly the possibility of the flute mode instability being observed in the experiment is considered. Owing to the configuration of

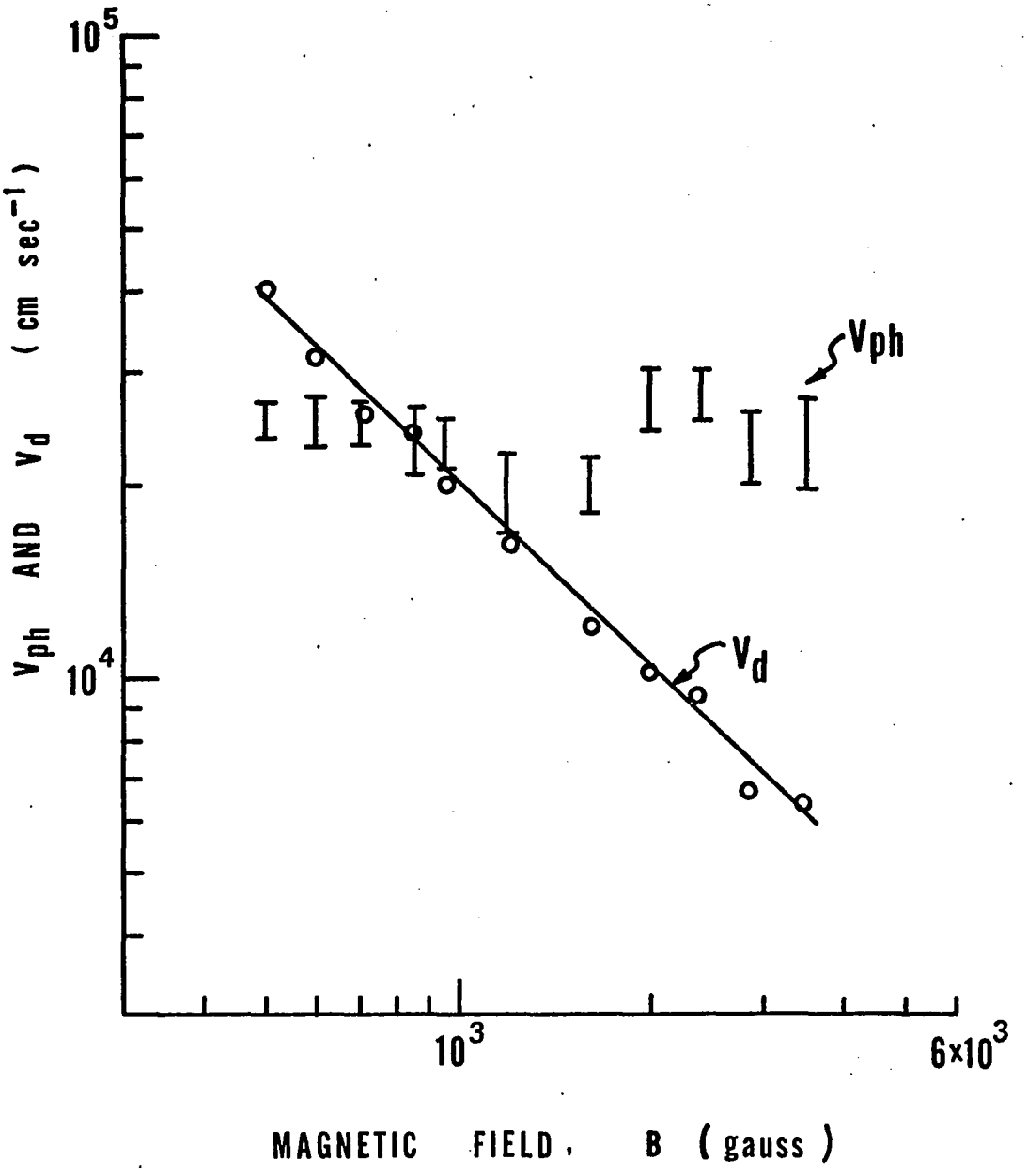

FIGURE 6.1 AZIMUTHAL PHASE VELOCITY, V_{ph} AND DIAMAGNETIC DRIFT, V_d

the plasma, in addition to the density gradient, the sharp potential gradient and the large temperature drop at the edge of the column, the plasma is subject to the Kelvin-Helmholtz type flute instability. The flute instability is characterized by the infinite longitudinal wave length ($k_z = 0$) and the maximum amplitude of oscillations at the column edge. In this experiment, however, at $B \geq 700$ gauss finite longitudinal wave length ($k_z \neq 0$) is observed. It negates the possibility of the flute instability being observed at $B \geq 700$ gauss. Furthermore, the observation of $m = 1$ mode at a higher magnetic field than that for the higher modes is contrary to the theoretical prediction and experimental observations of the flute mode.

From the foregoing discussions, together with measured characters of the instability (Sections 5.4 to 5.8), it is established that at $B \geq 1600$ gauss only helical instability is present in the plasma. The same conclusion, however, cannot be drawn for the range $700 \leq B < 1600$ gauss, in which the presence of the drift instability cannot be ascertained. Below 700 gauss, the helical instability is not excited and only the flute instability is present.

6.2 Characters of the Helical Instability

(a) General Description

The analysis of the helical mode instability is complicated by the existence of the longitudinal component in the predominant azimuthally

propagating wave in an asymmetrical plasma column. The instability occurs only in the presence of the longitudinal electric field and current flow and when the magnetic field exceeds B_c. At $B < B_c$ the plasma is stable against helical perturbations. The oscillations observed then are of the flute mode. The plasma column is generally symmetrical in a straight cylindrical form with flute-like density oscillations near the edge of the column.

At $B > B_c$, beyond the onset of the helical instability, the oscillations have a finite k_z, although they are predominantly azimuthal. The longitudinal wave length is large compared with the length of the column, which remains generally cylindrical with slightly helical density perturbations appearing as twisted flutes. Figure 6.2(a) is a schematic description of the column. This holds true for a moderate increase of the magnetic field above B_c (B = 700 to 1600 gauss) except with a decrease of the longitudinal wave length, or more "twist" in the density perturbations. When the magnetic field is raised to significantly higher than B_c (B = 1600 to 2800 gauss) the helical instability is fully developed. The density oscillations are no longer confined to the region near the column edge, nor does the column maintain its straight cylindrical geometry. Instead, helical density oscillations of high amplitude penetrate the bulk of the column. Figure 6.2(b) depicts the plasma column with the fully developed instability. The longitudinal wave length λ_z, i.e. the pitch of the helix is comparable to, or less than the length of the column.

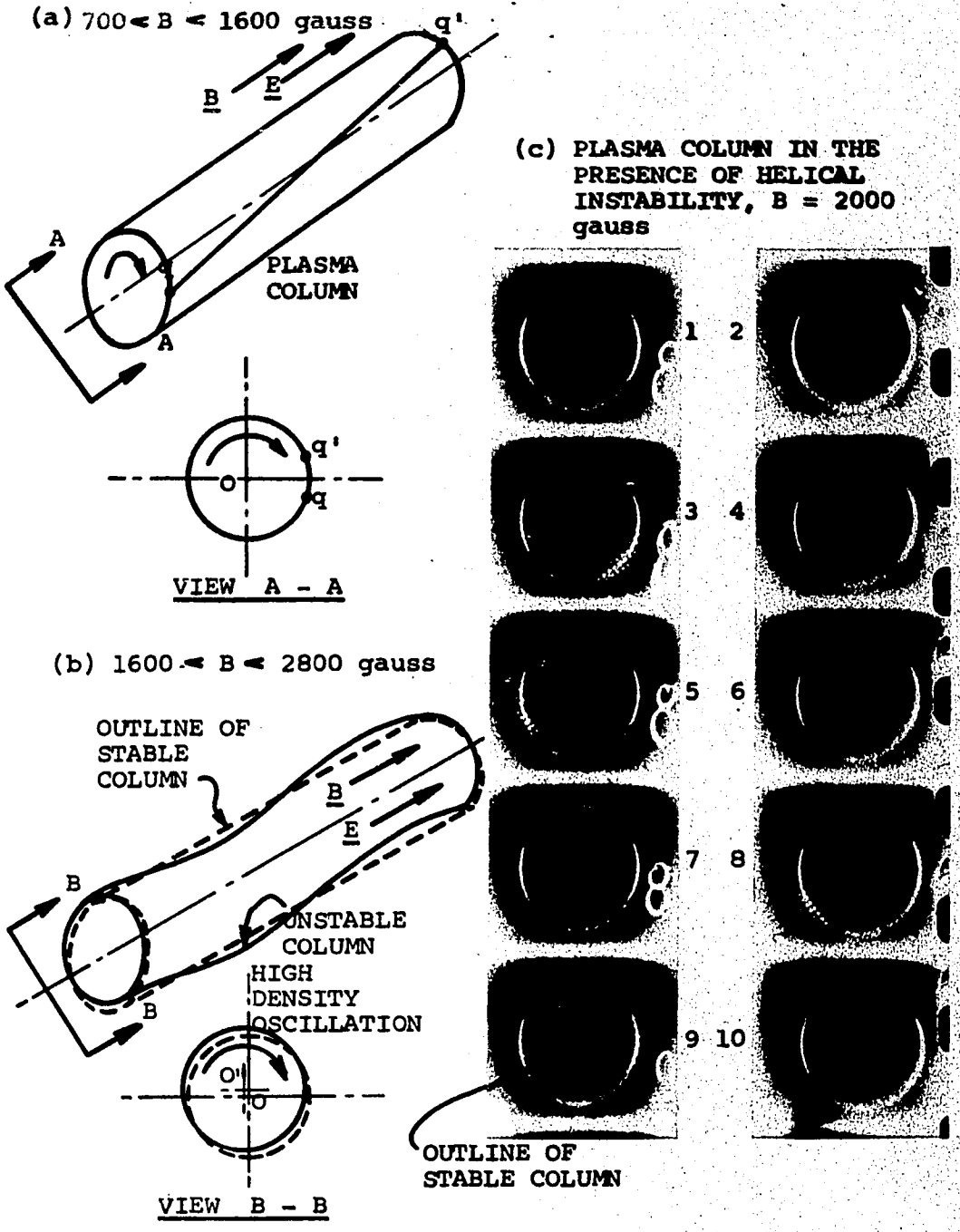

FIGURE 6.2 SCHEMATIC DESCRIPTION OF THE DEVELOPMENT OF THE HELICAL INSTABILITY IN A PLASMA COLUMN

While Langmuir probe measurements are responsible for the determination of λ_z, the form and extent of the density oscillations, the asymmetry or "off-set" of the column from the original stable geometry due to helicity are not readily detectable by the probe. They are observed and analyzed by the use of the high speed plasma camera. Figure 6.2(c) shows the typical high speed plasma camera photographs of the column, superimposed with the outline of a stable column to reveal the "off-set" of the column due to helical instability.

The unstable plasma with the helical instability develops into turbulence at strong, magnetic fields (B = 5000 to 6000 gauss) due to interactions of many excited modes.

(b) Plasma Density Oscillations - A Rotating Helix

Since the identification of the helical instability has been established, the salient features of the helical density oscillations are of interest. The direction of helicity was observed to be left-handed by moving the longitudinal probe and noting the change of the phase shift with respect to a fixed radial probe used as the trigger probe. Figure 6.3 gives a description of the method for determination of the direction of the helicity of the density oscillations. Since the azimuthal propagation of the wave is in the direction of the electron diamagnetic drift, if the helix is left-handed a travel of the longitudinal probe in the direction of the electric current flow will be accompanied by movement of the moving probe signal to the left with respect to the trigger signal. The reverse is true

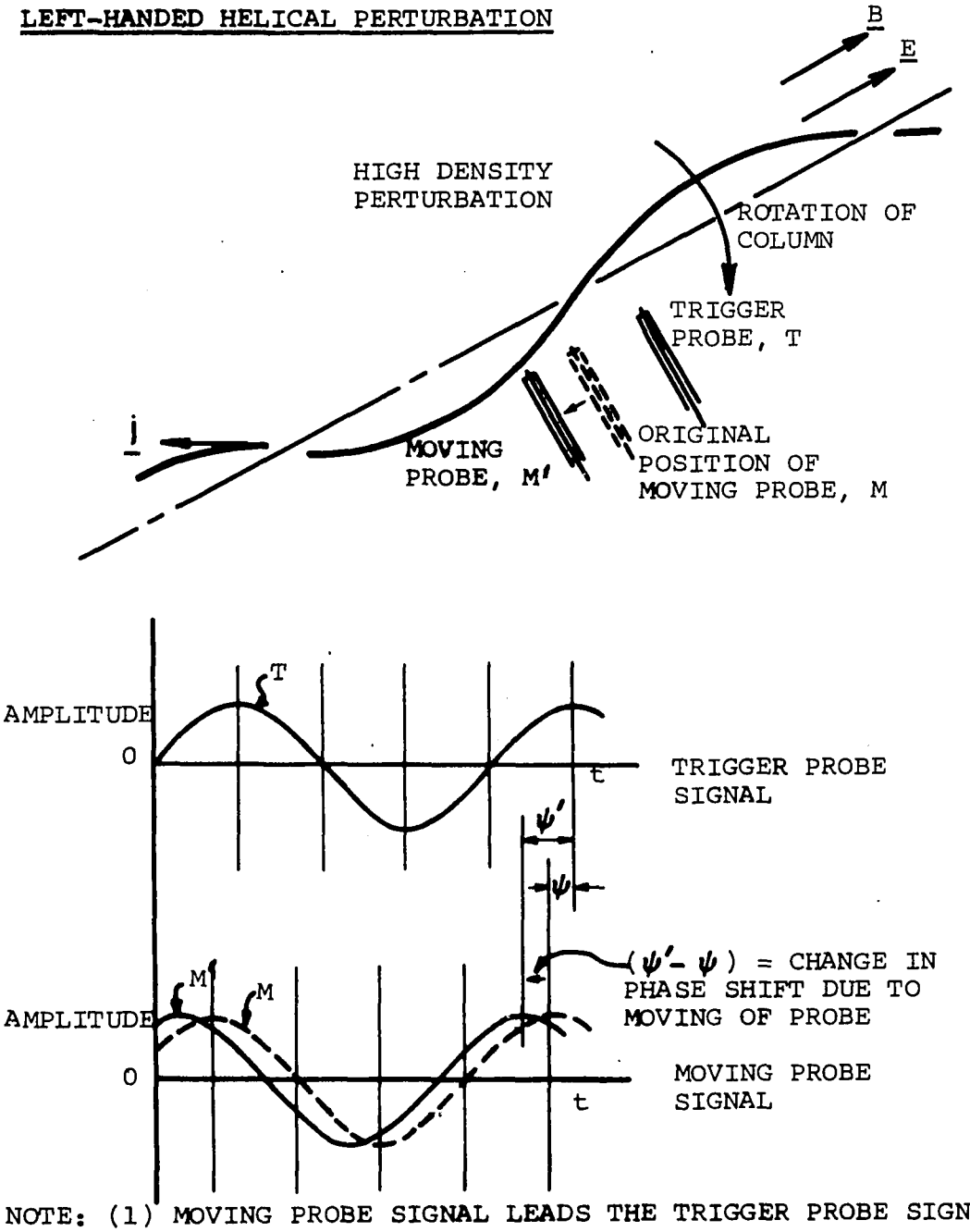

NOTE: (1) MOVING PROBE SIGNAL LEADS THE TRIGGER PROBE SIGNAL.

(2) MOVING THE PROBE IN THE DIRECTION OF THE STREAMING PLASMA RESULTS IN AN INCREASE OF THE LEAD (THE PHASE SHIFT), i.e. AN ADVANCING OF THE MOVING PROBE SIGNAL TO THE LEFT.

FIGURE 6.3 METHOD FOR DETERMINATION OF THE DIRECTION OF HELICITY

for a right-handed helix.

With regard to the direction of the helical wave, it should be noted that the difference between a rotating helix and an advancing helix cannot be detected by simple direct measurements using the radial Langmuir probes and the high speed plasma camera. The former measures the local properties of the wave and the latter visualizes the cross-sectional density distribution of the streaming plasma at constant time intervals. In each case, a rotating helix or an axially advancing helix will render similar oscillatory density variations. The helical oscillation can, however, be determined by an indirect method by comparison of the properties of the helical wave by those of the flute instability which occurs under similar experimental conditions except without the electric field and current along the column. The flute instability is known to propagate only in the azimuthal direction (Section 5.1a). The application of the longitudinal electric field in the case of the helical instability is not expected to affect any change in the azimuthal motion of the plasma from that of the flute instability. Hence any longitudinal propagation (axially advancing) of the helical wave will be reflected in the change in the measurement of density oscillations by the probe or by the high speed plasma camera. It will result in a decrease (or an increase) of the measured frequency if the helical wave is left-handed (or right-handed). As an example, we consider the case with B = 2000 gauss, $\lambda_z = 0.6\,L = 28$ cm. If the helical wave were advancing along the column

with a streaming velocity of the order of the ion thermal velocity $v_{ph} \approx 10^5$ cm/sec, the measured frequency v_{ph_z}/λ_z would have been ≈ 3.6 kHz. This frequency would have to be superimposed on, i.e. subtracted from the azimuthal frequency f/m (= 5 kHz), resulting in a frequency of 1.4 kHz, because the observed helical wave is in the left-handed direction. However, the experimental measurements indicate no such change in frequency when observing the helical wave. Figure 6.4 is a typical frequency spectrum of the helical wave as compared with that of the flute mode. From the above it is evident that the helical wave is in the form of a rotating helix with electrons moving freely along the helical density filament, but the helix itself does not advance or propagate along the column.

It should be remarked that in the case of the drift instability where the wave resembles that of the helical instability except the large λ_z ($(\lambda_z)_{drift} \geq 2L$) the linear theory also predicts a standing wave in the direction along the column.

6.3 Diffusion Across the Magnetic Field

Direct measurement of diffusion of plasma across the magnetic field obtained in the present experiment is more desirable than the indirect methods used by some investigators, because it can give a more accurate representation of the magnitude as well as the dependence on the magnetic field. However, the magnitude of the diffusion rate should not be over

(a) FLUTE INSTABILITY (m = 2, f/m = 5 k Hz)

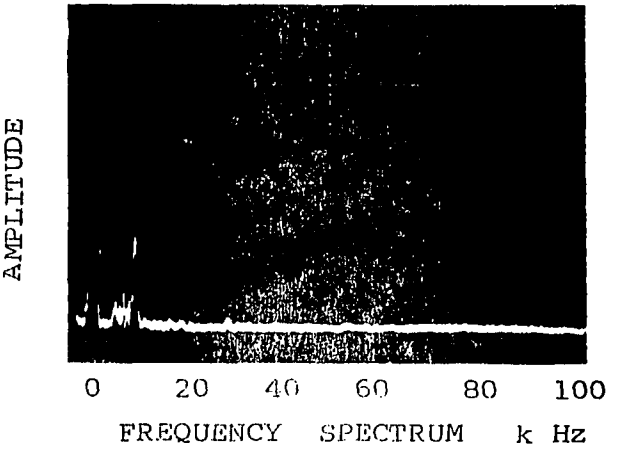

(b) HELICAL INSTABILITY (m = 1, f/m = 5.5 k Hz)

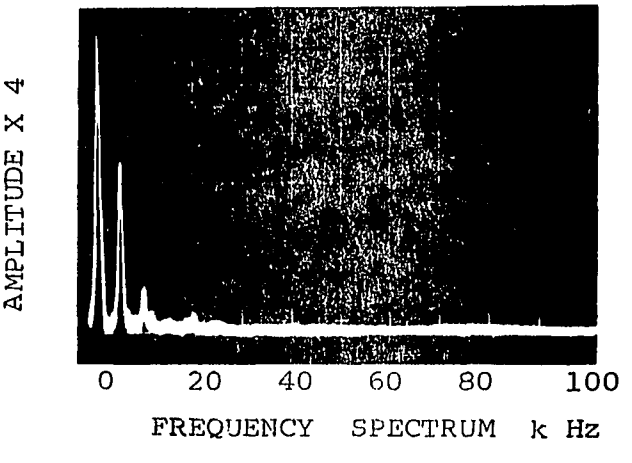

FIGURE 6.4 AZIMUTHAL WAVE SPECTRA - FLUTE AND HELICAL INSTABILITIES, B = 2000 GAUSS

emphasized as the diffusion measurements may be sensitive to the plasma oscillations, variations in plasma parameters, (n, T, p, etc.), and the design and the physical location of the measuring device with respect to the plasma column. They are representative only to the plasma under investigation at the specified experimental conditions.

In the experiment the unusual character of the transverse diffusion of plasma in the presence of the longitudinal electric and current flow is important to note (Fig. 5.3). The enhanced diffusion at $B > B_c$ signifies an abrupt change of the diffusion process, which in turn points to the onset of the helical instability, as verified by the Langmuire probe measurements of the longitudinal component of the wave. The increase of diffusion with an increasing magnetic field draws a parallel to that observed in weakly ionized plasmas in which a helical instability is also present. The range of the magnetic field, in which the diffusion increases abruptly with an increasing field, is relatively small. This abrupt increase of diffusion at the onset of instability is not dissimilar to that observed in the study of the collisional drift instability.

The presence of enhanced diffusion extends to magnetic fields about 20% higher than B_c (B = 700 to 850 gauss). In the range $850 < B < 3000$ gauss, the diffusion follows Bohm ($D \propto B^{-1}$), but is approximately one order of magnitude lower. The relatively high diffusion rate is attributed to the presence of the helical instability. At $B > 3000$ gauss the waves due to the helical instability start to breakdown due to the onset of

multi-modes. $D \propto B^{-2}$ dependency exists except that the diffusion is still large, about two orders of magnitude higher than the classical diffusion. At B = 5000 gauss, the plasma approaches a turbulent state.

A high diffusion rate does not occur when turbulence is present in the plasma, rather it occurs after the helical instability is excited. The perturbed azimuthal electric field resulted from the density oscillation due to the instability is responsible for the high rate of diffusion across the magnetic field.

6.4 Mechanism of Helical Instability

The helical instability is attributed to the growth of helical density perturbation of higher-than-average density in the plasma which has an inherent azimuthal drift due to the radial density gradient. With the helical density perturbations the longitudinal electric current follows the helical paths, hence the current j has a non-zero $j_\perp$ component. The $j_\perp$ component will interact with the magnetic field, and hence a $j_\perp \times B$ drift results in the direction away or toward the axis if the helix is left-handed or right-handed, respectively.

Figure 6.5 presents a schematic description of the mechanism of the helical instability. (a) depicts the effect of the longitudinal current along the left-handed helical path. The $j_\perp \times B$ drift is in the direction away from the axis, contributing the growth of the instability. (b) described the microscopic effects of the mobilities of the electrons and ions

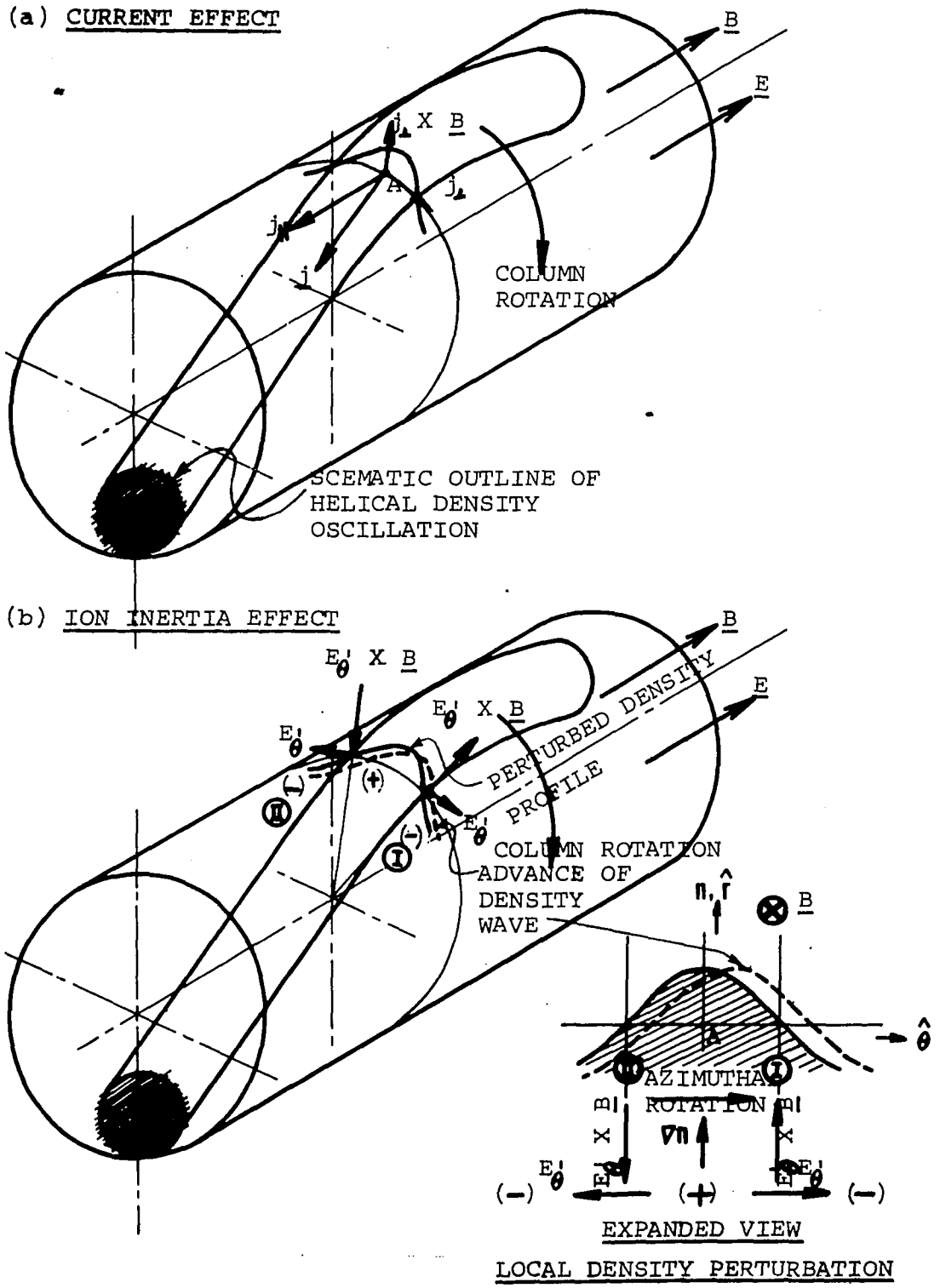

FIGURE 6.5 SCHEMATIC DESCRIPTION OF THE HELICAL INSTABILITY

on the instability.

The electric potential in the high density perturbation is higher than that of the background, because the electrons are more mobile and tend to move to the low density neighborhood. Azimuthally there are electric field perturbations, E'_θ resulting from the microscopic charge separation and acting away from the high density perturbation. The (+) sign indicates the region of high potential and the (-) sign refers to the opposite. The azimuthal electric field perturbations and the magnetic field give a $E'_\theta \times \underline{B}$ (radial) drift. The $E'_\theta \times \underline{B}$ drift is outward in region (I) bringing out high density plasma, and inward in region (II), pushing in the density perturbation there. This amounts to a propagation of the high density perturbation in the clockwise direction. Diagrams (a) and (b) should be superimposed to view the combined total effect.

The effects of the magnetic field are two-fold, one is tied with local diffusion of the high density perturbations, and the other is related to the finite Larmor radius effects of the ions.

Once a helical high density perturbation is formed, if the magnetic field strength is low, the perturbation will soon subside because the plasma is free to diffuse out from the high density region. If the magnetic field is increased, the local diffusion is reduced at a rate proportional to B^{-2}, while the radially outward $j_\perp \times \underline{B}$ drift decreases at a rate proportional to B^{-1}, i.e. the local diffusion decreases at a faster rate than that of the $j_\perp \times \underline{B}$ drift. At B_c the $j_\perp \times \underline{B}$ drift dominates and the high

density perturbation persists and grows. This explains the necessity of the longitudinal electric current and the critical magnetic field in the development of the helical instability.

The finite Larmor radius of the ions affects the magnitude of the density perturbation by the averaging effect of the ions gyrating near the boundary of the perturbation. It tends to "smear" out the potential difference there (Fig. 6.5(b)). In the range where the helical instability is present the ion Larmor radius is between 0.2 and 0.6 cm. Within this range, if the magnetic field is high the averaging effect of the ions at the boundary of the perturbation is low and the variation in potential is abrupt. Higher radial drifts are expected, and hence contribute to the growth of the perturbation. The increase of the amplitude of the observed helical wave with the magnetic field from 700 to 2000 gauss (Fig. 5.23) is in confirmity with this explanation.

When the magnetic field is high ($B > 3500$ gauss), onset of multi-mode waves occurs. They develop in a similar way as discussed above except that they become unstable at a higher critical magnetic field and grow to induce waves of many modes (not harmonics). The interactions among them cause the plasma to become electrostatically turbulent. The transition to turbulence can be seen from the wave spectra of Fig. 5.17 ($B = 2800$ gauss) to Fig. 5.21 ($B = 5000$ gauss).

With the presence of the helical instability, the electron motion along the column tends to equalize any transverse potential difference

due to the helical wave when they reach the ends of the column. This constitutes a stabilization factor which limits the helicity of the density wave. The longitudinal electron motion is governed by the electric current flow and the electric resistivity, η along the column. Low electric resistivity corresponds to less-hindered electron motion along the magnetic field and the helical instability then will not occur. In the experiment η is approximately 5×10^{8} e.m.u. and is not a controllable experimental parameter.

6.5 Conclusions

This investigation on a highly ionized potassium plasma produced by surface ionization in a Q-machine has attained the following goals and findings:

(1) The helical instability in a highly ionized plasma is observed and identified. While the helical instability has been observed in weakly ionized gas discharge plasmas, the present investigation is the first to identify its presence in a highly ionized plasma.

(2) The helical instability occurs when the longitudinal electric field and current are present and the magnetic field exceeds a critical value, B_c (= 700 gauss). The wave propagates azimuthally but has a standing longitudinal component resembling

a rotating helix, m = 1 mode dominates the azimuthal propagation when the magnetic field is high above B_c (B = 2000 to 2800 gauss).

(3) The rotation of the helix is in the direction of the electron diamagnetic drift. The helical density wave is left-handed and its longitudinal wave length, or pitch of the helix, is comparable to or less than the length of the column.

(4) The longitudinal electric current is essential for the helical instability to occur. However, its magnitude does not have significant effect on the amplitude of the instability in the range of the experiment. The system pressure, which ranges from 10^{-6} to 10^{-7} torr, does not have any significant effect on the instability.

(5) The general properties of the helical instability of a highly ionized plasma are analogous to those in a weakly ionized gas discharged plasma except in the latter case the system pressure is an important parameter, because the ionization process in the gas discharge plasma is by collisions between the emitted electrons and the gas neutrals. Thus the degree of ionization is governed by the pressure in the system.

(6) Direct measurements of plasma diffusion across the magnetic field have been made by using a transverse diffusion collector

specifically designed for the experiment. Enhanced diffusion is observed when the magnetic field is increased above B_c, and the diffusion increases with the confining magnetic field, instead of decreasing with B^{-2} dependency as is for the case of $B < B_c$. This abrupt change of diffusion process signifies the on-set of the helical instability which is verified by the measurements of the longitudinal wave length by the Langmuir probes.

When the magnetic field is high above B_c, i.e. $850 < B < 3000$ gauss, the diffusion changes to $D \propto B^{-1}$ dependency while large amplitude helical waves are observed. It changes, again, to $D \propto B^{-2}$ dependency for $3000 < B < 6000$ gauss, where the coherent waves start to breakdown and develop into turbulence. It indicates that Bohm diffusion corresponds closely to large amplitude oscillations rather than the turbulent state of the plasma.

(7) A high-speed photographic technique has been developed and applied to the study of plasma instability. The usefulness of this new diagnostic technique has been demonstrated by its ability to study the instantaneous density distribution and the time evolution of the plasma in the presence of instabilities. This method has the advantage of scanning the whole cross-section of the plasma without disturbance to it, in constrast

to the point-to-point local measurements by physical insertion of the Langmuir probe into the plasma.

This photographic technique in conjunction with the Langmuir probe provides more complete information on the behavior of the plasma. The adoption of the high speed photographic method has extended the measurements of the properties of the plasma to both the spatial and time regimes in the study of plasma instabilities, to which the time variation of plasma parameters in the complete domain of plasma is important. This is an improvement to the conventional probe method which can only obtain information of the time variation at fixed locations or information of the spatial variation at different times.

The photographic technique using the high speed plasma camera has been proven to be a powerful new diagnostic tool particularly useful not only in the investigation of the onset and evolution of plasma instabilities, but also in studies of the transient phenomena, mode-mode coupling and turbulence in the plasma.

(8) A turbulent plasma and its development from the helical instability have been observed. The theoretical analysis on the helical instability in weakly ionized gas discharge plasmas predicts the development of the instability into turbulence at

magnetic fields high above B_c. The turbulent state, however, has never been observed experimentally due to the failure to sustain the plasma column at magnetic fields significantly higher than B_c. In the present investigation the turbulent state of the plasma is not only detected by the frequency spectra of the waves, but also visualized by the high speed plasma camera photographs showing the plasma with fast and randomly changed density distributions.

(9) A description of the mechanism of the helical instability in a highly ionized plasma is given. This description, together with the results of the experiment, presents a physical model, upon which theoretical investigation may be based.

APPENDIX

METHOD FOR MEASURING THE AZIMUTHAL MODE NUMBER OF WAVES

A.1 General Description

Two Langmuir probes, the 2-dimensional (r, θ) probe and the radial probe, are used for the determination of the direction of the propagation and the mode number of the waves. The two probes are positioned at an angle, θ_1 apart but with the same r- and z-coordinates. With one probe used as the trigger and θ_1 predetermined, the direction of azimuthal propagation and the mode number can be computed from the observed phase shift between the density (or potential) oscillations of the two probes.

The method of setting the angle, θ_1 is shown in Fig. A.1. The determination of the direction of propagation and the mode number of the azimuthal wave are given in the following sections.

A.2 Determination of the Direction of Propagation

The direction of propagation of the azimuthal wave is determined by noting the change in the phase shift between the signals of the stationary trigger probe and the moving probe which moves only in θ direction. Basically this method is to determine the "lead" or "lag" of the signals of the moving probe with respect to the trigger probe signals on the dual beam oscilloscope. Since the relative positions of these probes are known, the "lead" or "lag" of the moving probe signals indicates the direction of the

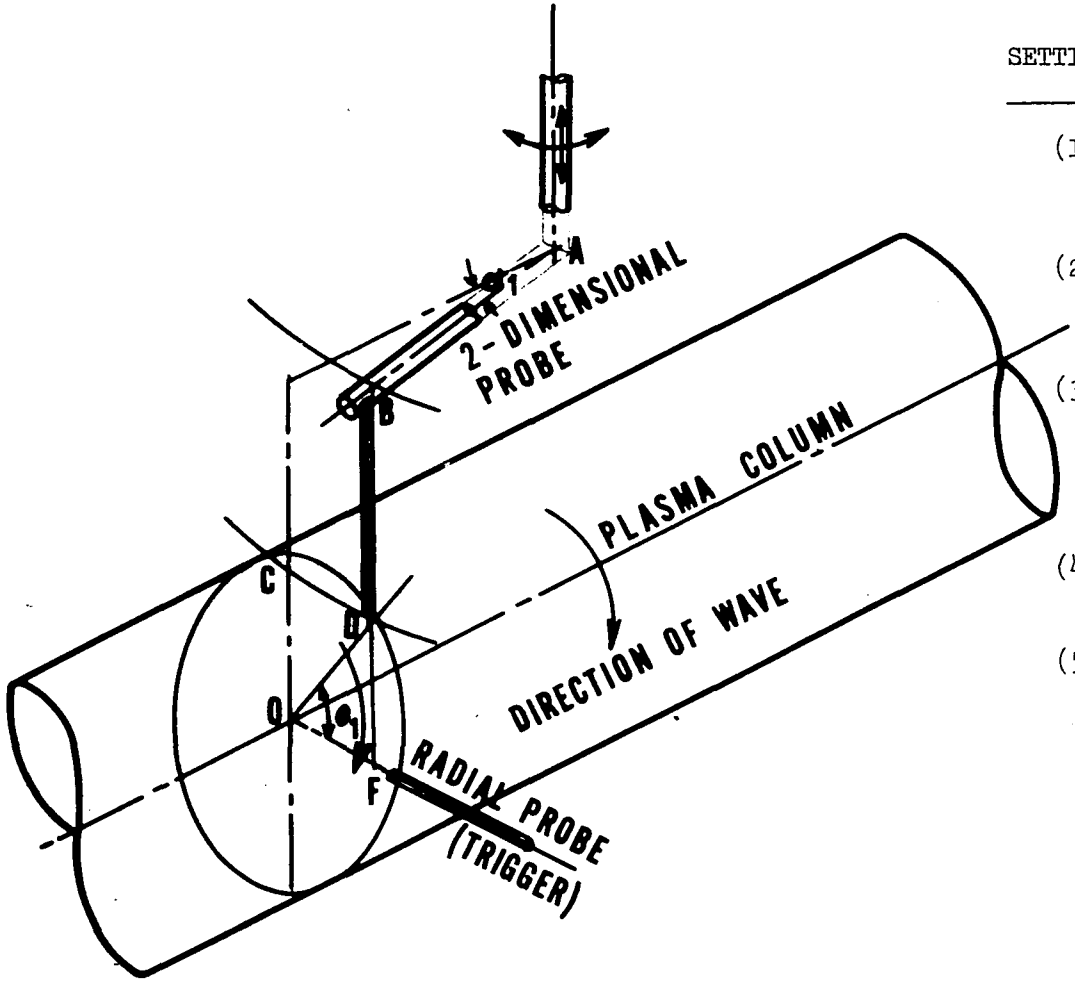

SETTING OF THE ANGLE, θ_1 BETWEEN THE TWO PROBES

(1) LOCATE O ON THE AXIS AS REFERENCE. THERE SET $r = 0$, $\alpha_1 = 0$ FOR 2-DIM. PROBE AND $r = 0$ FOR RADIAL PROBE.

(2) POSITION THE 2-DIM. PROBE AT D, DF (=OC) AND α_1 ARE THEN KNOWN; AB = ARM OF PROBE, ALSO KNOWN.

(3) FOR THE 2-DIM. PROBE, OBTAIN r AND θ_1 FROM

$\theta_1 = \tan^{-1} DF/DC$, WHERE $DC = AB \sin\alpha_1$
$r = OD = DF/\sin\theta_1$.

(4) POSITION THE RADIAL PROBE AT $r = OF = OD$.

(5) NOW THE TWO PROBES ARE AT AN ANGLE, θ_1 APART, BUT AT THE SAME r AND z.

NOTE: DEVIATION FROM CONSTANT z IS LESS THAN ONE-HALF PERCENT.

FIGURE A. 1 ARRANGEMENT OF THE TWO-DIMENSIONAL AND THE RADIAL PROBES FOR MODE NUMBER MEASUREMENT

azimuthal wave propagation. Figure A.2 illustrates how the direction of propagation is determined.

A.3 Determination of the Azimuthal Mode Number

The azimuthal mode number, m indicates, in a physical sense, the number of cycles of the wave propagating one complete path around the plasma column. The wave is the density oscillations measured by the Langmuir probes held stationary relative to the wave. Figure A.3 is a schematic diagram illustrating the azimuthal waves and the corresponding density oscillations in the plasma column. With the aid of the high speed plasma camera, the density oscillations of various mode numbers have been observed. Good agreement between the mode number measured by the probes and the density oscillations observed by the plasma camera can be seen in Figs. 5.11 to 5.14 with m = 2, and in Figs. 5.15 to 5.18 with m=1.

Before the actual determination of the phase shift between the probe signal and the trigger signal, the direction of propagation of the waves has to be known, as it establishes the proper relation between these signals. Figure A.4 gives the values of m determined from the phase shift measured at the two probes.

As can be seen from Fig. A.4, uncertainty may arise in the determination of m, because in the oscilloscope display the phase shift of 1/4 wave length and that of 1-1/4 wave length are not differentiable. For example, with $\theta_1 = 90^{\circ}$, phase shift = 1/4 wave length, the mode number,

CASE I MOVING PROBE SIGNAL "LEADS" THE TRIGGER SIGNAL

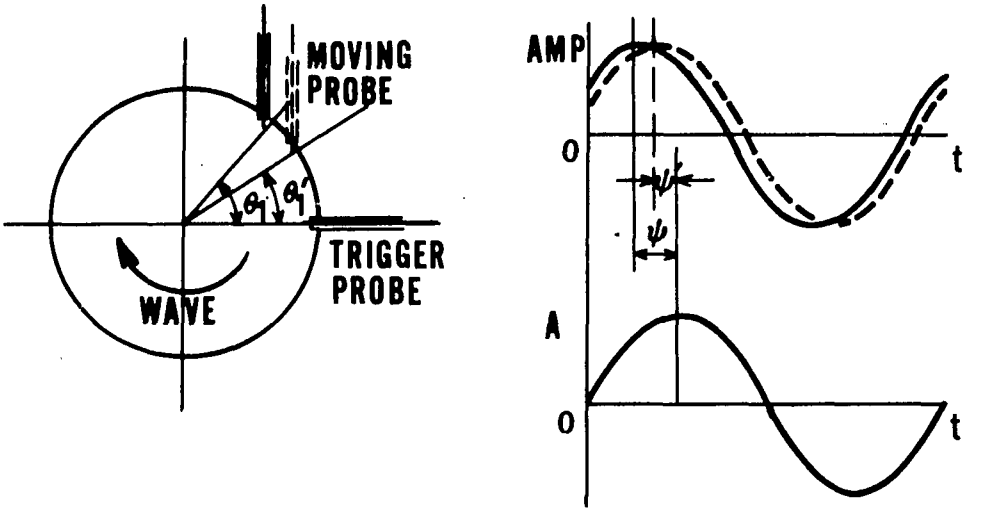

WAVE PROPAGATES IN THE DIRECTION OF THE MOVING PROBE:

-WITH DECREASING θ_1, THE PHASE SHIFT ψ DECREASES RESULTING IN A REDUCED LEAD; $\psi \rightarrow 0$ FROM THE LEFT ON THE DUAL-BEAM OSCILLOGRAM.

CASE II MOVING PROBE SIGNAL "TRAILS" THE TRIGGER SIGNAL

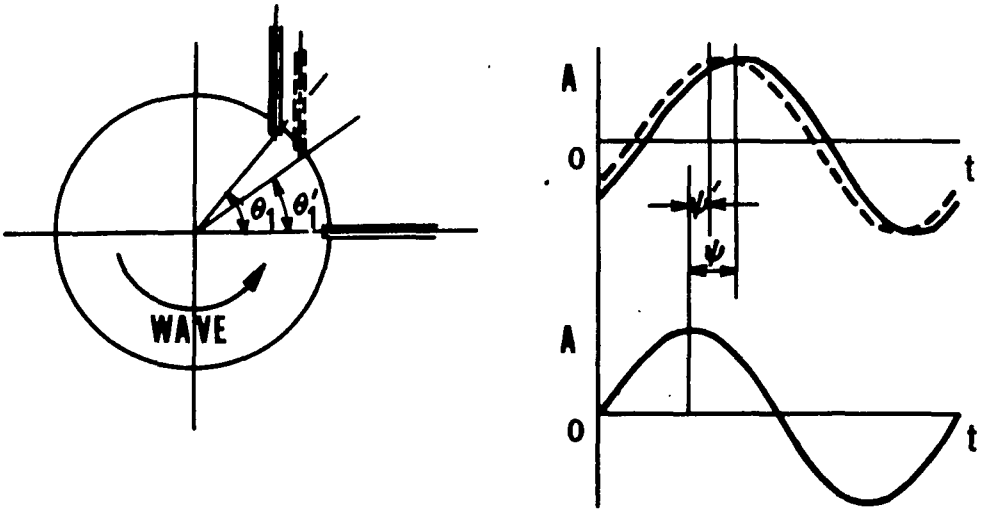

WAVE PROPAGATES IN THE DIRECTION OPPOSITE TO THE MOVING PROBE:

-WITH DECREASING θ_1, THE PHASE SHIFT ψ DECREASES RESULTING IN A REDUCED LAG; $\psi \rightarrow 0$ FROM THE RIGHT OF THE DUAL-BEAM OSCILLOGRAM.

FIGURE A. 2 DIRECTION OF THE AZIMUTHAL WAVE PROPAGATION

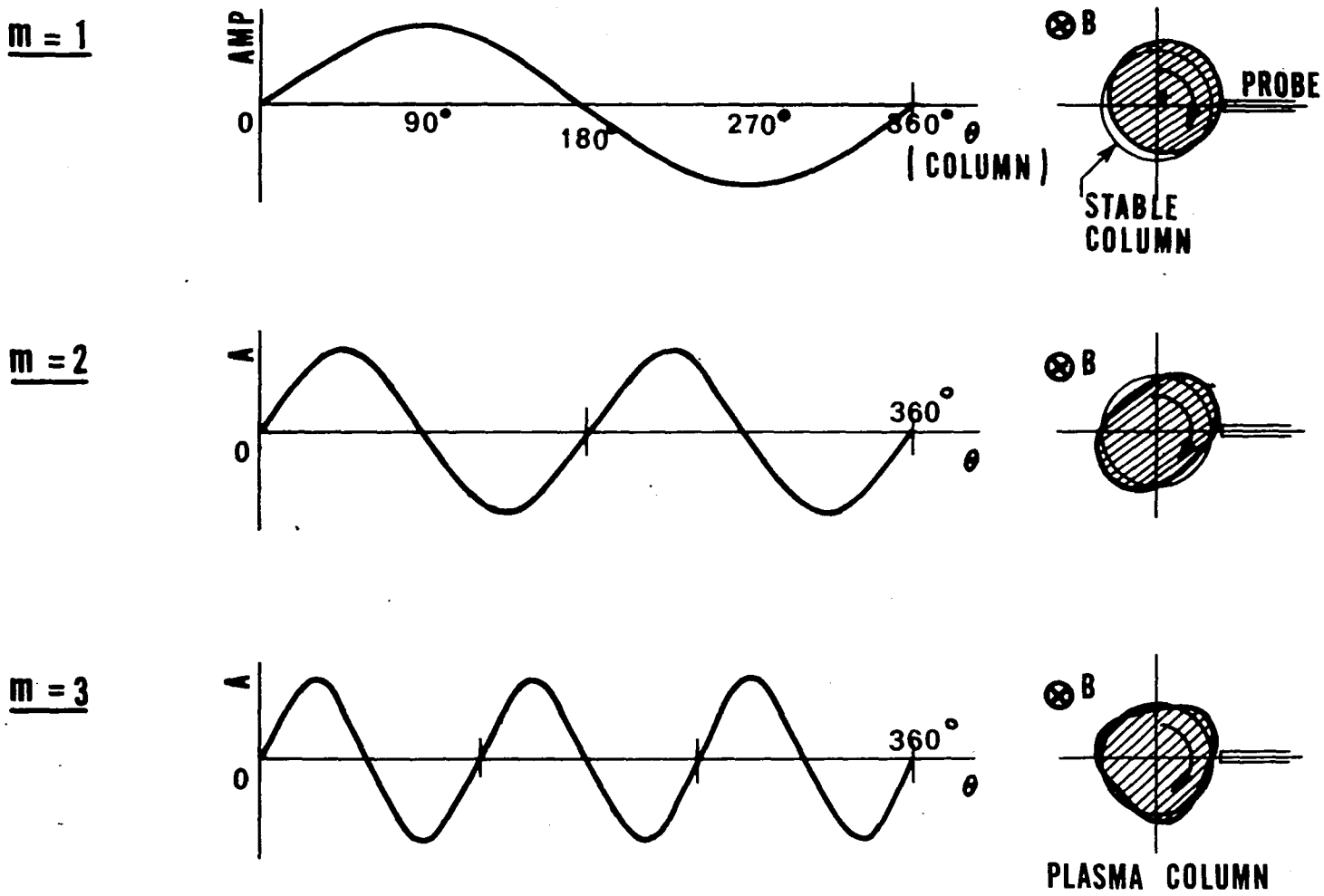

FIGURE A. 3 AZIMUTHAL WAVE AND PLASMA DENSITY OSCILLATIONS, m = 1, 2 AND 3.

MODE No. m	θ PER WAVE LENGTH λ	PHASE SHIFT IN FRACTION OF THE WAVE LENGTH		
		$\theta_1 = 90°$	$\theta_1 = 45°$	$\theta_1 = 30°$
1	360	90/360 = 1/4	45/360 = 1/8	30/360 = 1/12
2	180	90/180 = 1/2	45/180 =1/4	30/180 = 1/6
3	120	90/120 = 3/4	45/120 =3/8	30/120 =1/4
4	90	90/90 = 1	45/90 = 1/2	30/90 = 1/3
5	72	90/72 = 1-1/4	45/72 = 5/8	30/72 = 5/12
6	60	90/60 = 1-1/2	45/60 = 3/4	30/60 =1/2
7	51.43	90/51.43 = 1-3/4	45/51.43 = 7/8	30/51.43 = 7/12
8	45	90/45 = 2	45/45 = 1	30/45 = 2/3
9	40	90/40 = 2-1/4	45/40 = 1-1/8	30/40 = 3/4
10	36	90/36 = 2-1/2	45/36 = 1-1/4	30/36 = 5/6

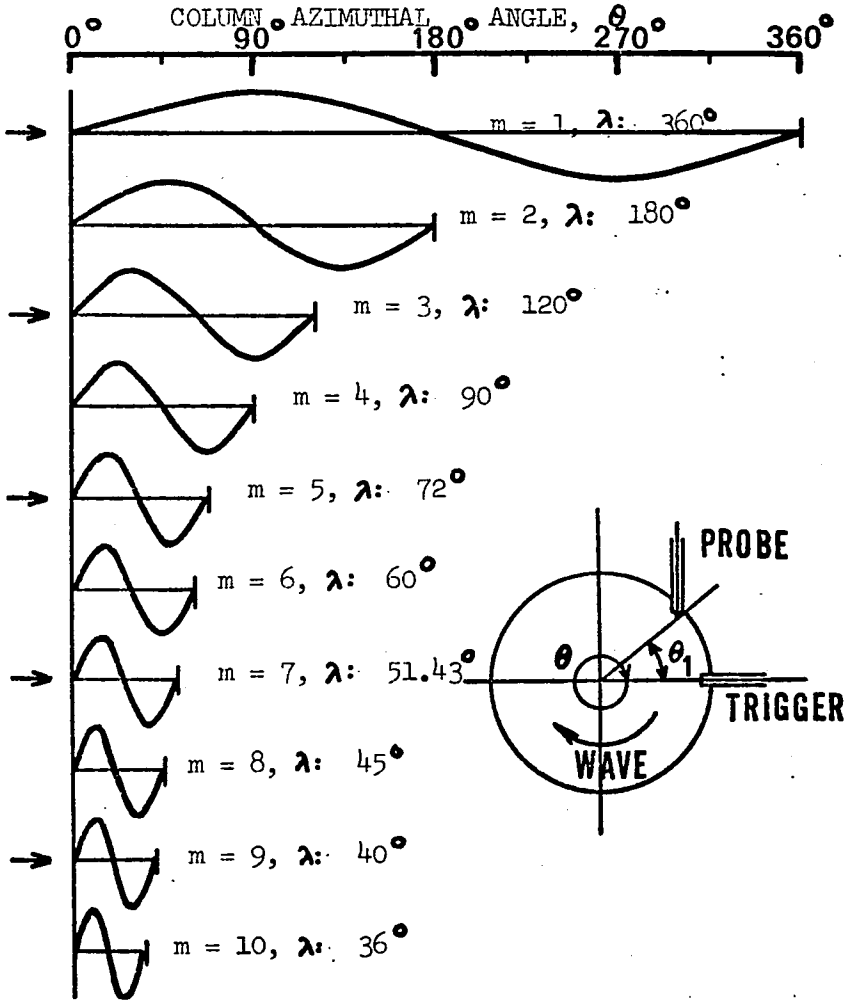

FIGURE A. 4 DETERMINATION OF THE AZIMUTHAL MODE NUMBER, m

m is determined to be one. However, the same phase shift can also be observed for m = 5, 9 .... etc. This difficulty can be overcome by verifying the mode number with the two probes set at a different angle. For the above example, if in further measurements a phase shift of 1/8 wave length is obtained with $\theta_1 = 45^{\circ}$, m = 1 is ascertained. In the experiment the mode number of the wave was determined by taking at least two different θ_1's.

BIBLIOGRAPHY

1 Lehnert, B., Proc. 2nd U.N. Intern. Conf. on the Peaceful Uses of Atomic Energy, 32, 349 (1958).

2 Goeler, S.V. and D'Angelo, N., Phys. Fluids 8, 1570 (1965).

3 Buchel'nikova, N.S., Nuclear Fusion, 6, 122 (1966).

4 Buchel'nikova, N.S., Kudryavtsev, A.M. and Salimov, R.A., Soviet Physics - Tech. Phys. 10, 53 (1965).

5 Chu, T.K., Hendel, H.W. and Politzer, P.A., Phys. Rev. Letters 19, 1110 (1967).

6 Buchel'nikova, N.S., Salimov, R.A. and Eidelman, Yu. I., Soviet Phys. - JETP 25, 252 (1967).

7 D'Angelo, N. and Motley, R.W., Phys. Fluids 6, 422 (1963).

8 Buchel'nikova, N.S., Salimov, R.A. and Eidelman, Yu.I., Soviet Phys. - JETP 25, 548 (1967).

9 Hendel, H.W., Chu, T.K., and Politzer, P.A., Phys. Fluids 11 2426 (1968).

10 Kent, G.I., Jen, N.C. and Chen, F.F., Phys. Fluids 12, 2140 (1969).

11 Paulikas, G.A. and Pyle, R.V., Phys. Fluids 5, 348 (1962).

12 Hoh, F.C. and Lehnert, B., Phys. Fluids 3, 600 (1960).

13 Kadomtsev, B.B., Nedospasov, A.V., Plasma Physics, 1, 230 (1960).

14 Kadomtsev, B.B., Soviet Phys. - Tech. Phys. 6, 882 (1962).

15 Allen, T.K., Paulikas, G.A. and Pyle, R.A., Phys. Rev. Letters, 5 409 (1960).

16 Hoh, F.C., Phys. Rev. Letters 4, 559 (1960).

17 Guest, G. and Simon, A., Phys. Fluids 5, 503 (1962).

18 Woods, L.C., Phys. of Fluids 6, 725 (1963).

19 Akhmedov, A.R. and Zaitsev, A.A., Soviet Phys. - JETP 18, 977 (1964).

20 Holter, ø and Johnson, R.R., Phys. Fluids 8, 333 (1965).

21 Friedman, H.W., Phys. Fluids 10, 2053 (1967).

22 Sheffield, J., Phys. Fluids 11, 222 (1968).

23 McPherson, D.A., Phys. Fluids 9, 1373 (1966).

24 Huchital, D.A. and Holt, E.H., Phys. Rev. Letters 16, 677 (1966).

25 Reynolds, J.F., Holt, E.H., Jennings, W.C. and Noon, J.H., Applied Phys. Letters 11, 148 (1967).

26 Reynolds, J.F., Jennings, W.C. and Gunshor, R.L., Phys. Fluids 11, 1048 (1968).

27 Chen, F.F., Plasma Physics 7, 399 (1965).

28 Chen, F.F., Phys. Fluids 8, 1323 (1965).

29 Sato, M., Applied Phys. Letters, 9, 423 (1966).

30 Tao, C.H., Mansfield, I., and Jen, N.C., Bull. Am. Phys. Soc. 13, 1558 (1968).

31 Tao, C., Jen, N.C., and Mansfield, I., Proceedings of the Electro-Optical System Designs Conference, Sept. 22-24, 1970, N.Y. (in press).

32 Rynn, N. and D'Angelo, N., Rev. Sci. Instr. 31, 1326 (1960).

33 Cataldo, J.C. and Jen, N.C., Phys. Fluids 11, 2057 (1968).

34 Chen, F.F., Chapter 4, Plasma Diagnostic Techniques, Huddleston, R.H. and Leonard, S.L., Editors (Academic Press, New York and London, 1965).

35 Langmuir, I., in "Collected Works of Irving Langmuir" (G. Suits, ed.) MacMillan (Pergamon) N.Y. (1961).

36 Bohm, D., Burhop, E.H.S., and Massey, H.S.W. in "The Characteristics of Electrical Discharges in Magnetic Fields" (A. Guthrie and R.K. Wakerling, Eds.) McGraw-Hill, N.Y. (1949).

37 Lam, S.H., Phys. Fluids 8, 73 (1965).

38 Demetriades, A. and Doughman, E.L., Jour. AIAA 3, 451 (1966).

39 Sanmartin, J.R., Phys. Fluids 13, 103 (1970).

40 Wada, J.Y. and Knechtli, R.C., Proc. I.R.E. 1926 (1961).

41 Fatora, D.A., J. Soc. Motion Pict. and Telev. Engrs., 74, 912 (1965).

42 Lashinsky, H., Phys. Rev. Letters 12, 121 (1964).

43 JEDEC Electron Tube Council, JEDEC Pub. No. 16A (1966).

44 D'Angelo, N. and Rynn, N., Phys. Fluids 4, 1303 (1961).

45 Spitzer, L. Jr., "Physics of Fully Ionized Gases", John Wiley, N.Y. (1967).

46 Chen, F.F., Phys. Fluids 8, 912 (1965).

47 Tchen, C.M., Proc. Symposium on Turbulence of Fluids and Plasmas, Polytechnic Press, 47-54 (1969).

48 Tchen, C.M., Proc. Symposium on Turbulence of Fluids and Plasmas, Polytechnic Press, 55-64 (1969).

49 Tchen, C.M., AIAA Transactions on Electronic Devices, 247-251 (1970).